UNIVERSITÀ DEGLI STUDI DI MILANO

Dottorato di Ricerca in Biologia Molecolare e Cellulare

XXIX Ciclo

IMPROVING TRAFFICKING AND KINETICS OF A SYNTHETIC LIGHT-GATED POTASSIUM CHANNEL

L. S. ALBERIO

PhD Thesis

Scientific tutor: Prof. A. Moroni

Academic year: 2015-2016

SSD: BIO/11

Thesis performed at Università degli Studi di Milano, Dipartimento di Bioscienze (Milano, Italy) and Columbia University, Department of Physiology and Cellular Biophysics (New York, USA)

CONTENTS

PART I 1

Abstract 2

1 – State of the Art 3

1.1 – Optogenetics and optogenetic tools 3

1.2 – Shortcomings of chloride-driven neuronal inhibition 8

1.3 – Creating a light-gated K+ channel: SPARK, HyLighter, PIRK and Lumitoxin 9

1.4 – BLINK1 12

1.5 – Trafficking to the PM: an overview 18

1.6 – Improvement of NpHR surface expression 21

2 – Aim of the Project 24

3 – Results 25

3.1 – Immunolocalization of BLINK1 on the plasma membrane of HEK 293T cells 25

3.2 – The linker and its influence on the properties of BLINK –type channels 28

3.3 – The N terminal helix of LOV2 domain and its role in controlling channel properties 31

3.4 – Anchoring of LOV domain to the PM 33

3.5 – Addition of C-terminal targeting signals 38

3.6 – BLINK2 characterization 53

3.7 – Mutations in LOV domain affect channel kinetics and trafficking 60

4 – Conclusions and Future Perspectives 66

PART II 73

CONTENT 74

PART III 127

Materials and methods 128

1 – Molecular biology 128

1.1 **–** Constructs Preparation 128

1.2 **–** Insertion of mutations 128

1.3 – Expression vectors 128
2 – Western blot analysis.....130
2.1 – Yeast growing conditions 130
2.2 – Western blot.....130
3 – Immunocytochemistry.....131
4 – Electrophysiology recordings in HEK 293T cells.....131
5 – Microinjections and touch response assays in zebrafish 132
6 – Light conditions.....132

PART I

ABSTRACT

Optogenetics uses light-regulated ion channels and pumps to modulate the activity of neurons with high temporal precision. To date, inhibition of neuronal firing is obtained by means of hyperpolarizing pumps, and/or chloride channels. However, a light-gated potassium (K^+) channel would represent a more physiological tool because of the universal role of K^+ in repolarizing membrane potential in animal cells.

We recently engineered a synthetic light-gated channel by fusing the LOV (light oxygen voltage) domain of the plant blue-light receptor AsPhototropin1 to the viral K^+ channel Kcv-PBCV1. The resulting channel BLINK1 (Blue Light Induced K^+ channel) is reversibly activated by blue light and shows K^+ selectivity and high single channel conductance, when expressed in HEK 293T cells. However, BLINK1 low expression rate at the plasma membrane (PM) (less than 10% in HEK 293T cells) prevented so far its application in optogenetics.

The goal of my PhD thesis has been to improve BLINK1 expression in HEK293T cells and to test it in two model systems, zebrafish and mouse. To this end, I have applied molecular and cellular approaches for modifying the trafficking and the overall folding and stability of the channel. Both the LOV domain and the pore domain have been modified by either the addition of PM anchoring motifs and structural elements (LOV domain) or the addition of trafficking motifs (Kcv). The outcome of this study, BLINK2, was obtained by adding a 14-3-3 signal peptide to the C terminus of BLINK1. It showed a moderate increase in PM expression (26% vs 10%) compared to BLINK1, but responded to light with a delay of about 90 s. We further improved BLINK2 by introducing a point mutation (Q513D) in the LOV domain that reduced the delay to about 30 s. When tested in mouse, BLINK2 Q513D efficiently inhibited spontaneous firing in brain slices. BLINK2 Q513D is currently undergoing a test *in vivo* in a mouse behavioral experiment.

1 - STATE OF THE ART

1.1 – Optogenetics and optogenetic tools

The term “optogenetics” refers to the ability to control defined cellular processes combining genetics and light [1]. This approach allows high spatial and temporal precision, since it relies on the activation of light modulated proteins whose expression can be specifically targeted.

This technique allows neuroscientists to dissect the complexity of neural circuits and investigate neuronal functions *in vivo* in freely behaving animal models and it is based on the manipulation of the electrical activity of excitable cells by means of optogenetic actuators [2, 3, 4].

Optogenetics actuators are natural occurring ion channels and pumps identified in algae and microbial genomes and they can be divided into two main categories: excitatory or inhibitory tools (Fig. 1).

When transfected into neurons, excitatory tools promote membrane depolarization, by mediating

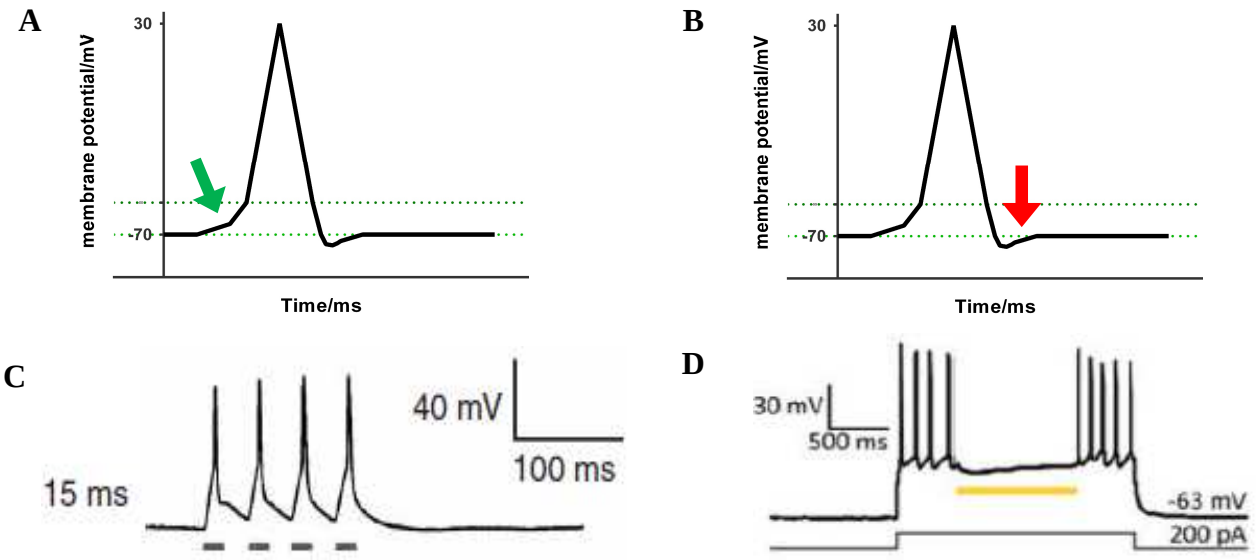

Fig. 1

Modulation of membrane excitability

A and B: schematic representation of action potential. Dotted lines indicate cell resting potential (-70mV) and threshold potential (-55mV). Excitatory tools can promote action potentials by depolarizing the PM to reach threshold potential value (green arrow). Inhibitory tools prevent action potential rise by maintaining the cell membrane at hyperpolarized values (red arrow).

C: example of light-induced neuronal firing; dotted line below the trace represents time of light on modified from ref [5]. *D: example of light driven firing inhibition in a neuron excited by current injection (grey step), yellow bar represents light exposure, modified from ref* [7]

cation influx and thus leading to the rise of action potentials [5].

On the other hand, inhibitory tools impair neuronal firing by maintaining cell membrane potential to hyperpolarized values with two different mechanisms: extrusion of protons from the cell cytosol [6] or influx of chloride ions [7].

The main actuator used to promote neuronal activity is Channelrhodopsin 2 (ChR2), a natural occurring light-gated cation non-specific channel isolated from the green alga *Chlamydomonas reinhardtii* [8].

ChR2 is a seven transmembrane domain opsin that contains an all-trans-retinal molecule as chromophore. Following blue light (470 nm) absorption, the chromophore undergoes isomerization inducing conformational changes in the protein leading to pore opening. In neurons the non-selective influx of cations (H+>>Na+>Ca2+) driven by ChR2 causes cell membrane depolarization, promoting neuronal firing (Fig 1c) [5].

ChR2 has been extensively characterized during the past decade and, as shown in Fig. 2, many improved versions have been engineered to obtain faster activation kinetics, shifted activation spectra,

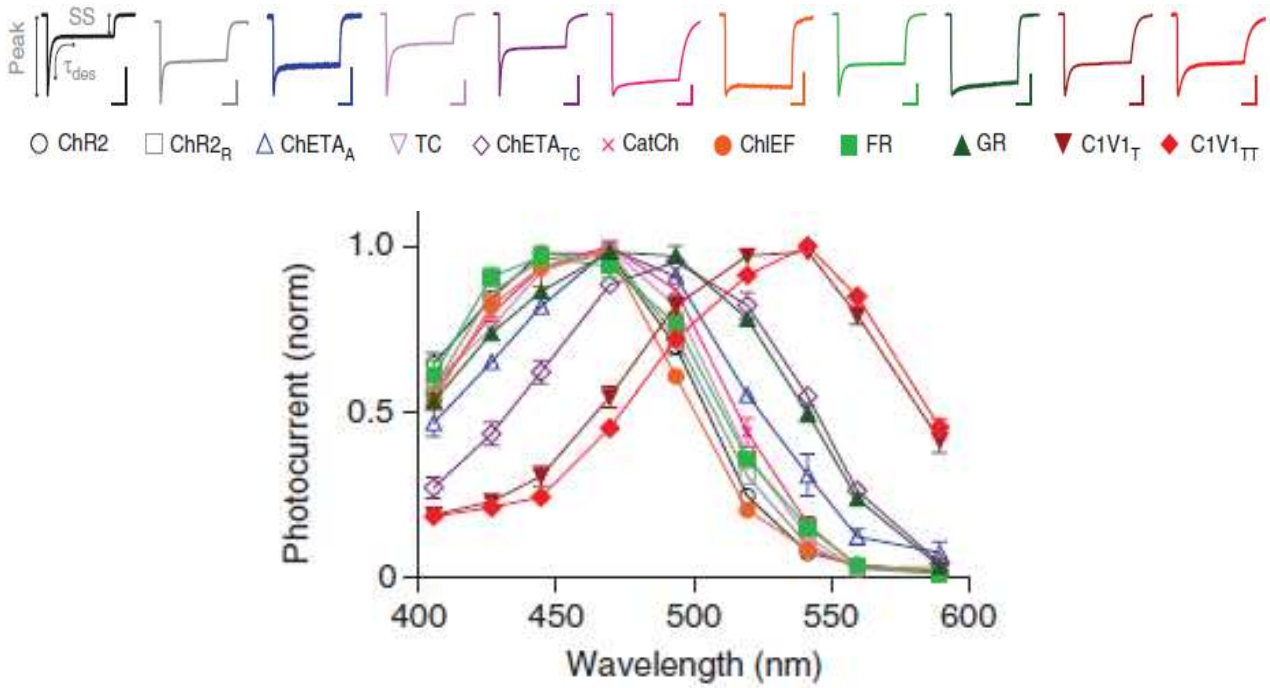

Fig. 2

Comparison between wild type ChR2 and improved spectral variants.

Upper panel: Normalized photocurrent. Scale bars: 400pA, 200ms.

Lower panel: action spectra for each variant. Color- and symbol- codes are the same reported in the upper panel. The names of the constructs are also indicated below each measurement. Modified from reference [9]

increased depolarizing currents and higher light sensitivity [9]. ChR2 and its variants are widely and successfully employed as activators in all optogenetic experiments.

As for the inhibitory tools, the most used are two microbial light-driven pumps: eNpHR3.0 and eArch3.0. eNpHR3.0 belongs to the family of halorhodopsins, discovered in the archaeon *Natronomonas pharaonis.* Following yellow light illumination (590 nm), eNpHR3.0 pumps chloride (Cl^-) ions inside the cell leading to membrane hyperpolarization [10] and inhibition of neuronal firing (Fig 1D) [11]. eArch3.0, on the contrary, is an outward proton (H^+) pump isolated from *Halorubrum sodomense*. Following light absorption (560nm) eArch3.0 moves H^+ out of the cell establishing a membrane hyperpolarization that inhibits neuronal activity [6].

When measured in the same conditions, eArch3.0 showed larger photocurrents than eNpHR3.0 and could induce a stronger hyperpolarization [9] (Fig. 3). However, it has been reported that pH shift following sustained eArch3.0 activity activates calcium influx in synaptic terminals leading to spontaneous vesicle release [12]. For this reason, eNpHR3.0 is preferentially employed as a hyperpolarization tool, given that Cl^- influx into cells is considered a more physiological condition. Noticeably, it was recently shown that also Cl^- accumulation beyond its electrochemical equilibrium promotes neurotransmitter release, thus leading to neuronal excitability [12].

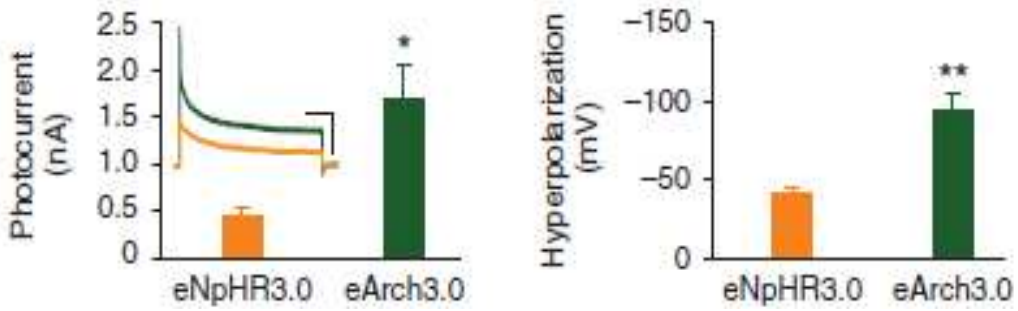

Fig. 3

Comparison between eNpHR3.0 and eArch3.0 measured in the same experimental conditions.

Left, exemplary current measurements and mean peak currents of the two pumps (n= 8 and 10); right, mean hyperpolarization measured in 6 and 10 cells after light on. Modified from reference [9]

eArch3.0 and eNpHR3.0 show similar EPD50 values, in the order of 5-10mW/mm^2 [9], where EPD50 is the light power density at which 50% of maximum photocurrent in recorded. These values are relatively high (ChR2 EPD50 value is 1-2mW/mm^2) and will not allow hyperpolarization of large tissue areas, since cells located far from the light source will need longer exposure to achieve the same hyperpolarization degree than those located closer [9].

A general issue regarding the use of pumps to inhibit neuronal firing is that high expression levels are required since only one ion per photon is pumped across the PM [6]. Such a low transport rate cannot completely abolish spiking activity when the input currents have bigger magnitude than the elicited photocurrent [13]. For this reason, the optogenetic community has long been searching for a light-regulated inhibitory channel. To this end, ChR2 has been engineered to become selective for chloride ions [14, 15]. When expressed in neurons, these chloride channels prevent firing by shunting inhibition as they move the value of Cl- reversal potential to the cell membrane potential value.
Recently, a natural occurring Channelrhodopsin selective for chloride ions has also been identified during a screening of microbic genomes [16]. When expressed *in vitro* in cultivated neurons, iC++ showed a more efficient inhibition of firing than NpHR3.0 [13]. Neurons expressing the channel showed no spike during light exposure while in some cases eNpHR expressing cells showed some firing activity (Fig. 4A). On the other hand, when these two tools were employed *in vivo*, this difference was not evident anymore and mice behavior was affected by both with the same efficiency (Fig.4B) [13].

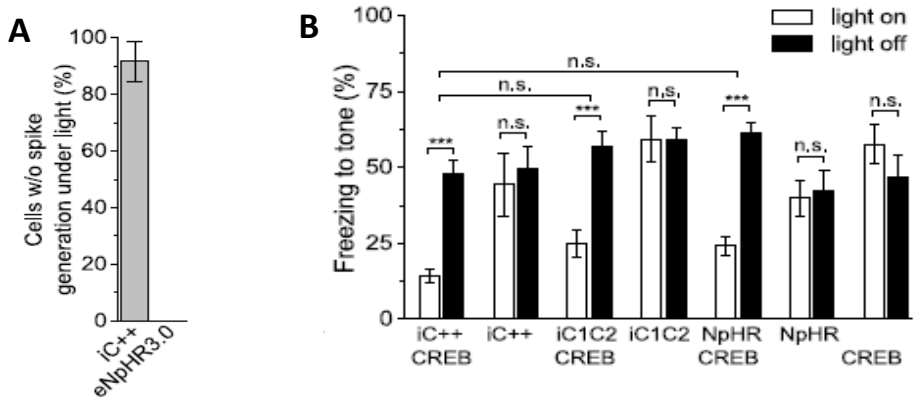

Fig. 4

Comparison between iC++ and eNpHR3.0 effects in vitro and in vivo

A: Percentage of cells expressing either iC++ or eNpHR3.0 that did not show spiking activity under light at any current injection level.

*B: Assay for memory performed on mice expressing iC++, iC1C2, or eNpHR3.0 in wild type neurons as well as in neurons overexpressing CREB (transcription factor that preferentially allocates neurons to the engram that supported fear memory). Silencing these neurons reversibly disrupted memory retrieval, resulting in freezing to tone. Disrupting the activity of the same number of neurons that are not allocated to the fear engram (those not overexpressing CREB) did not impair memory retrieval. n.s.: P > 0.05; ***P < 0.005. Error bars indicate SEM.*

Modified from reference [13]

1.2 – Shortcomings of chloride-driven neuronal inhibition

Despite the positive results obtained with chloride pumps and chloride channels as inhibitors of neuronal activities, inhibition of firing mediated by the influx of chloride into neurons has some shortcomings.

Chloride is an important anion in neurons, playing a major role in synaptic inhibition. The latter is mediated by the action of $GABA_A$, $GABA_C$ and glycine receptors that are Cl^- permeable ligand-gated channels. In addition, Cl^- is also responsible of the modulation of the cell volume and for the loading of transmitters into vesicles [17, 18, 19].

Interestingly, it has been reported that chloride gradients are not constant in neurons during developmental stages in vertebrates [20]. In particular, it was reported that in immature neurons the intracellular chloride concentration was higher than in neurons from adult brain. This is shifting the value of chloride reversal potential (E_{Cl}) to more depolarized voltages than the membrane resting potential (V_{rest}). In these conditions, activation of $GABA_A$ receptors leads to a depolarization instead of the usual hyperpolarization and the consequent inhibitory effect reported for mature neurons [21]. Moreover, chloride gradients in a single cell have been observed to undergo dynamic changes, following a circadian rhythmicity. As a result, this attributes to GABA either an excitatory or an inhibitory role on firing depending on the time of day [22].

In a recent publication, eNpHR3.0-mediated intracellular chloride accumulation has been used to augment excitability of cellular membrane in neuronal cells in order to simulate an epileptic condition [23]. The intracellular accumulation of Chloride ions driven by eNpHR3.0 shifts in E_{GABA} in neurons. Therefore, when the GABA receptors open, they drive an excitatory current (due to chloride ions leaving the cell) that has been used as a model for the study of chloride gradients misregulation in epilepsy [23]. The results of these experiments show that modulation of neuronal activity by chloride influx into cells can give conflicting effects. Inhibitory tools such as NpHR3.0 can also mediate an increased synaptic transmission, due to rebound excitation [12, 24].

A better alternative to provide a more stabilized inhibition of neuronal activity would be the use of a light-gated potassium (K^+) channel. K^+ ions efflux via K^+ channels is the physiological process occurring during an action potential to achieve repolarization. For this reason, a light-gated K^+ channel would represent a very desirable optogenetics tool. Indeed, synaptic inhibition mediated by a chemo-regulated K^+ channel has already been achieved [25]. The use of a light-modulate actuator would allow a more rapid, remote and non-invasive control of the process.

1.3 - Creating a light-gated K+ channel: SPARK, HyLighter, PIRK and Lumitoxin

The screening of microbial genomes conducted so far has not yet identified a light modulated K^+ channel. In the last years, several attempts have been made by a number of researchers to engineer different kind of synthetic light-gated K^+ channels.

In 2004 Banghart *et al.*, reported the creation of SPARK, a synthetic photoisomerizable azobenzene-regulated K^+ channel [26]. SPARK is composed of a modified Shaker K^+ channel engineered with a photoswitchable K^+ channel blocker, a TEA ion. A molecule called MAL-AZO-QA (MALamide, AZObenzene, Quaternary Ammonium) was engineered and linked to a cysteine in one of the channel outer loops, at a distance known to allow the quaternary ammonium molecule (QA) to block the channel pore. Following UV light exposure (380 nm), the AZO moiety in the molecule isomerizes. This reduces the total length of the MAL-AZO-QA molecule and thus removes the pore blocker (Fig. 5). The latter process is almost completely reverted by exposing the channel to green light (500nm).

In vivo experiments confirmed that SPARK was able to inhibit neuronal firing. However, this synthetic channel requires the addition of external cofactors (MAL-AZO-QA molecule is not naturally occurring). This makes an application in organisms difficult. An additional negative effect is that SPARK is activated by UV light, e.g. light which is potentially harmful.

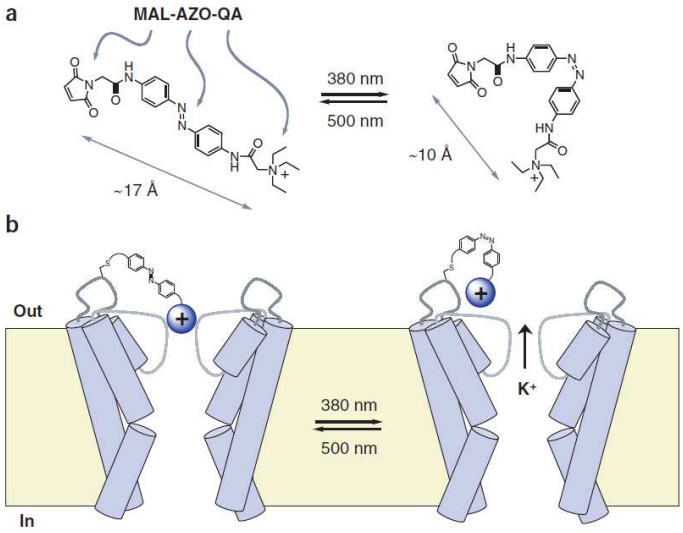

Fig. 5

SPARK channel activation/deactivation mechanism

A: MAL-AZO-QA photoisomerzation: UV light (380 nm) induces the trans to cis isomerization of the molecule. The process reverts exposing the molecule to visible light (500 nm). B: schematic representation of SPARK activation mechanism. Modified from reference [26]

With a similar strategy, a synthetic molecule called MAG (Malamide, Azobenzene, Glutamate agonist) was used to modulate the activity of a K^+ selective bacterial glutamate receptor [27]. The obtained synthetic channel has been named HyLighter, and it was reported to generate hyperpolarizing currents following UV light exposure. In particular, when expressed in motor neurons, HyLighter can inhibit neuronal firing in brain slices and impair Zebrafish escape behavior after UV illumination [27]. The channel however shares many of the negative features with SPARK; it also requires the cofactor supplementation for channel activation and UV light for stimulation.

Following another approach, Schmidt *et al.*, created a two components light-sensitive K^+ channel by tethering a pore blocker (in this case a toxin) to a photoreceptor (LOV domain) [28]. The LOV domain reversibly exposes or retrieves the toxin upon illumination. The photoreceptor is expressed on the plasma membrane by means of a TM domain. The proximity of the blocker to endogenous K^+ channels is sufficient to block their conductance and this block can be removed by light [28]. This modular construct is known as Lumitoxin. Following blue light exposure, conformational changes in the LOV domain lead to a removal of the toxin, which serves as a blocker of the channel. The light generated removal of channel blocking in turn causes channel activation (Fig. 6).

This design of this system is versatile, since it can potentially be used to modulate any pore using different toxins. However, its activity depends on the proximity of the Lumitoxin to the channel pore; this may not ensure in all cases a total current block in the dark (Fig. 6B).

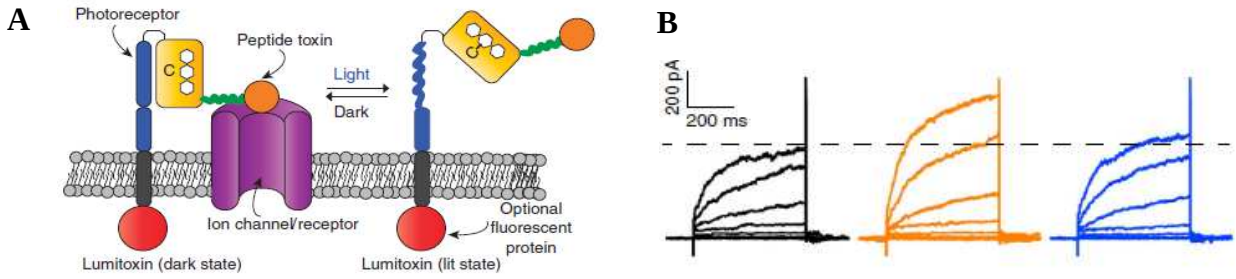

Fig. 6

The Lumitoxin system

A: schematic representation of Lumitoxin inhibition of an ion channel

B: recorded currents from cells expressing Lumitoxin in dark (black), during light application (orange) and after light application (blue)

Modified from reference [28]

PIRK (Photoinducible Inwardly rectifying K^+ channel) [29] is yet another engineered light sensitive channel. It is a modified version of Kir2.1 channel, an inward rectifying channel that is one of the key players in the control of neuronal excitability [30]. In this channel, unnatural amino acids (4,5-dimethoxy-2-nitrobenzyl-cysteine (Cmn)) have been inserted into the protein to create a block, which is removed after UV illumination. When expressed in neurons, PIRK can indeed reduce the firing frequency by hyperpolarizing the cell. However, the light-induced channel activity is not reversible and can only be blocked with the addition of specific blockers, such as Barium ions (Fig.7). Moreover, the need of inserting unnatural aminoacid is technically very demanding and, more importantly, precludes its usage *in vivo*.

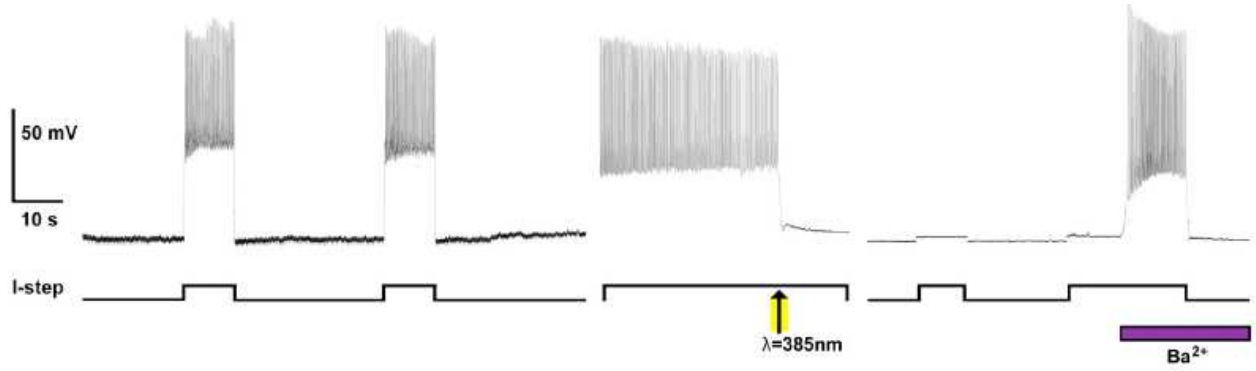

Fig. 7

PIRK mediated firing inhibition in hippocampal neurons.

Arrow indicates a single UV light pulse. After the channel activation, current injection cannot promote firing. Only in presence of a channel blocker (Ba2+), current injection can restore firing activity. From reference [29]

Finally, in 2015, our group has engineered a light-driven K^+ channel, BLINK1, that is fully genetically encoded. Moreover, BLINK1 does not require exogenous cofactors; another desirable features for application as an optogenetics inhibitory tools. In the next paragraph, I will describe the channel features in more details.

1.4 - BLINK1

To engineer a light gated K^+ channel, Cosentino *et al.*, took advantage of the light induced conformational changes in the LOV2 (light oxygen voltage2) domain. The latter is part of the blue-light receptor Phototropin1 from *Avena sativa*. The light sensitive LOV2 domain (from now on called LOV) is used to modulate the activity of the K^+-selective viral channel PBCV-1 Kcv (from now on called Kcv) [31].

LOV domains can covalently bind Flavin Mono Nucleotide (FMN), their cofactor, when exposed to blue light (450 nm) (Fig. 8). This leads to the formation of a covalent bond between C4a in FNM and the thiol in the side chain of a highly conserved Cysteine residue (C450 in the protein from *Avena sativa*) in the core of the protein. The formation of the covalent adduct causes the breaking of all the hydrogen bonds between FMN and other residues also located in the LOV domain core. This network of hydrogen bond is involved in the stabilization of the cofactor inside the binding pocket in the dark. As a result, some rearrangements occur in the LOV structure, among which the partial unfolding and displacement of the C-terminal helix called Jα [32]. In the native protein Phototropin, the Jα movement leads to the activation of a downstream kinase domain. The conformational changes are reversed when the covalent bond between the protein and the cofactor spontaneously breaks in about 60 seconds in the dark [33].

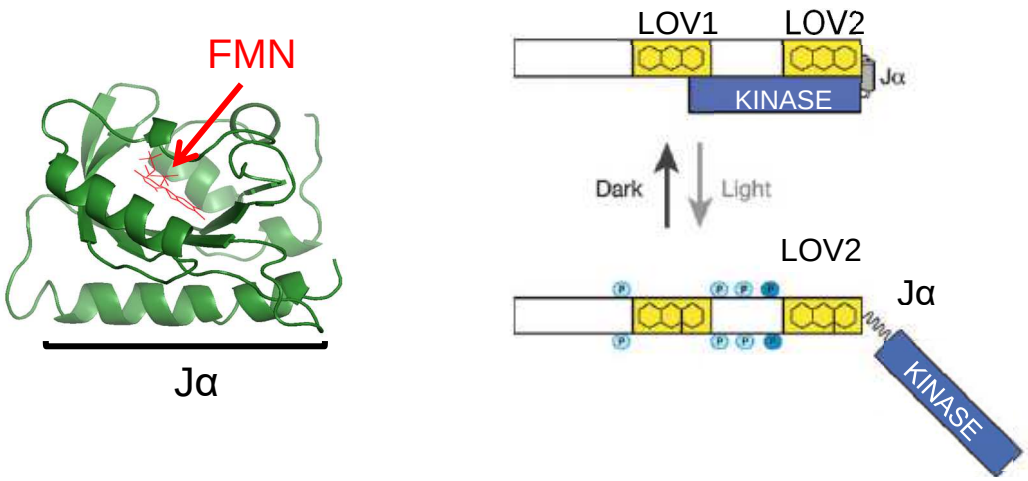

Fig. 8

Structural details of LOV2 domain in light and dark

A: crystal structure of AsLOV2 in which the chromophore Flavin mononucleotide (FMN) (in red) is bound to the core domain. Jα is indicated by a black bar (PDB:2V1B). B: schematic representation of the role of LOV2 domain in Phototropin activation/deactivation by light and dark. Modified from reference [32]

The light-induced movement of the Jα-helix has been used in BLINK1 to modulate the gating of the small viral K^+ pore Kcv. The pore of the channel, Kcv, is part of a family of small (82 to 94 residues long) viral channels, which are highly selective for K^+ [34]. The tetrameric Kcv channel represents the minimal functional K^+ channel found so far. The monomer is composed by two transmembrane domains and a pore loop that contains the selectivity filter sequence; a short (12 aa) amphipathic alpha helix called slide-helix is found at the N-terminus and is presumably located at the interface between the lipid membrane and the cytosol [35].

In order to obtain a functional light-gated channel, a number of chimeras were generated by connecting the LOV domain to different positions of the Kcv monomer. A yeast-based functional complementation assay was employed to screen for functional and light-regulated K^+ channels (Fig.9).

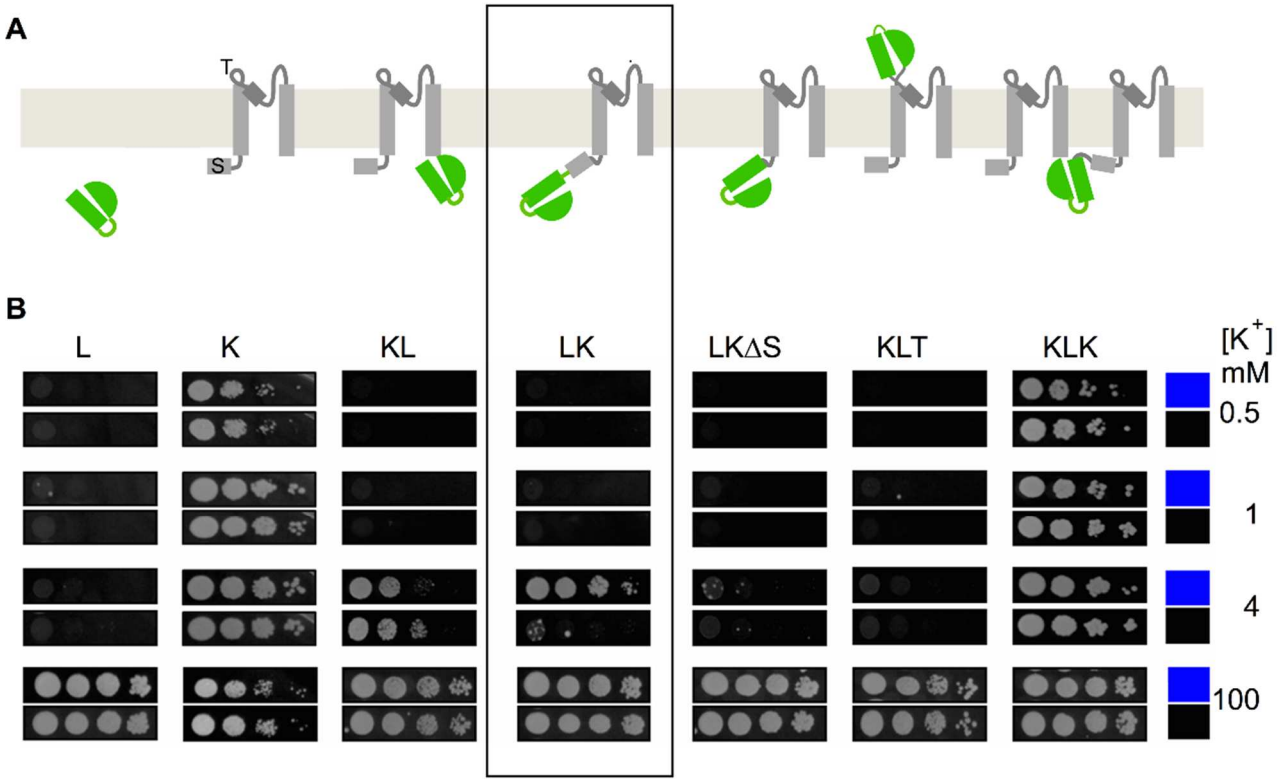

Fig. 9

Yeast-based functional screening for light sensitive channels.

A: schematic representation of the tested construct. LOV domain is in green, Kcv monomer is in grey. T and S indicate Turret and slide helix respectively. B: Results of functional complementation of a K^+-uptake deficient Yeast strain at different K^+ concentrations. Blue square and black square indicate light- or dark-exposure respectively. Construct giving the desired phenotype (LK) is boxed. Modified from reference [31]

For this purpose, we used a yeast strain (SGY1528) that can only grow in high external K^+ concentration (100mM K^+) and only regains the ability to grow in low external K^+ when transformed with a functional K^+ channel [36]. This screening allowed the identification of a chimera, named LK, which had the LOV domain fused to the N-terminal region of Kcv. When tested in x. laevis oocytes, LK was giving rise to a small and irreversible light-gated current (Fig10A)

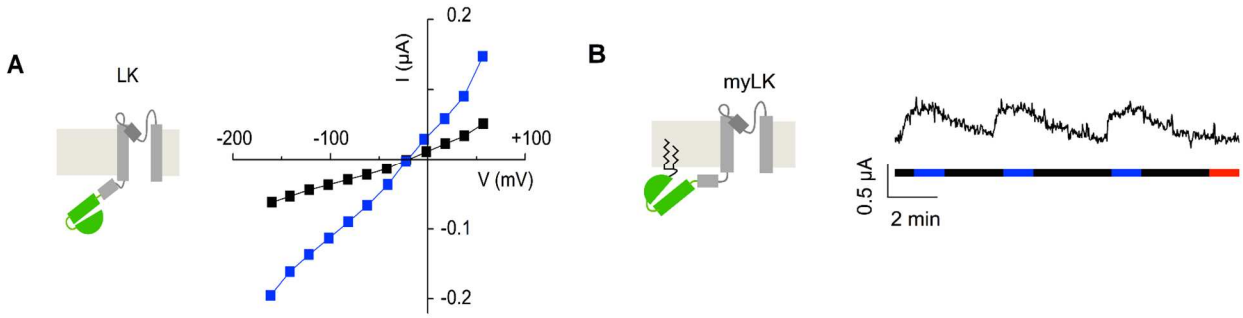

Fig. 10

Structural modifications in LK and functional consequences.

Monomer representation and currents recorded in X. laevis oocytes of LK (A) and myLK (B) constructs. myLK current is recorded at -60mV. Modified from reference [31]

To anchor the LOV domain to the membrane, in LK, a short N-terminal myristoilation and palmytoilation consensus site was added. This resulted in the clone myLK, which exhibited in *X. laevis* oocytes a reversible light induced response (Fig 10B).

myLK was further improved by a combination of rational design and protein evolution leading to the identification of myLK33, a clone showing very desirable features. The difference with the original myLK channel was the presence of three mutations: A7T in the myristoilation/palmitoylation site, N538A in the LOV domain and P13L in the Kcv pore.

The N538A mutation was introduced because it was reported in the literature to have a positive effect on the dynamic range of the LOV domain [37]. When introduced in myLK, mutation N538A increased current amplitude of the light stimulated K^+ currents in *X. laevis* oocytes. The clone was chosen as template for subsequent sequence randomization (Fig11A).

The two additional mutations A7T and P13L were inserted by sequence randomization. In particular, the first mutation, located in the myristoilation site, resulted in an improved consensus site for the binding of yeast N-Myristoyltransferase (NMT) [38]. P13 is a residue located in a key position of the Kcv sequence. In fact, this Proline residue represents the point where the slide-helix ends and the first transmembrane domain begins. Mutations in this residue have been demonstrated to affect gating of Kcv [39].

myLK33 exhibited good expression levels in *Xenopus* oocytes and in mammalian expression systems such as HEK293T cells. In these cells, light-gated currents could be detected in about 36% of transfected cells. However, myLK33 showed a substantial dark current, which compromised any *in vivo* application of the channel (Fig. 11).

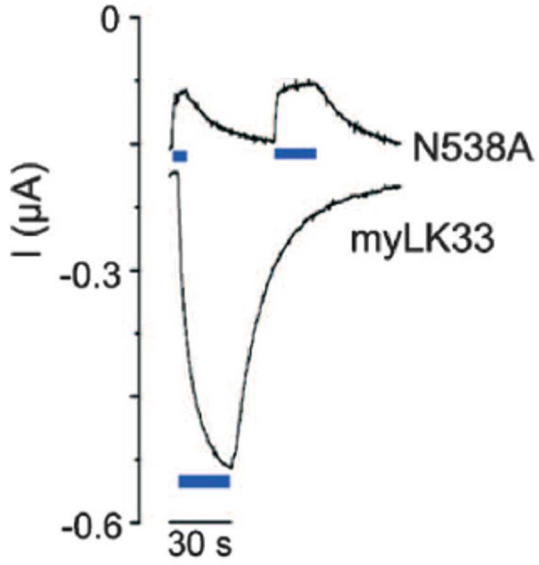

Fig. 11

Comparison between myLKN538A and myLK33 currents

Comparison of current amplitude between different myLK-based constructs expressed in X. laevis oocytes and measured in the same conditions (-60mV, 100mM K^+). Modified from reference [31]

A critical point in the design of synthetic proteins is the way in which two functionally related domains are connected in a chimera. In a previous work from our laboratory, in which a synthetic channel was engineered by fusing Kcv to the voltage sensor domain of a phosphatase [40], we have shown that the length of the linker region greatly affects the properties of the channel.

In the construct of a light gated K^+ channel we considered as linker the residues belonging to the LOV domain Jα helix and to the Kcv Slide helix (Fig. 12). Both, Jα helix and Slide helix (Sh) have an amphipathic nature. The first one exposes its hydrophobic residues to the core of the LOV domain [41, 42]. MD simulation have shown that the slide helix of Kcv on the other hand lies parallel to the membrane at the interface with the cytosol [39, 43].

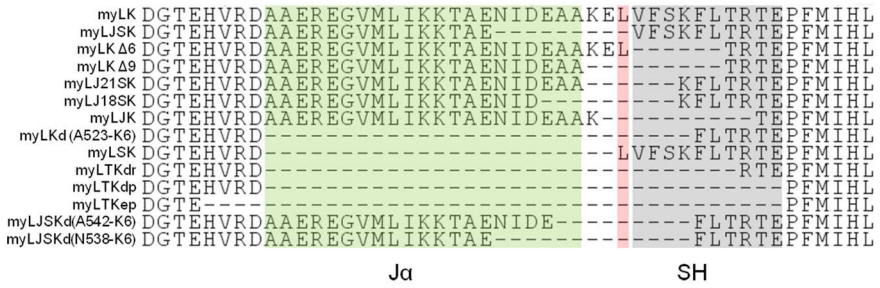

Fig. 12

Alignment of myLK-based construct bearing differences in the length of linker region

Alignment of myLK linker region with rationally designed deletion mutants. Residues boxed in green and grey belong to Jα and slide helix respectively.

Using rational design, an array of new clones was created by inserting progressive deletions in the linker region (Fig. 12). After testing the performance of the new constructs by yeast functional complementation screening, a new clone, called myLJSK, has been identified. HEK293T cells expressing myLJSK showed light activated potassium currents but no residual dark activity (Fig.13).

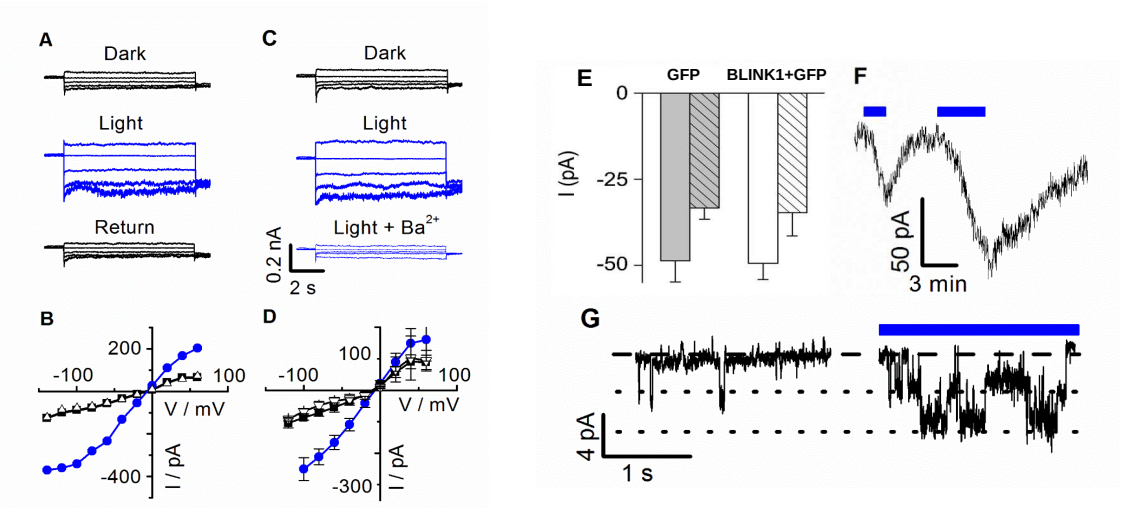

Fig. 13

BLINK1 (myLJSK) currents recorded in HEK293T cells

A and C: BLINK1 currents recorded in HEK293T in dark or light conditions as indicated. B and D: steady state IV relationship of traces in A and C. E: comparison between current levels in dark in HEK293T expressing GFP or BLINK1 and GFP in absence or in presence (diagonal pattern) of Barium ions. F: Gapfree recording of whole cell BLINK1 currents at -60mV. G: single channel measurements recorded at -70mV. Blue bars indicate blue light on. Modified from reference [31]

The currents measured in the dark were comparable with the endogenous current level of non-transfected cells (Fig.13E). This clone, which reveals a light sensitive gating and no dark current has been renamed BLINK1.

BLINK1 is reversibly activated (Fig. 13F) by blue light and maintains biophysical features of Kcv, including K^+ selectivity and high single channel conductance (70-80 pS, calculated from Fig.13G). Preliminary test to verify *in vivo* applicability of this channel were performed in Zebrafish embryos (Fig. 14): ectopic expression of BLINK1 reversibly inhibited the escape response of larvae, which were exposed to blue light but not in those kept in the dark. The results of these experiments stress that BLINK1 provides a single-component optogenetic tool that can establish prolonged, physiological hyperpolarization of cells at low light intensities (80µW/mm^2).

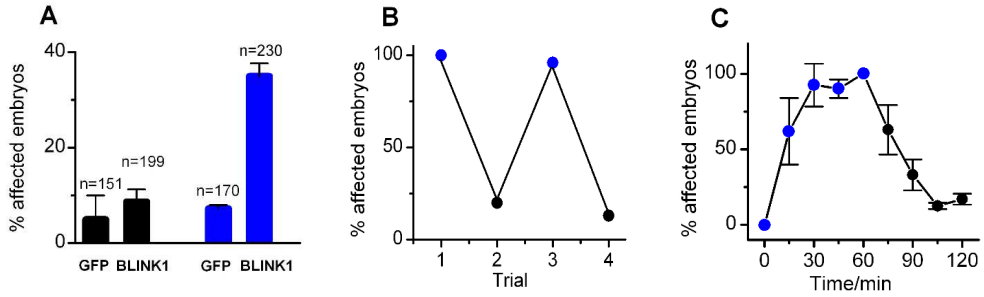

Fig. 14

Effect of BLINK1 expression on escape response in 2-days-old zebrafish larvae.

A: affected phenotype displayed in dark (blue bars) or after light exposure (blue bars) in GFP- or BLINK1-expressing larvae. B: Reproducibility of the light effect following repetitive light exposure. C: Kinetics of BLINK1-induced affected phenotype in light (blue dots) or dark (black dots) conditions. Modified from reference [31]

Even though BLINK1 was apparently successful in inhibiting the *in vivo* escape response of zebrafish larvae in response to blue light, electrophysiological experiments in mammalian cell lines (HEK293T, CHO) highlighted a very low surface expression of this channel in these systems. In patch clamp experiments, a light-gated current could only be detected in 8-10% of the transfected HEK293T cells analyzed [31]. The results of electrophysiological measurements on mammalian cells suggested a possible intracellular retention of BLINK1 and therefore an impaired channel presence on the PM.

1.5 - Trafficking to the PM: an overview

Trafficking of integral membrane proteins to the PM is a complex and strictly regulated process; a schematic representation of the key steps is reported in Fig. 15.

For a correct sorting and trafficking to the PM along the secretory pathway, the newly-synthetized peptides contain short sorting sequences. These can be recognized by adaptor proteins, which control the correct progression of protein sorting through the compartments of the secretory pathway [44].

As shown in this Figure, the pathway of a membrane protein begins with co-translation in the ER. In the ER, the nascent protein undergoes a Quality Check (QC) step: protein chaperons and folding sensors have the role to control if the protein exposes long stretches composed of hydrophobic residues, shows unpaired Cysteine residues or has other features that can lead to the formation of aggregates [45]. As a result, QC proteins retain in the ER the proteins that are recognized as not properly folded until they either reach a stabilized conformation or are modified by the addiction of specific secondary modifications that will target the protein to degradation pathway (i.e. glycosylation, ubiquitination, and others) [45].

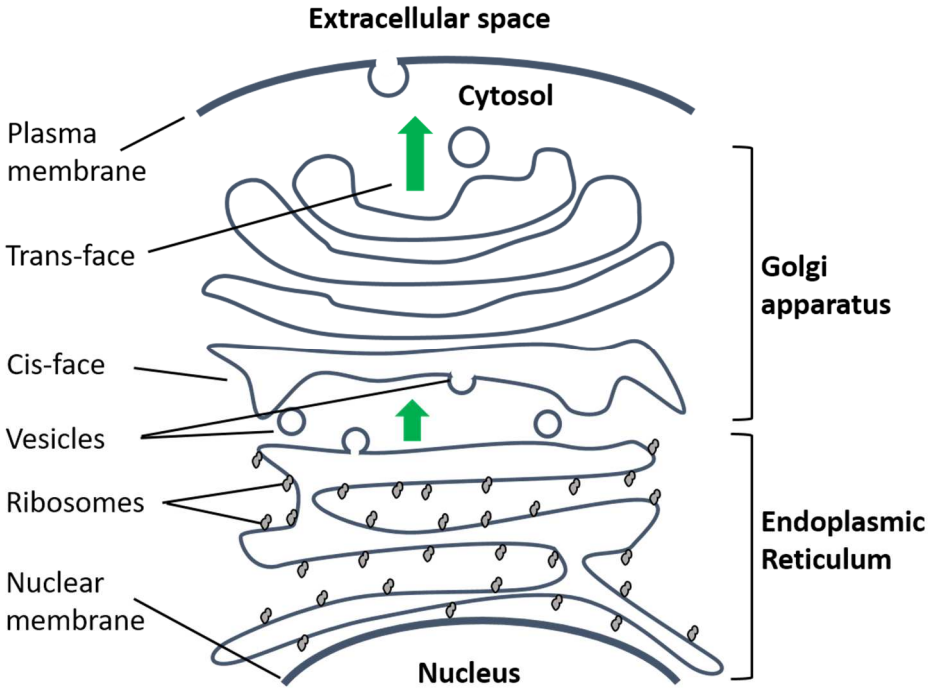

Fig. 15

Schematic representation of the main steps in the trafficking of membrane integral proteins to the PM.

Green arrows represent the forward trafficking steps from the ER to the PM, for a protein properly folded.

When a protein is recognized as stable and properly folded, it undergoes a series of vesicle-mediated and protein-controlled sorting steps before it reaches, via the Golgi apparatus and secretory vesicles, the PM (Fig. 15).

The first sorting step is the exit from the ER. This step is mediated by short sequences named diacidic motifs, embedded in the native protein sequence. The name comes from two or more acidic residues, which are critical in this sorting motive [46, 47]. Once the cargo protein is folded properly, the signal sequence is recognized by Sec24, one of the components of the COPII complex that specifically recognized transmembrane cargo proteins [48]. To allow Sec24 recognition, the cargo protein is recruited in specific ER areas, called ERES (ER Exit Sites), where it is coated in COPII vesicles and transported to the Golgi apparatus [49].

Golgi is the organelle where final secondary modification of cargo proteins occurs (i.e. phosphorylation, glycosylation, and others), and it is responsible of the proteins sorting to their final destination. Golgi apparatus presents a cis-trans orientation: vesicles containing cargo proteins from ER fuse to the cis Golgi, facing the ER; budding vesicles containing the mature cargo protein, directed to the PM or other subcellular compartment leave from the Trans-face of the organelle [50].

Export from the Golgi is mainly regulated by sorting signals contained in the cargo protein sequence, in particular tyrosine-based consensus site (YXXΦ) play an important role in the forward sorting of the protein [44, 47] through the Trans-Golgi Network (TGN).

Both class of signals mentioned above, ER-export and Golgi forward trafficking sequences, have been identified in many membrane protein sequences [47, 46]. They were then successfully inserted in different heterologous proteins to improve their sorting to the PM [11, 51, 52, 53].

Another factor that can serve as targeting signals for PM sorting of membrane proteins are posttranslational covalent modifications such as phosphorylation, prenylation, and lipidation [54, 55]. Among these, we have focused our attention on myristoylation and palmytoilation, because of their striking effect on BLINK1 current (see paragraph 1.4).

N-Myristoyltransferase (NMT) is the enzyme, which is responsible for the addition of the myristic acid during the protein translation, at the ER level. The resolution of its structure has provided new insights into its catalytic mechanism: this enzyme strictly requires a Glycine right after the initial Methionine residue (position +1) and a Serine (or Threonine) residue in position +5 [56]. Glycine is the residue that will be lipidated while Serine establishes Hydrogen bonds with residues inside the NMT catalytic site for stabilizing the interaction between the two proteins [56].

The determination of the enzyme structure has also underlined the relevance of the residues in position +7 to +10, since the amino acids occupying these positions are also entering the enzyme

catalytic site [57, 56]. However, no general rule regarding these residues has been established yet. Palmytoilation is another form of lipidation. In this case, a molecule of palmitic acid is covalently bound to a Cysteine residue located in position +3 in a peptide, which is already modified by the activity of NMT [58, 54]. This type of lipidation has also been reported to serve as a PM sorting signal [59].

Finally, a number of plant and animals channels and pumps (TASK, PMHA, and KAT1) are sorted to the PM following interactions with 14-3-3 proteins [60, 61, 62]. 14-3-3s are a class of adaptor proteins, which are conserved within eukaryotes [63, 64] where they are involved in many different processes, from trafficking to signalling [65, 66]. They establish a direct interaction with their partners by binding to specific aminoacid motifs containing a phosphorylated serine/threonine but also binding to non-phosphorylated ligands has been reported. The binding motifs for 14-3-3 proteins can be found anywhere in the target protein (MODE I and II), or only at the very end of the C-terminus (MODE III). In the latter case, the phosphorylated residue of the motif is the penultimate residue of the protein [67].

It has been demonstrated in several cases that the addition of 14-3-3 binding motifs to a membrane protein with poor membrane expression, could indeed increase its trafficking rate to the PM [11, 54, 52, 68].

1.6 – Improvement of NpHR surface expression

Impaired trafficking to the PM of mammalian expression systems appears to be a common problem of other optogenetic tools for which an *in vivo* applicability had already been assessed. One example is the NpHR-based inhibitory actuators [11].

It has been reported that most of the synthesized NpHR-EYFP protein was retained in the ER when expressed in cultured hippocampal neurons at high levels (Fig. 15) [69, 51]. A reduction in the aggregate formation was observed after reducing the expression level of the protein. This however does not solve the problem because a high expression level of the pump is required for an efficient membrane hyperpolarization [51].

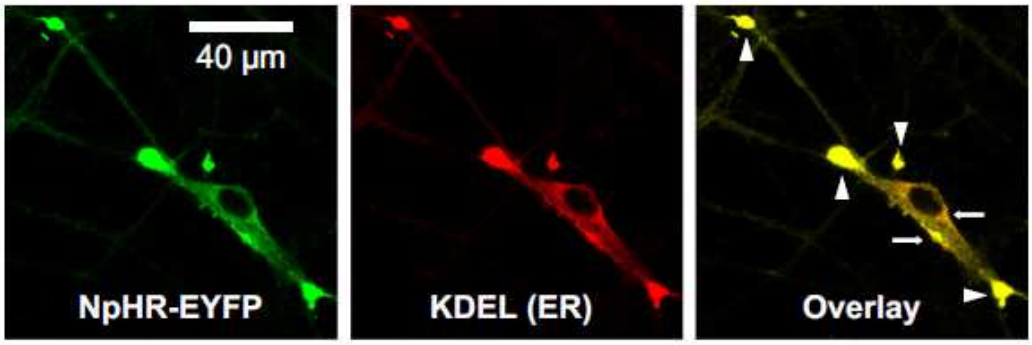

Fig. 16

Immunolocalization of NpHR-EYFP in hippocampal neurons.

In green is shown the detection of EYFP-tagged NpHR (left panel). ER is marked by red fluorescent KDEL marker protein (central panel). The two signals colocalize as shown by the overlay (right panel). From reference [7]

ER retention of membrane proteins is either the result of protein misfolding or due to the presence of retention signals in the protein sequence [45]. Since the NpHR sequence did not contain any known ER-retention signal and since the protein was functional in previous *in vivo* experiments, an ER export sequence has been added to overcome the aggregate formation in ER. This was done because the trafficking rate of many channels and receptors to the PM is strongly augmented by the presence of a C-terminal ER-export sequence [70, 46, 71].

The ER-export sequence chosen to improve the trafficking of NpHR is an established trafficking motive from the mammalian inward rectifier K^+ channel, Kir2.1. It is composed of a stretch of seven residues, ^{374}FCYENEV^{380}, which are located in the C-terminal region of the native channel sequence [70, 47]. It has been reported that the addition of this diacidic motif to the C-terminal region of other channels e.g. a lobster voltage gated K^+ channels, could improve the PM expression of the channel in neurons [52].

Addition of the ER-export sequence to NpHR resulted in the clone named eNpHR (also named eNpHR2.0) [7]. The construct shows an improved intracellular distribution, since the aggregate formation was apparently reduced; the channel could be located in the Golgi network suggesting an improved ER-export (Fig 17A) [7]. Increased surface expression was also validated by detection of photocurrent with bigger amplitude than from the wild type construct (Fig. 16B).

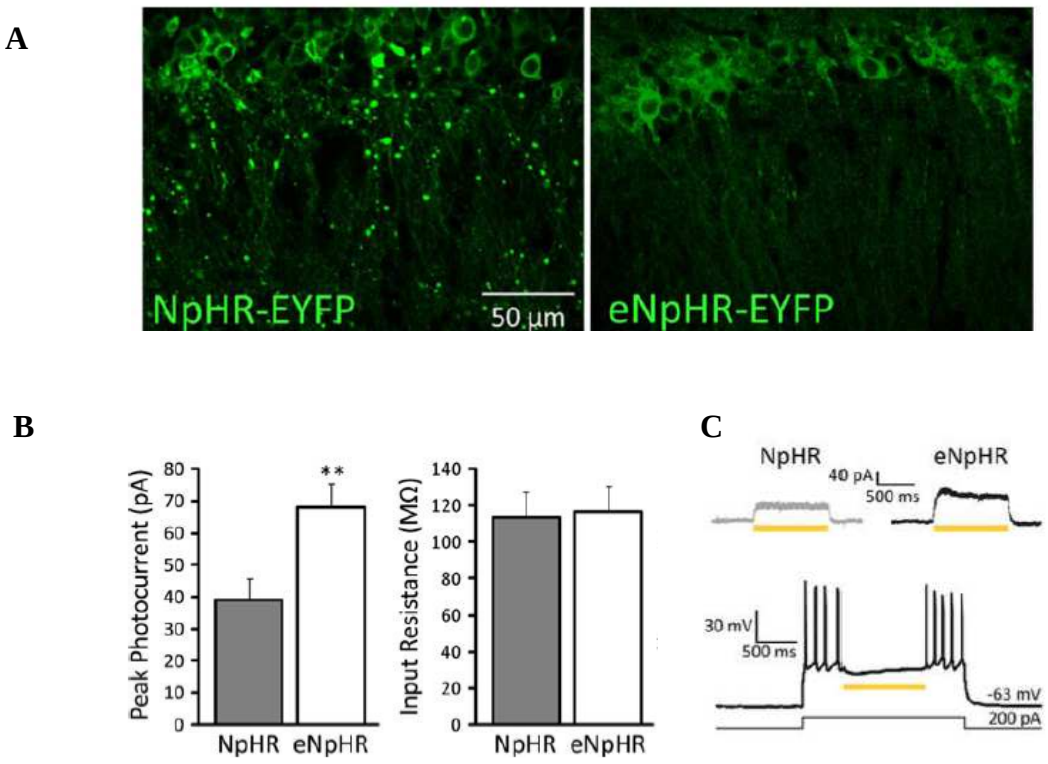

Fig. 17

Comparison between expression of NpHR and eNpHR in the PM of neurons.

A: Fluorescence detection of EYFP tag in neurons expressing the two constructs. B: Graphs showing mean values photocurrent and input resistance measured in neurons expressing NpHR (grey, n=12) or eNpHR (white, n=10). Reported error bar is SEM. C: Current traces recorded after yellow light exposure (top) and light-induced inhibition of firing (bottom).
Modified from reference [7].

However, expression of the construct in hippocampal neurons still suffered of poor membrane localization. To further improve the sorting of the pump another targeting sequence from Kir2.1 channel has been added [11]. In the C-terminal region of the mammalian channel Kir2.1, a tyrosine-dependent (YXXΦ) consensus motif for Adaptin binding has been identified [68]. The sequence core is composed of four residues, ^{242}YIPL^{245}, where the Tyrosine residues is followed by two random amino acids (XX) and a third residue with a bulky hydrophobic side chain (Φ). This is typical for canonical tyrosine-based trafficking signals [53]. However, this YXXΦ consensus also requires

additional specific residues in flanking regions, which altogether defines a 20 residue long targeting signal (residues from 233 to 252 in Kir2.1 channel).

Such a sequence has been added to eNpHR obtaining eNpHR3.0; the new chimera was showing an improved trafficking rate to the neuronal PM and increased labelling of neuronal processes (Fig. 18A from ref. [11]). In addition, in this case the improved PM localization was confirmed by detection of larger photocurrents and consequently stronger hyperpolarization in yellow light compared to the parental construct recorded in the same conditions (Fig. 18B). The improved construct generated a stronger hyperpolarization (Fig 18C) [11]. Adding sorting signals seems to be a valid strategy for improving surface expression of synthetic membrane protein. The aforementioned combination of the two trafficking signals has also been demonstrated to improve surface expression of Bacteriorhodopsin (BR) in hippocampal neurons [11]. This implies that the addition of trafficking sequences can indeed improve the PM localization of optogenetics actuators expressed in mammalian cells including neurons.

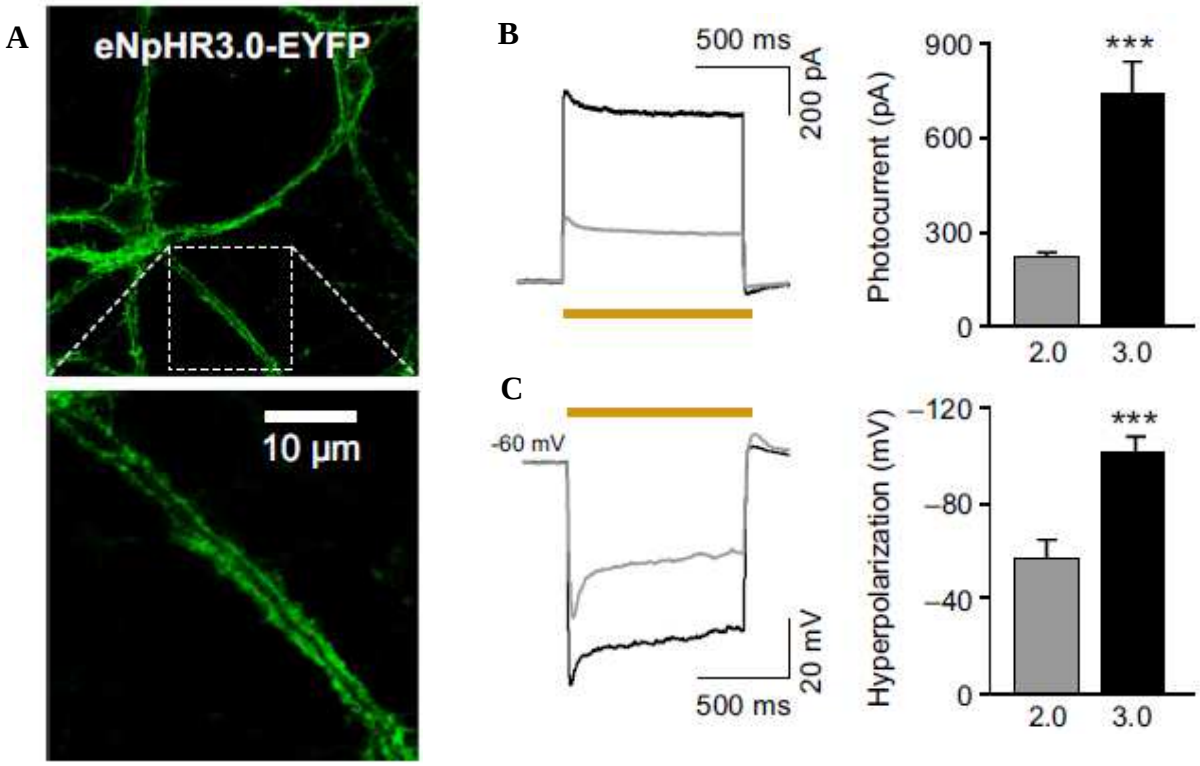

Fig. 18

eNpHR3.0 generates higher photocurrents in neurons than parental eNpHR

A: EYFP tag detection in neurons expressing eNpHR3.0.

B and C: measured photocurrents and membrane hyperpolarization values in neurones expressing eNpHR (grey) or eNpHR3.0 (black). Modified from reference [11]

2 - AIM OF THE PROJECT

The aim of this work was to improve PM localization of the light-gated potassium channel BLINK1. BLINK1 is a newly engineered light-gated K^+ channel with desirable features for optogenetics, such as large single channel conductance and high K^+ selectivity. Moreover, preliminary *in vivo* test in Zebrafish larvae have demonstrated the effectiveness of this optogenetic tool [31]. However, the channel showed quite low expression levels in mammalian cell line HEK293T, as well as in cultivated mammalian neurons. Since the goal would be to use BLINK1 in *in vivo* behavioral experiments in mice, in this study we have tried different strategies to improve PM expression of the channel in mammalian cells. The aim was not to understand the trafficking details of the BLINK1 channel, but to screen, on the basis of literature reports, for modifications, which increased surface expression and measurable currents in animal cells, including neurons.

First, we examined the linker region connecting the LOV domain to the channel, as a potential source of misfolding and consequent intracellular retention of the channel. Then, following the hypothesis that the engineered channel was prone to misfolding, we have introduced in BLINK1 structural elements belonging to the LOV domain, in order to promote a more stable conformation and possibly to increase PM expression level of the chimeric protein. Finally, we added different trafficking signals to promote forward transport of BLINK1 from the ER, through the Golgi and to the PM.

The addition of a 14-3-3 mode III consensus site, from the plant channel KAT1, moderately improved PM expression of the channel without impacting on its properties (light-regulation in particular), therefore this channel, renamed BLINK2, was further characterized in vitro and in vivo. BLINK2 showed an initial delay in current activation, in addition to the already slow activation kinetics typical of the parental channel BLINK1. Therefore, we tried to manipulate the photocycle kinetics of the light sensor, the LOV domain, in order to improve the overall kinetics of the channel. To this end, we inserted point mutations reported to tune the photocycle in the isolated LOV protein. BLINK2 Q513D gave the best result and was consequently tested *in vivo* and *ex vivo* in two model systems (zebrafish and mouse respectively) to assess the channel effectiveness. *In vivo* behavioral experiments on mice expressing BLINK2QD in the amygdala are also currently ongoing.

3 – RESULTS

3.1 – Immunolocalization of BLINK1 on the plasma membrane of HEK 293T cells

We previously reported that the expression levels of BLINK1 in HEK293T cells are quite low. The number of cells expressing BLINK1 current over the total number of transfected cells tested by patch clamp is in the order of 8-10% (n= 400 cells tested in n= 34 experiments) [31]. Such a low frequency of expression prevents a more detailed characterization of the biophysical properties of the channel. Moreover, BLINK1 was released to several neuroscience laboratories that reported poor expression of the channel in mammalian neurons (T. Fellin, department of Neuroscience and Brain Technologies at IIT, in Genova; O Yizhar, Department of Neurobiology at Weizmann Institute of Science, Israel; S. Tonegawa, Tonegawa Laboratory, MIT; personal communications)

In order to validate the low surface expression level estimated with electrophysiological measurements, we performed immunohistochemical experiments on BLINK1-transfected HEK 293T cells using 8D6, a monoclonal antibody that specifically recognizes the tetrameric but not the monomeric form of the native Kcv pore [72].

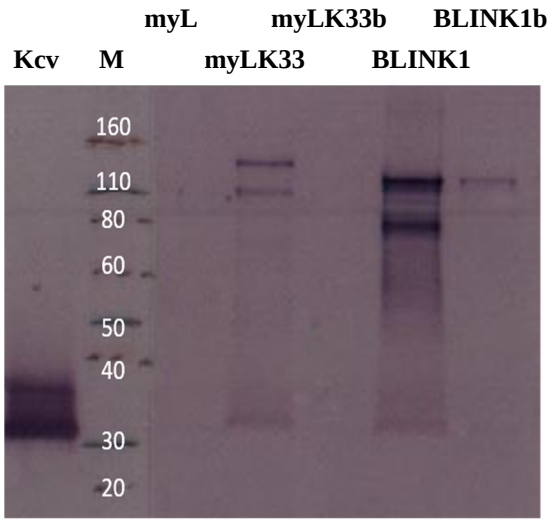

Fig. 19

Western blot on microsomal preparation of yeast cells.

Kcv: positive control, myL: myristoilated LOV domain, negative control; myLK33: non boiled or boiled (LK33b), BLINK1 non boiled or boiled (BLINK1b). MW of the markers (M) is in kDa. The blot was immunodecorated with 8D6, the monoclonal antibody that recognises Kcv tetramer but not the monomeric form.

Recognition of BLINK1 channels by the 8D6 antibody was first assessed by western blot on yeast cells, where we observed high level of channel expression [32]. Yeast cells were transformed with

myLK33 and BLINK1 [32], both channels contain the Kcv region recognized by the antibody linked to LOV domain. myLK33 serves as control; this chimeric protein can still be recognized by the 8D6 antibody. Moreover, yeast cells transformed with Kcv and myLOV were used, as positive and negative controls, respectively. After growing under selective conditions on solid plates for three days, cells were collected and the microsomal fraction was purified and separated on SDS-PAGE. Proteins blotted on PVDF membrane were immunodecorated with the 8D6 antibody following the protocol reported in Part III, paragraph 7. The 8D6 antibody recognizes a band at the expected height of the LK33 tetramer (111kDa) and of BLINK1 (106 kDa) (Fig. 19). Also for the positive control Kcv, a two-band pattern was observed (expected m.w. 42kDa). The specificity of the antibody for the tetrameric conformation of the channels was confirmed by the decrease (BLINK1) or disappearance (myLK33) of the signal after boiling the samples before loading (Fig. 19). This procedure, which is known to disassemble the otherwise rather stable tetrameric form of Kcv into monomers [72], seems to apply to Kcv-derived channels as well. As for the appearance of a double band in all Kcv – based constructs, this might depend on post translational modification of Kcv (for example phosphorylation and/or glycosylation) that have not been investigated further in this work.

In the next step, we used the 8D6 antibody to detect channels at the plasma membrane (PM) of HEK293T cells by immunofluorescence. Figure 20 shows the results from one representative experiment, out of 10 performed on non-permeabilized cells. In each experiment, BLINK1 expression could be detected at the PM level in less than 10% of cells, confirming the low surface expression estimated from patch clamp experiments. The immunostaining was repeated on permeabilized cells to investigate the intracellular localization of the channel (Fig. 21). The percentage of positive cells is similar to that found with the detection of the channel in non-permeabilized cells. Moreover, a closer scrutiny of the antibody signal shows that the fluorescent signal is localized in intracellular compartments. These have no obvious reminiscence to any known subcellular compartment such as ER and/or Golgi (Fig. 21).

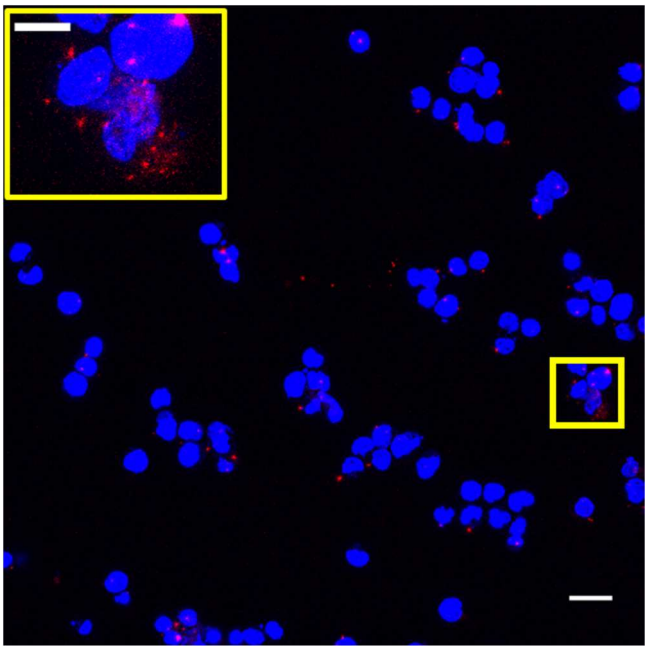

Fig. 20

Immunolocalization of BLINK1 on cell membrane.

Immunolocalization of BLINK1 channel tetramers in living non-permeabilized HEK293T cells. DAPI staining of nuclei is shown in blue, Alexa594 secondary antibody recognizing 8D6 is in red. Bar: 25 µm. Image acquired with 40x lens. Inset: magnification of the cell boxed. Bar: 10 µm

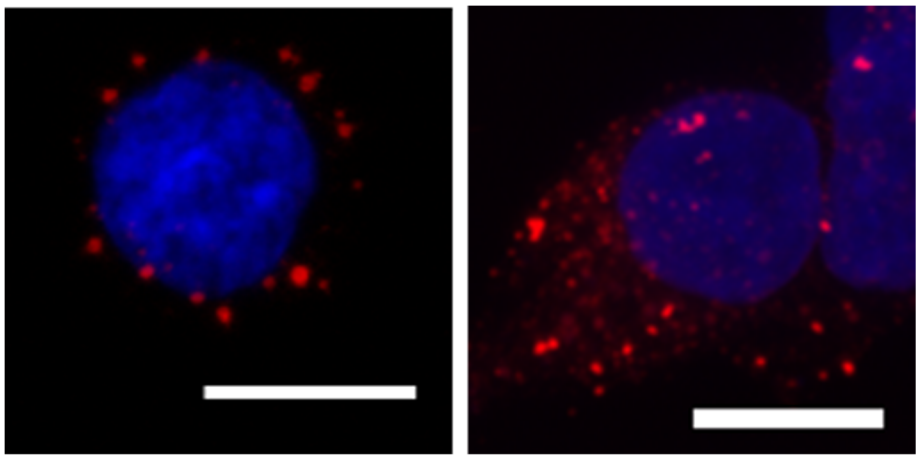

Fig. 21

Immunolocalization of BLINK1 in permeabilized and non-permeabilized cells.

Immunolocalization of BLINK1 channel tetramers in living non permeabilized (left) or in fixed permeabilized (right) HEK293T cells. DAPI staining of nuclei is shown in blue, Alexa594 secondary antibody recognizing 8D6 is in red. Image acquired with 63x oil lens. Bars: 10 µm

3.2 – The linker and its influence on the properties of BLINK –type channels

As previously reported [40], we found differences between the behavior of BLINK1 and another clone with a longer linker, called myLK, when they were expressed in HEK 293T cells.
myLK has been one of the first functional chimera tested in the attempt to generate a light-gated K+ channel. It contains the full-length LOV domain, tethered to PM through the myristoilation and palmytoilation consensus site, fused to the N-terminus of Kcv [31].
In terms of sequence, myLK and BLINK1 differ in a short region composed of nine residues (from N538 to L546, numbered according to native AsPhotI sequence) belonging to Jα helix. This region is present in myLK but not in BLINK1 (Fig. 22).

Fig. 22

Alignment of myLK and BLINK1 aminoacidic sequences.

Residues belonging to Jα helix are boxed in green, residues belonging to Slide helix (Sh) are boxed in grey. The L residue boxed in pink is common to both protein sequences. Residue numbers according to the numbering in original protein sequences. Modified from ref. [31].

When expressed in HEK 293T cells, BLINK1 exhibits a perfect light regulation but a poor presence at the PM [31]. In contrast to this, we found that myLK, which has an unfavorable dark current, has an improved PM localization, since we could record currents in 36% of GFP positive HEK293T cells (n=14).
Since the only difference between the two channels is in the length of the linker region, we speculated that these residues might be important for a proper folding of the chimeric construct. According to this hypothesis, a deletion of these amino acids could promote the formation of a protein that is recognized as toxic by the host cells and therefore degraded. This may then result in the low signal, which was detected when performing immunofluorescence assays on permeabilized cells (Fig. 21). However, as shown by the immunolocalization on non-permeabilized cells (Fig. 20 and 21), a certain amount of BLINK1 channels can still fold properly and reach the PM, where they show a perfect light regulation of the channel conductance.
According to our hypothesis, in myLK both helices can maintain their natural conformations and positions (Fig. 23A). In this way, the Jα domain can be docked against the core of the LOV domain

and Slide-helix is able to interact with the PM. This means that both domains of the channel are properly folded.

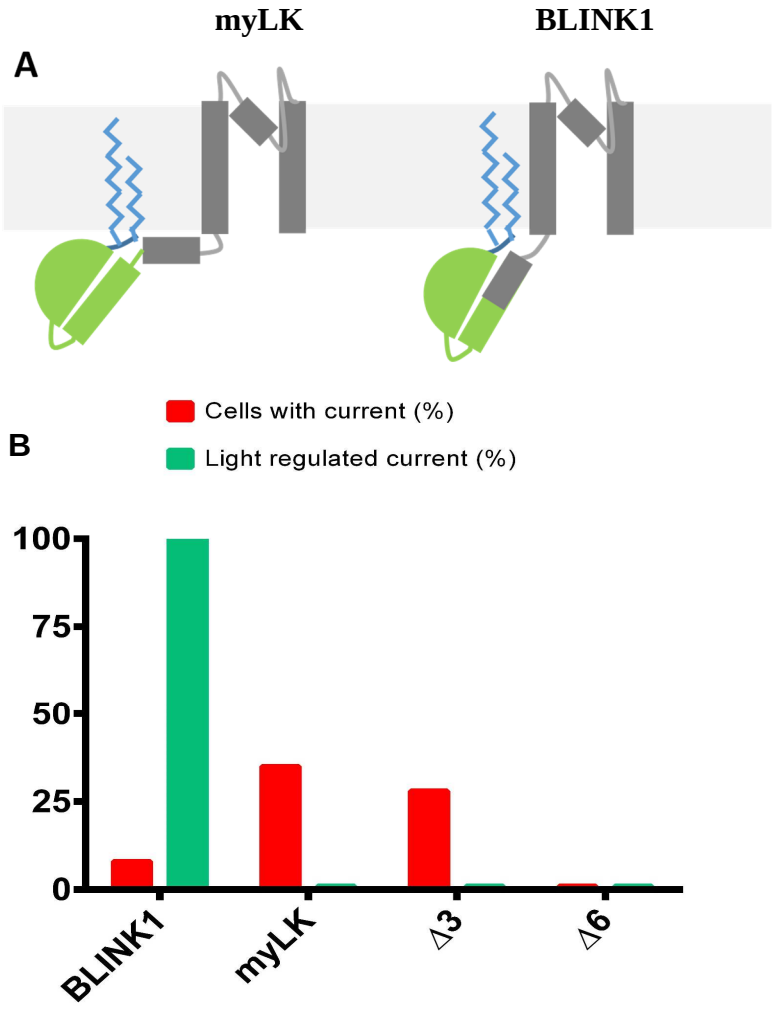

Fig. 23

The connection of LOV and Kcv domains affects channel function

A: Hypothetic configuration of myLK and BLINK1 monomers. LOV domain is represented in green, Kcv is in grey and lipid secondary modifications are represented in blue.

B: PM expression and light regulation of BLINK1 (n=400), myLK (n=14), Δ3 (n=7) and Δ6 (n=9). Surface expression of channels was quantified from positive detection of respective currents in patch clamp experiments.

In BLINK1, on the other hand, six residues belonging to the last helical turns of the Jα have been removed and replaced with the residues belonging to the Slide helix. This is forcing the connection between the two helices. The result of this direct coupling is a presumable a long α helix. It is reasonable to speculate that this helix could create trafficking defects to the channel. The long helix

might be prone to misfolding which may in turn have a negative effect on ER export and/or trafficking to the PM. All this remains as a speculation and cannot be verified here.

To test whether the elongated helix is indeed causing trafficking defects for BLINK1, we introduced deletions in the myLK sequence in order to generate two constructs with different linker regions: the first one has been named Δ3 and only lacks the last three linker residues (K544, E545, L546), the second one, Δ6, lacks the last six residues (E540, A541, A543, K544, E545, L546) of the linker.

When expressed in HEK293T cells, the Δ3 mutant channel shows a slightly decreased PM expression (Δ3= 28% vs myLK= 35%, n=7 and 14). Still it shows the same absence of light-regulated currents as the full-length construct. The three residues that were removed, KEL, are not part of the Jα helix. Hence, presumably the two helices are still properly folded, resulting in a behavior similar to that of full-length myLK (Fig. 23B).

The second mutant that we tested was Δ6, where we removed three residues of Jα helix in addition to KEL residues removed in Δ3. We have not yet been able to record any currents in HEK293T cells transfected with Δ6 channel (n=9). Since similar amounts of cells transfected with the two constructs have been tested (Δ3 n= 7, Δ6 n=9), it seems as if Δ6 has an impaired trafficking rate; it seems to behave in a way more similar to BLINK1 (Fig.23B).

The results of these experiments show that we cannot increase the length of the linker without losing light-regulation of the channel. Therefore, we decided to try to increase trafficking by other means.

3.3 – The N terminal helix of LOV2 domain and its role in controlling channel properties

A paper published in 2015 [73] shows that in Phototropin1 from *Arabidopsis thaliana*, a N-terminal α-helix, called A'α-helix, is involved in the signal transmission mechanism through direct interactions with the Jα-helix of LOV2 domain. The aminoacidic sequence of A'α-helix is 20 residues long, from D391 to R410 in *Avena sativa* (Fig. 24A).

A'α-helix is missing in our chimera, that is based on the LOV2 domain crystal structure (PDB:2V1B) that does not include this helix (Fig. 24B).

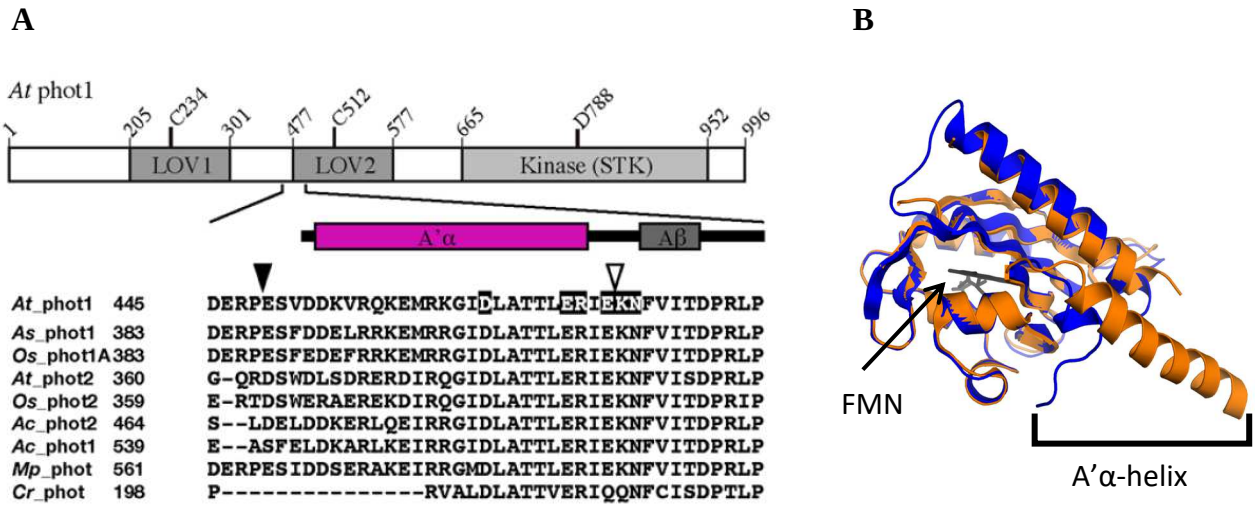

Fig. 24

Structural conservation of A' α helix in Phototropin

A: Sequence alignment of different Phototropins show conserved residues pattern in A' α helix. Modified from reference [73].

B: Superimposition of A. sativa and A. thaliana LOV domain crystal structures with truncated (blue, PDB:2V1B) or complete (orange, PDB:4HHD) A'α helix respectively.

Since A'α-helix is physically interacting with Jα [73, 74], our hypothesis was that its presence could help to stabilize proper folding of the linker helix of our construct that is composed of Jα and Slide helix residues, thus promoting channel stability the PM level. We generated three different constructs named AnBLINK1, nBLINK1 and GID-BLINK1 (Fig. 25). AnBLINK1 has the full-length helix, nBLINK1 has the second half of the helix (starting from residue R398) and GID-BLINK1 has only its last three amino acids.

The three channels tested in patch-clamp experiments, did not show any improvement in the number of cells with light-gated currents, when compared with those expressing BLINK1.

The lack of effect could be due to the fact that in our protein the C-terminal part of the Jα-helix is replaced by Kcv slide helix. Following these results, we decided to maintain the shorter N-terminal helix in the LOV domain and we looked for other strategies to improve channel expression at the PM.

Fig. 25

Alignment of N-terminal sequence of BLINK1 and the three constructs containing the gradually re-introduced A' a helix.

Myristoylation/palmytoilation consensus site is in black, residues belonging to the A'a helix are in orange, other LOV domain residues are in grey. Residues not present in the parental BLINK1 channel are underlined.

3.4 – Anchoring of LOV domain to the PM

A successful step in the rational engineering of BLINK1 has been the addition of a myristoilation/palmytoilation consensus site at the very N-terminus of the LOV domain sequence. The presence of this sequence increased the amplitude of the light-gated current (Fig. 10). At this point is however not clear if this positive effect was a consequence of an increased number of channels in the PM or an effect on the dynamic range of individual channels.
Inspired by the positive effect of anchoring, we further pursued this strategy assuming that this could increase the amount of channels, which are reaching the PM. To this end, we decided to introduce either an N-terminal transmembrane domain or a different myristoilation/palmytoilation consensus site.

3.4.1 – Addition of an N-terminal transmembrane domain

A modified version of BLINK1, called TJSK+, was prepared. This channel had an additional N-terminal transmembrane domain, called TM23, carrying a Red Fluorescent Protein (RFP) at the extracellular side (Fig. 26A). TM23 is a transmembrane domain of the human lysosomal membrane protein 1 (LAMP1). It was reported to provide an efficient anchoring system for proteins in heterologous systems [75]. To verify the presence of the channel in the PM, we used confocal laser scanning microscopy to visualize non-permeabilized cells: an RFP signal could be detected in only 5% of the cells present in each optical field acquired with a 20x lens.
In these cells, the red signal was as expected localized at the level of the plasma membrane (Fig. 26B) but in a rather diffuse manner. The presence of the channel in the membrane was additionally detected on the same cells by means of the monoclonal antibody 8D6. The latter specifically recognises the tetrameric conformation of the Kcv channel (Fig. 26B and C).
The two signals show a very different pattern: the RFP signal is much more abundant than that of the 8D6 antibody. While the red signal is seen throughout the plasma membrane, the 8D6 antibody is only detected in localized spots at the level of the PM.
The difference between the two signals suggests that RFP and the channel tetramers do not share the same distribution in the PM. A reasonable explanation for these unexpected results is that the RFP might have been cleaved from the rest of the channel and sorted by itself to the PM along with the TM domain. An alternative explanation is that the majority of the protein is in the monomeric form. This would be detected by the fluorescent signal of RFP associated to the extracellular side of TM23

domain. The small fraction of tetrameric protein on the other hand would only be labelled by the 8D6 antibody, which only recognizes the channel tetramer.

Since the addition of the TM domain at the N terminus of the channel did not increase the amount of cells displaying BLINK in the PM, we decided to test the effect of an alternative anchoring system.

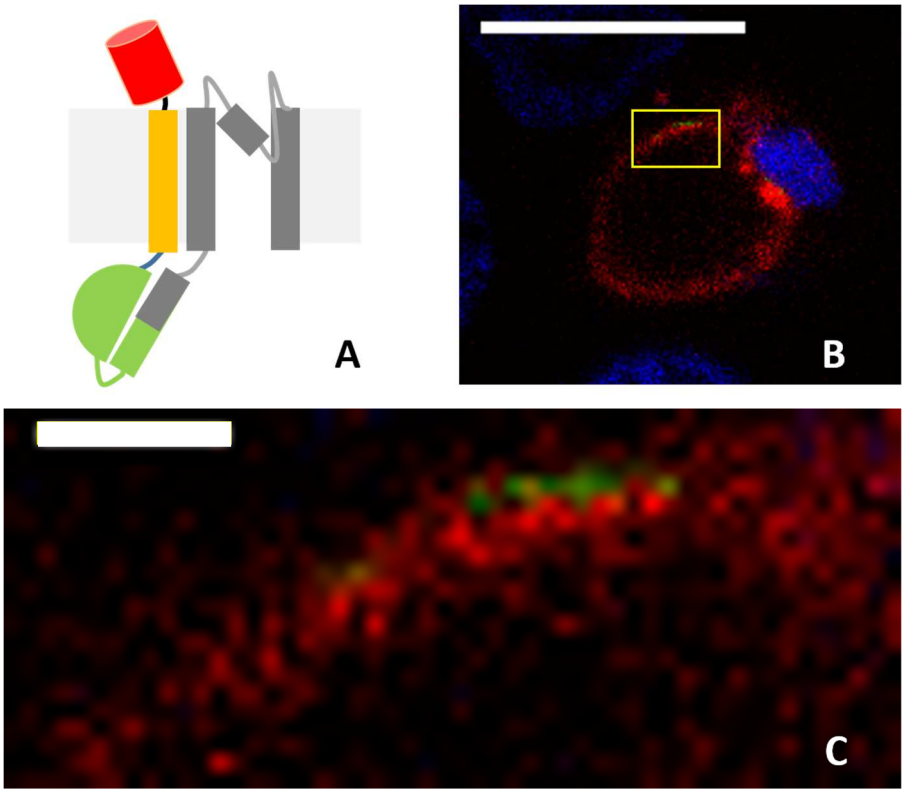

Fig. 26

Detection of TJSK+ construct in plasma membrane of HEK293T cells via labelling of additional transmembrane domain and channel pore.

A: Representation of TJSK+ monomer: RFP is in red, LAMP1 transmembrane domain is in yellow, myristoilation/palmitoylation consensus site is in blue, LOV domain is indicated in green and Kcv is in grey. B: Non permeabilized HEK 293T cells expressing TJSK+. RFP signal is shown in red, secondary Alexa 488 antibody recognizing 8D6 is shown in green. DAPI staining of nuclei is in blue. White bar: 10µm C: magnification of PM region boxed in yellow in B. Bar: 1µm

3.4.2 – Improving the N-terminal myristoilation/palmytoilation sequence in BLINK1

The BLINK1 channel already has at the N terminus a consensus site for myristoilation and palmytoilation for mammalian cells [76, 31]; the crucial sequences are reported in Fig. 27. Hence, the N-terminus of BLINK1 already contains all the key elements necessary for the protein lipidation (see paragraph 1.5). However, since this consensus site is only eight residues long it only represents the minimal sequence, which is required for NMT recognition [56].

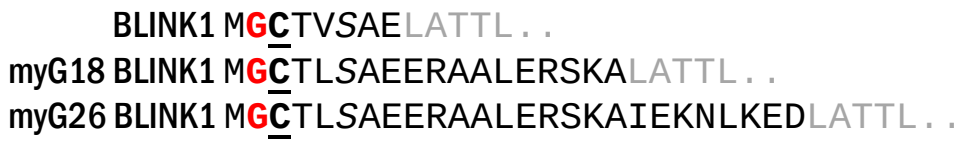

Fig. 27

Comparison between N-terminal sequences of BLINK1 and myG constructs.

Myristoylation and palmytoilation consensus site is in black, Gly and Ser residues important for myristoilation are highlighted in red or italic respectively. Cys residue important for palmitoylation is in bold and underlined. Residues belonging to LOV domain sequence are in grey.

To overcome this limitation, we decided to test a longer consensus sequence displaying all the desired features. Such a site has been described in the human Guanine nucleotide-binding protein G(o) subunit alpha (Gαo codified by the gene GNAO) [54]. In this protein, lipidation is clearly involved in trafficking to the PM, however the exact length of a myristoilation/palmytoilation consensus sequence is not yet known. For this reason, we decided to test two different constructs sharing the N-terminal sequence from Gαo.

The two channels, which have an 18- and a 26-aminoacid long N-terminal consensus sequence, have been named myG18 BLINK1 and myG26 BLINK1 respectively (Fig. 27).

The function of the channels and their localization in the plasma membrane were tested by patch clamp and immunofluorescence respectively. In none of these assays, we were able to detect an improvement. Neither the number of cells in which we could detect light-gated currents nor the fluorescent signal of the protein in the PM was better than that of the parental BLINK1 channel (Fig. 28).

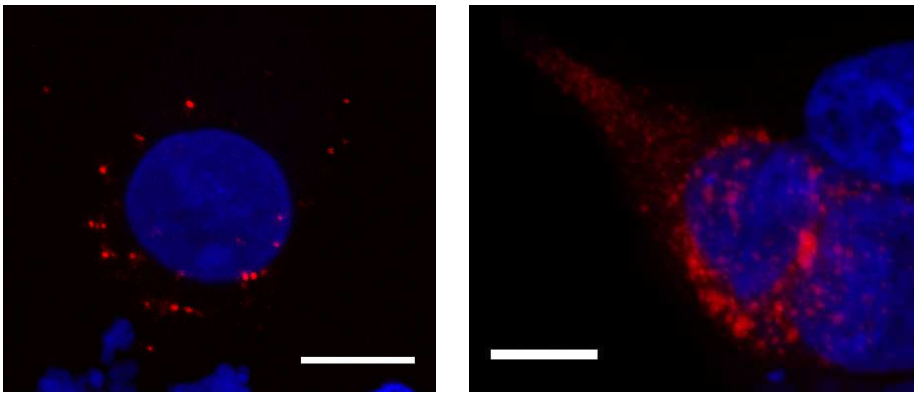

Fig. 28

Microscopic detection of myYG18 BLINK1 in HEK293T cells

Non permeabilized (left) and permeabilized (right) HEK293T cells expressing myG18 BLINK were stained with specific monoclonal antibody 8D6 against the tetrameric Kcv channel. Secondary Alexa 594 antibody recognizing 8D6 is shown in red. DAPI staining of nuclei is in blue. Bars: 10µm

So far, our attempts to improve PM sorting of BLINK1 were only focused on modifications at the N-terminal region of the channel. Our experiments included the introduction of A'α-helix (paragraph 3.3) and addition of an extra TM domain (paragraph 3.4.1). We furthermore modified the existing

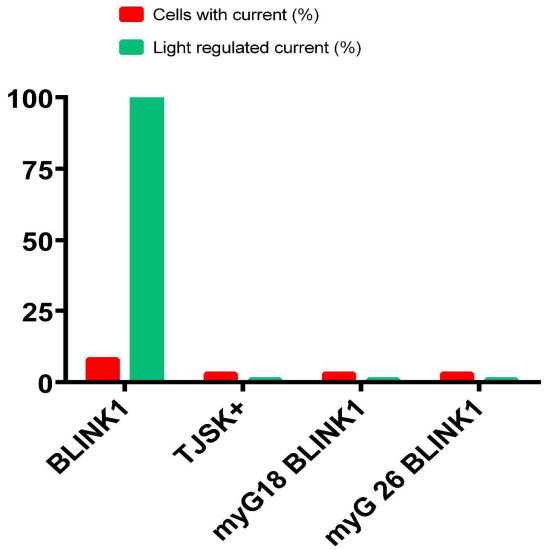

Fig. 29

Modifications at the channel N-terminus did not improve PM localization of BLINK1.

Graph summarizing the results obtained with clones modified to improve PM anchoring (Paragraph 3.4)

myristoylation/palmitoylation sequences to improve sorting. However, so far none of these N-terminal modifications could improve the expression level of the channel at the PM (Fig. 29).
After all these attempts demonstrated to be not successful, we decided to promote the PM targeting of the channel by using specific signal peptides, which we added to the C-terminal region of BLINK1.

3.5 – Addition of C-terminal targeting signals

Other optogenetic tools, derived from algae and/or microorganisms, showed poor trafficking to the PM when first expressed in mammalian cells [11]. This problem was solved by adding ER-export and Golgi forward trafficking sequences taken from mammalian channels and transporters. Therefore, at the beginning of our engineering effort, we decided to follow the same strategy.

3.5.1 – ER-export motifs and Golgi forward trafficking sequences improve surface expression of BLINK

Improved membrane localization of eNpHR3.0 was achieved by fusing to the C-terminal region of the pump two targeting sequences found in the native sequence of the mammalian channel Kir 2.1 [11]. The two motifs can promote ER export (FCYENEV, residues 374-380 in mKir2.1 sequence) (ER) or trafficking from Golgi to PM (KSRITSEGEYIPLDQIDINV, residues 233-252) (TS) [68]. We decided to follow a similar strategy and we generated six different chimeras containing the two sequences differently spaced.
The first three were designed according to reference [11], simply adding the trafficking signals to the C-terminus of the channel. In our case, the C-terminus of Kcv is not cytosolic, as the channel ends with the second transmembrane domain.
The C-terminal sequences of the three channels, named BLINK-ER, BLINK-TS and BLINK-EYFP, are shown in Figure 30.

BLINK-EYFP ...V L T L A A A K S R I T S E G E Y I P L D Q I D I N V::*EYFP*::F C Y E N E V-COOH
BLINK-TS ...V L T L K S R I T S E G E Y I P L D Q I D I N V-COOH
BLINK-ER ...V L T L F C Y E N E V-COOH

Fig. 30
Alignment of C-terminal sequences of BLINK1 clones with additional ER and TS sequences. *Transmembrane domain of BLINK1 is in grey (^{91}VLTL^{94}). TS sequence is in pink and ER sequence is in blue.*

BLINK-ER and BLINK-TS have the diacidic ER sequence and TS sequence respectively, while BLINK-EYFP has both sequences and a EYFP inserted in-between. When tested in patch-clamp experiments none of the three constructs showed an improved PM trafficking rate compared to BLINK1.

The three other chimeras, named BKir, BKir2 and BKir3, were designed by adding at the C terminus of BLINK1 the full-length C-terminal sequence or portions of the Kir 2.1 channel. BKir was obtained by fusing the full-length C-terminal region of Kir2.1 (residues 180-428 of the original mKir2.1 sequence); BKir2 and BKir3 were made by fusing two shorter regions, residues 233-428 and 233-380 respectively (Figure 31).

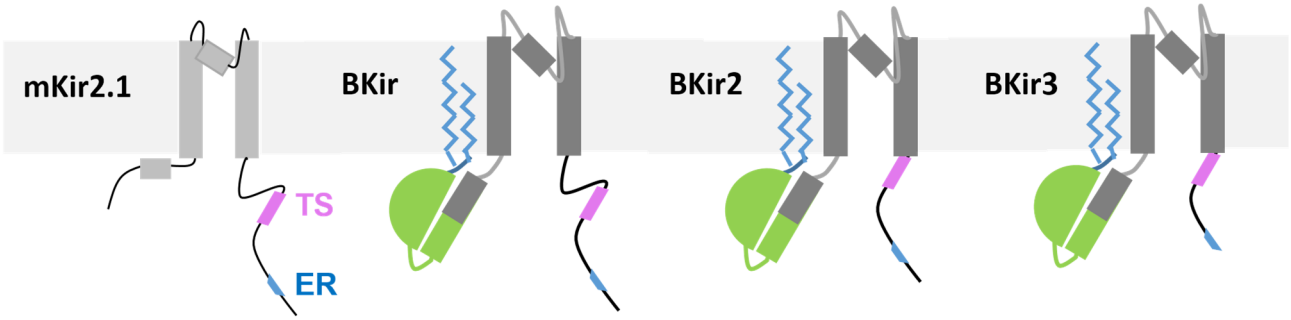

Fig. 31

Schematic representation of monomeric structure of mKir2.1 and BKir chimeras.

The elements of the channel protein are the same as in Fig. 24A. ER and TS represent the diacidic ER export motive and the Golgi forward trafficking sequence respectively.

Notably, with these constructs we measured for the first time an improved trafficking rate of BLINK1 to the PM. BKir was present at the PM in 37% of tested cells (n=30). In 64% of these cells, the current was perfectly light-regulated (Fig. 32), while in the remaining 46% the current was already present in the dark (Fig. 33A).

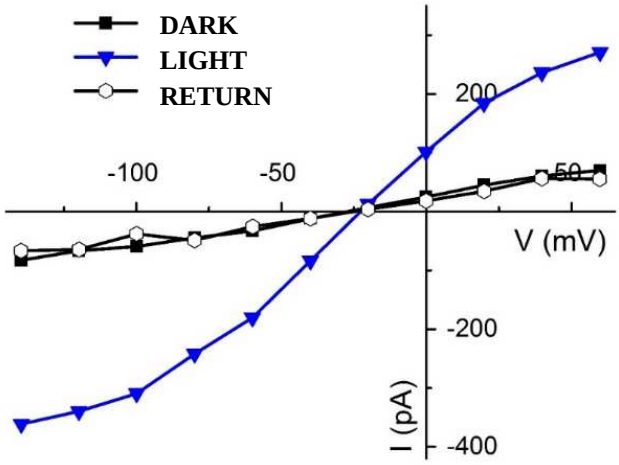

Figure 32

BKir currents detected in HEK93T cells

Steady state IV curves recorded in dark or light in a HEK293T cell expressing BKir. In this case, the channel shows a proper sensitivity to blue light

In order to test whether the current measured in the dark was due to non-regulated BLINK1 channels, we blocked this current with Ba^{2+} (Fig. 33B), an inhibitor of the BLINK1 channels. The difference current, e.g. the portion of the current, which was sensitive to Ba2+ is shown in Figure 33C and D. The difference current has the typical features of the BLINK1 conductance with a saturation at negative voltages. The results of these experiments confirm that the dark current, which is measured in BKir expressing cells, is carried by the synthetic channel protein.

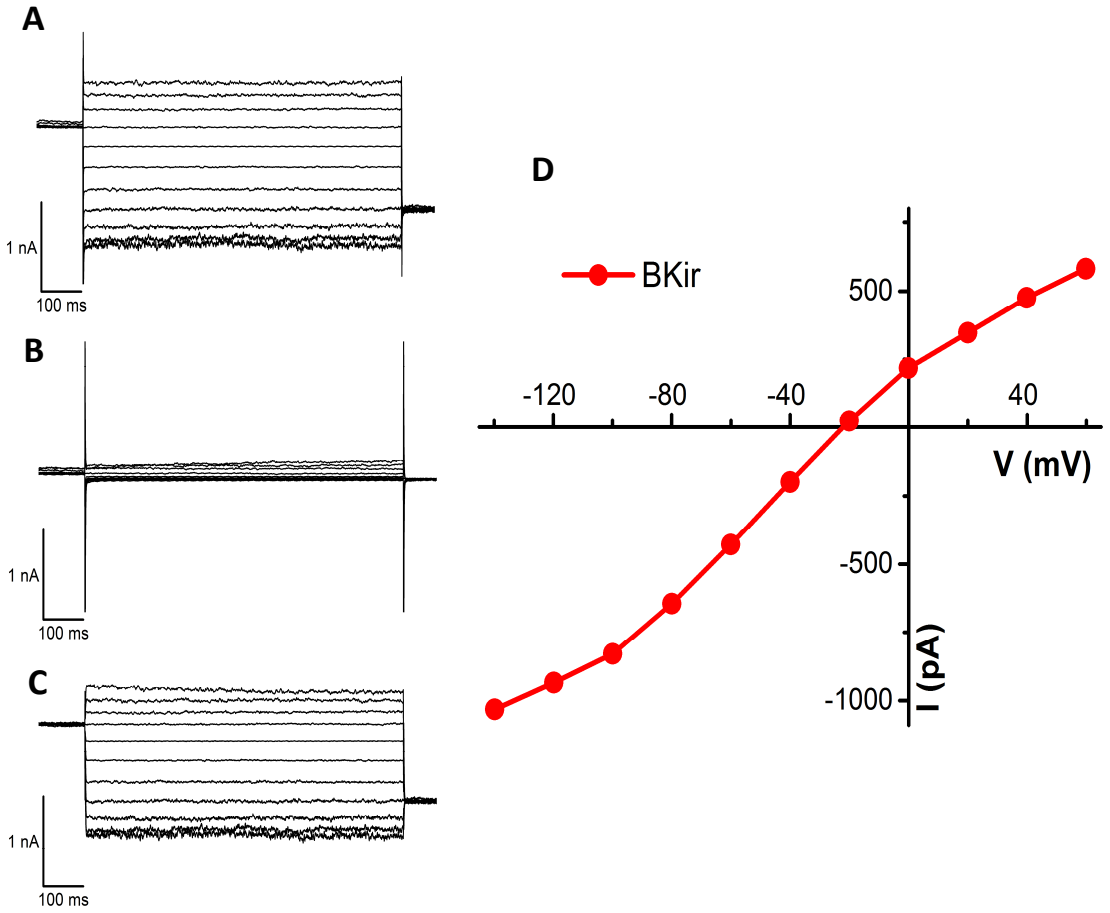

Fig. 33

The construct BKir shows dark current

A and B: currents recorded in whole cell configuration from the same cell expressing BKir, in the dark, before (A) and after (B) the addition of 5mM $BaCl_2$.

C: Barium sensitive current obtained by subtracting B from A.

D: Steady state I/V curves from currents in C. IV difference curve resembles IV relation of BLINK1 (Fig.13) and light-regulated BKir (Fig. 32)

We also measured a BLINK1 current in 27% of cells transfected with BKir2 (n=11) and in 46% of cells transfected with BKir3 (n=13). However, in the case of BKir2 the currents were completely light-insensitive, meaning that in 100% of the cells in which we found the current, the channel was already open in the dark; this current could not be further increased in the light. Also in this case we could assign the dark current to BLINK1 by analysing the kinetics and the I/V curve as in Fig. 32 of the Ba^{2+} sensitive current.

In the case of BKir3 expressing cells, we could finally find a light-induced current in 30% of the cells, which revealed a BLINK1-like conductance. In the remaining 70% of the cases, the current was already present in the dark.

In conclusion, all the chimeras, which were designed by fusing parts or the entire C-terminus of mKir2.1 to the C-terminus of BLINK1, resulted in a large improvement in the PM expression of the synthetic channel (Fig. 34A). However, the new channel variants had the drawback that they were not is in all cases not perfectly regulated (Fig. 34B). A large proportion of the cells or in one case all of them, showed a dark-current. It seems as if there is a negative correlation between the number of channels at the PM and their regulation by light. The causal relation between these two features remains unexplained. Since the present work was designed as a screening of sorting motives, this aspect was not further investigated.

Since the aforementioned modifications corrupted the light-regulation of the channels we went on to test the effect of other trafficking motifs.

A

SOURCE	SEQUENCE ADDED TO BLINK1 C-TERMINUS	CLONE NAME
Kir 2.1/ NpHR3.0	MEMBRANE TRAFFICKING + ER-EXPORT (aa 233-252 of Kir2.1+ EYFP + aa 374-380 of of Kir2.1)	BLINK-YFP
Kir 2.1	GOLGI EXPORT + ER-EXPORT (aa 180-428)	BKir
	GOLGI EXPORT + ER-EXPORT (aa 233-428)	BKir2
	GOLGI EXPORT + ER-EXPORT (aa 233-380)	BKir3
	ER-EXPORT (aa 374-380)	BLINK-ER
	GOLGI EXPORT (aa 233-252)	BLINK-TS

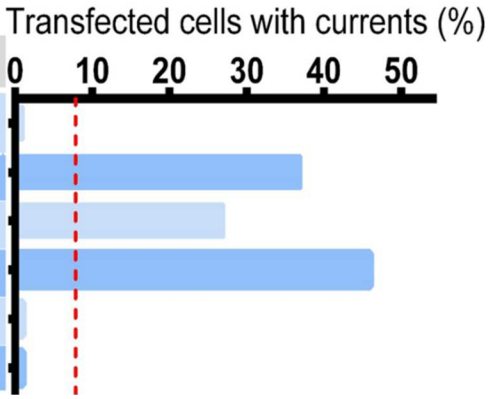

B

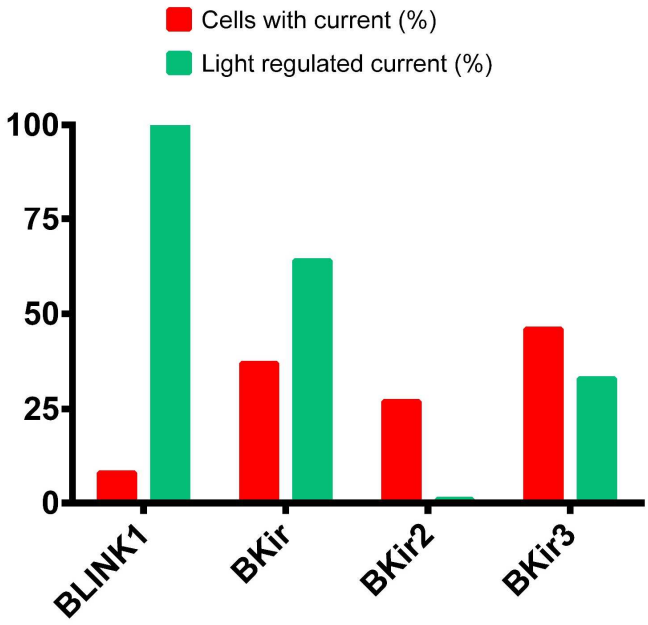

Fig. 34

The BKir mutants enhance surface expression of BLINK1

A: Table summarizing the results obtained with all the chimeras in which ER and TS sequences from other channels were included into BLINK1. Surface expression of BLINK1 is given for reference by red dotted line.

B: Graph summarizing the results obtained with BKir clones in terms of PM expression and light-regulation

3.5.2 – Addition of 14-3-3 binding signals

The surface expression of many membrane proteins (such as TASK and KAT1 channels or PMHA2 proton pump) is regulated by their interaction with 14-3-3 proteins [60, 61, 77].
Since the addition of trafficking sequences to the C-terminal region of the channel had proved to be a successful strategy to promote PM expression of BLINK (see paragraph 3.5.1 and Fig. 33B), we decided to add a C-terminal 14-3-3 binding signals to our channel. The effect of this modification was then tested in HEK293T cells.

```
mTASK1     LVVLRFMTMNAEDEKRDAEHRALLTHNGQAVGLGGLSCLSGSLGDGVRPRDPVTCAAAAG
mTASK3     LVVLRFLTMNTDEELLEGEVAEILAGNPRRVSVRAPQRR---------KR----------
           ******:***:::*  :.*   :*: * : *.: . .           *
mTASK1     GVGVGVGGSGFRNVYAEVLHFQSMCSCLWYKSREKLQ---------YSIPMIIPRDLSTS
mTASK3     -----HHAMYFLRKYGRTLCYLCFPGTNWGKDDDDDDDDDVVDNVVVTAPISAPAPAPAP
                  .  * . *...* : .: .  * *. :. :          : *:  *    :
mTASK1     DTCVEHSHSSPGGGGRYSDTPSHPCLC-----------SGTQRSAISSVSTGLHSLAAFR
mTASK3     AP--APAAVAAGATIRSVRATVHTVSCRVEEIPPDVLRNTYFRSVFGAIPPGMHTCGDHR
                 :  : *.  *   :  *   *           .   **.:.::  *:*: . .*
mTASK1     GLMKRRSSV
mTASK3     LHLRRKSI-
             ::*:*
```

Fig. 35

Alignment of C-termini from mTASK1 and mTASK3.

Sequence alignment of TASK channels starting with residue 241. Residue R245 is highlighted in red and represents the first residue of the sequence fused to BLINK1 for creating BT1D and BT3D chimeras. Green highlights the Serine residue that requires phosphorylation for recognition by 14-3-3 protein. In both chimeras, the residue is replaced by an Aspartate.

We first tested the 14-3-3 binding peptide from the mammalian K^+ channel TASK. Therefore, we designed two different chimeras, BT1D and BT3D, which were obtained by fusing the cytosolic C-terminal region of mTASK1 (residues 245-394 in original sequence) or mTASK3 channels (residues 245-402), respectively to the C-terminus of BLINK1. Both added domains contain the mode III binding motif $XXXXpSX_{\text{-COOH}}$ at the very C-terminus (see Fig. 35). The highlighted pS is the Serine residue, which needs to be phosphorylated for the binding of 14-3-3. X in the sequence can be any amino acid and $X_{\text{-COOH}}$ is the last protein residue. In both cases, the residue that should be phosphorylated (S393 in mTASK1 and S401 in mTASK3) was replaced by an Aspartate. This mutation allows the negative charge in Aspartate lateral chain to mimic the presence of the negative charge of the phosphate group in the phosphoserine residue.

We tested both chimeras in HEK293 cells and we obtained different results. While we did not detect the current (n= 12 cells) with BT3D, we could measure BLINK1 K^+ currents in 38% of the cells expressing the BTD1 construct (n=8) (Fig. 36). But like in the case of chimeras with Kir (Fig. 32) also the addition of the domains from the TASK channels abolished the light regulation of the synthetic channel, in that only 33% of the cells showed a proper light-induced current increase (Fig. 36B).

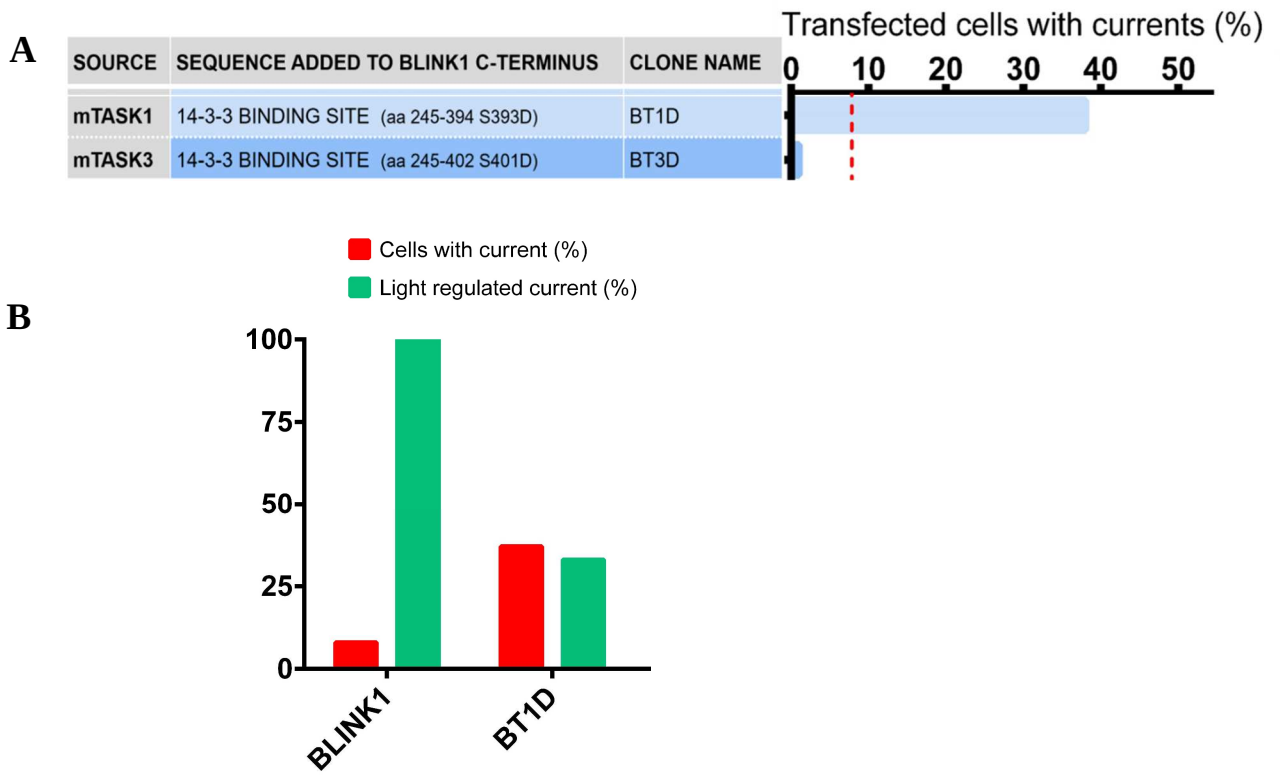

Fig. 36

Different binding site for 14-3-3 proteins in BLINK2 affect channel sorting

A: Table summarizes the results obtained with chimeras comprising binding sites for 14-3-3 proteins from TASK channels. Surface expression of BLINK1 is represented with the red dotted line. B: Graph summarizing the results obtained with BKir clones in terms of PM expression and light-regulation

We did not expect such a different behaviour of the two chimeras, since the sequences of the two channels are overall conserved. Still some of the larger differences between the two channels are located in the C-terminal region (Fig 34). In particular, mTASK3 shows a stretch of Aspartate residues (308-316) and repeated sequences (329-341) that suggest interaction sites with unknown partners. We speculate that in the absence of those interacting partners, the 14-3-3 protein loses its ability to regulate trafficking of the channel. For this reason, we may not see any improvement in the trafficking of the chimera.

In a complementary project, a mode III 14-3-3 motif on the C-terminus of the plant channel KAT1 was discovered in the laboratory (A. Saponaro, personal communication). We decided to test this motive, ^{673}YFSpSN^{677} (numeration follows the sequence of KAT1), on BLINK1 because it can also be recognized by the endogenous 14-3-3 proteins of HEK293T cells.

Therefore, we fused the last 170 amino acids of the C-terminal region of KAT1 (from residue 506 to 677 in original sequence) to BLINK1 generating two different chimeras named BK6S and BK6D (Fig. 37A). S and D indicate here the presence of the original Serine or of an Aspartate acting as a phosphomimetic. We decided to generate both constructs because we knew from complementary project data that the wild type sequence of KAT1 is recognized by endogenous kinases and 14-3-3 isoforms of HEK293T cells. The phosphomimetic mutation was inserted to test if, in case of positive results, the constitutive presence of a phosphorylated residue could enhance the trafficking rate of the synthetic channel to the PM even further.

In the following experiments, we measured an improved surface expression of the channel with both constructs: 22% and 26% of cells transfected with BK6S (n=8) and BK6D (n=147) respectively, displayed potassium currents attributable to a BLINK channel. In the case of the BK6S construct the channel has again lost its light-regulation; it was already open in the dark (Fig. 37B).

Surprisingly, all BK6D expressing cells showed the desired features. The K+ current was, apart from the endogenous channels of HEK293T cells, absent in the dark. Upon stimulation with blue light, the current was activated (Fig. 37C). This type of light regulated BLINK type currents were recorded in 26% of 147 cells tested in 20 experiments. Given the positive result, the new version has been renamed BLINK2.

The different behaviour of the two clones suggests that 14-3-3 proteins influence both, channel trafficking and light-regulation in BLINK2. This observation finds a parallel in the effect of 14-3-3 binding to KAT1. Also, this interaction promotes, in HEK293T cells, PM trafficking and channel function. We can therefore assume that the 14-3-3-binding motive from a plant is recognised by 14-3-3 proteins from animals and that this interaction is in the present case responsible for an augmented surface expression of BLINK2. The different effect of the BK6S and BK6D motive indicates that the phosphorylation state of the motif is crucial for light-regulation: only a stable complex with 14-3-3, which is provided by the phosphomimetic mutation of the serine, results in a perfectly regulated channel.

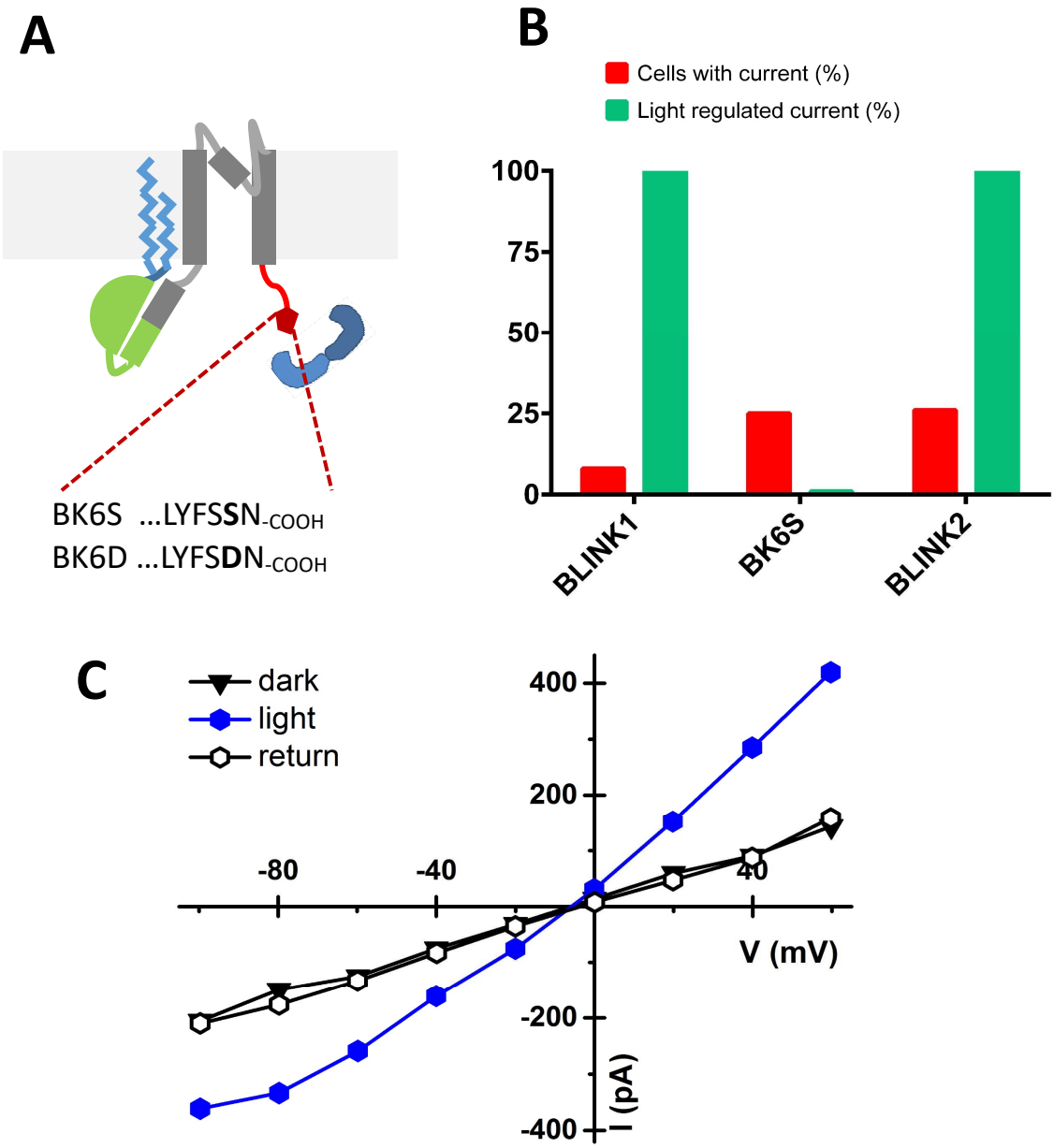

Fig. 37

Properties of BK6S and BK6D mutants.

A: Cartoon representing BK6S and BK6D monomers. They only differ in the amino acid in position 676 with a Serine in BK6S and an Aspartate in BK6D (both in bold). Myristoilation/palmytoilation consensus site and lipids are in blue, LOV domain is in green, Kcv pore is in grey, C-terminal 14-3-3 binding peptide is in red. A 14-3-3 dimer is represented in dark blue. B: Graph summarizing the results obtained with clones modified with KAT1 C-terminus, in terms of PM expression and light-regulation C: Steady state IV curves of HEK293T cells expressing BK6D – BLINK2. Data recorded in dark (black triangle), during light (blue hexagon) and after the return to dark (empty hexagon).

This difference in the behaviour of the two channels could be due to the fact that not only endogenous kinases can recognize and phosphorylate the serine in the KAT1 motif. By the same logic, also the endogenous phosphatases will recognize the motive and remove the modification. This scenario would explain why only the aspartate substitution with its phosphomimetic character is able to recruit 14-3-3 proteins in HEK293T cells to make a permanent and stable complex with the channel.

At the same time, the complex with the 14-3-3 protein cannot be the only requirement for light-regulation of the channel. This is apparent from the observation that the channel loses its regulation in constructs with the BTD1 and BTD3 motives. Both are carrying a phosphomimetic mutation in the serine and should generate stable complexes with 14-3-3 proteins.

Collectively the data suggest that the C terminal portion of KAT1, which was added to BLINK1, carries other domains besides the 14-3-3 motif that we are not aware of. These additional motifs may, in combination with the phosphomimetic motif, prevent a loss of regulation of the channel.

3.5.3 – Combination of 14-3-3 binding signals and ER-export motifs

In order to test if we could increase the percentage of cells expressing the channel, which is still relatively low even in BLINK2, we combined the 14-3-3 binding signal with an ER export motif. We know that the ER sequence from Kir2.1 improves PM trafficking but impairs at the same time the light regulation of the channel. To avoid this negative effect we decided to use a KAT1 native ER export sequence [46], which was not originally included in the BLINK2 clone. KAT1 bears a diacidic motif, DIDAE, in its C-terminus (residues in position 392-396). This domain augments the surface expression of KAT1 and other channels [46, 68] by interacting with a receptor protein of COPII vesicles. We inserted the DIDAE sequence in two different positions in the C-terminus of BLINK2 creating the clones BLINK2.1 and BLINK2.2 (Fig. 38).

```
BLINK2.2    MGCTVSAELATTLERIEKNFVITDPRLPDNPIIFASDSFLQLTEYSREEILGRNCRFLQG
BLINK2      MGCTVSAELATTLERIEKNFVITDPRLPDNPIIFASDSFLQLTEYSREEILGRNCRFLQG
BLINK2.1    MGCTVSAELATTLERIEKNFVITDPRLPDNPIIFASDSFLQLTEYSREEILGRNCRFLQG
            ************************************************************

BLINK2.2    PETDRATVRKIRDAIDNQTEVTVQLINYTKSGKKFWNLFHLQPMRDQKGDVQYFIGVQLD
BLINK2      PETDRATVRKIRDAIDNQTEVTVQLINYTKSGKKFWNLFHLQPMRDQKGDVQYFIGVQLD
BLINK2.1    PETDRATVRKIRDAIDNQTEVTVQLINYTKSGKKFWNLFHLQPMRDQKGDVQYFIGVQLD
            ************************************************************

BLINK2.2    GTEHVRDAAEREGVMLIKKTAEVFSKFLTRTEPFMIHLFILAMFVMIYKFFPGGFENNFS
BLINK2      GTEHVRDAAEREGVMLIKKTAEVFSKFLTRTEPFMIHLFILAMFVMIYKFFPGGFENNFS
BLINK2.1    GTEHVRDAAEREGVMLIKKTAEVFSKFLTRTEPFMIHLFILAMFVMIYKFFPGGFENNFS
            ************************************************************

BLINK2.2    VANPDKKASWIDCIYFGVTTHSTVGFGDILPKTTGAKLCTIAHIVTVFFIVLTLDDSNTS
BLINK2      VANPDKKASWIDCIYFGVTTHSTVGFGDILPKTTGAKLCTIAHIVTVFFIVLTLDDSNTS
BLINK2.1    VANPDKKASWIDCIYFGVTTHSTVGFGDILPKTTGAKLCTIAHIVTVFFIVLTLDDSNTS
            ************************************************************

BLINK2.2    GHENRDFKSMGWDIDAESRKDGYGLDVTNPTSDTALMDAIHKEDTEMVKKILKEQKIERA
BLINK2      GHENRDFKSMGWEEWRDSRKDGYGLDVTNPTSDTALMDAIHKEDTEMVKKILKEQKIERA
BLINK2.1    GHENRDFKSMGWEEWRDSRKDGYGLDVTNPTSDTADIDAEHKEDTEMVKKILKEQKIERA
            ************:   :****************** :** ********************

BLINK2.2    KVERSSSETAGRSYANDSSKKDPYCSSSNQIIKPCKREEKRVTIHMMSESKNGKLILLPS
BLINK2      KVERSSSETAGRSYANDSSKKDPYCSSSNQIIKPCKREEKRVTIHMMSESKNGKLILLPS
BLINK2.1    KVERSSSETAGRSYANDSSKKDPYCSSSNQIIKPCKREEKRVTIHMMSESKNGKLILLPS
            ************************************************************

BLINK2.2    SIEELLRLASEKFGGCNFTKITNADNAEIDDLDVIWDGDHLYFSDN
BLINK2      SIEELLRLASEKFGGCNFTKITNADNAEIDDLDVIWDGDHLYFSDN
BLINK2.1    SIEELLRLASEKFGGCNFTKITNADNAEIDDLDVIWDGDHLYFSDN
            ***********************************************
```

Fig. 38

Alignment of BLINK2, BLINK2.1 and BLINK2.2 amino acidic sequences.

Sequence alignment of different BLINK2 variants. The second transmembrane domain of Kcv is highlighted in blue, DIDAE ER-export sequence is in green, phosphomimetic mutation at the 14-3-3 binding site is in red.

In BLINK2.1, the DIDAE motif was inserted in position 547 (numbering follows KAT1 original sequence) 130 residue upstream of the 14-3-3 binding motif (Fig. 38). In this case, the channel displayed an improved presence at the PM. In 39% of the cells transfected with BLINK2.1 (n= 28) we could record BLINK type K^+ currents. But also in this case the improvement of sorting was connected to a loss of light regulation, since 70% of the cells were already showing a K^+ current in the dark (Fig. 39).

The next clone, BLINK2.2, was designed by moving the ER-export motif further upstream in position 524. This should reduce potential steric hindrance between the trafficking proteins recruited by DIDAE and the 14-3-3 proteins recruited by the C-terminal motif (Fig. 38). BLINK 2.2 also exhibited an increased percentage of cells with current (33%, n=12). The improved surface expression over the parental BLINK2 channel, however, was again paid, like in the twin construct BLINK2.1, with a loss of light regulation (Fig. 39). In this case, 50% of cells had a light-gated current.

A third chimera was then obtained by fusing the full-length C-terminal sequence of KAT1 (residues

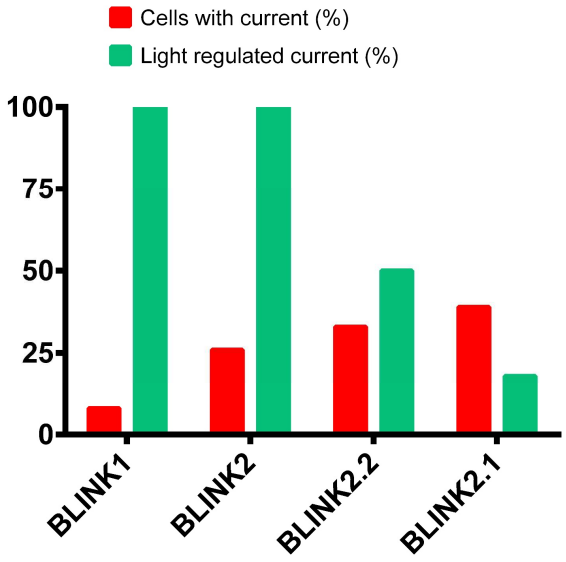

Fig. 39

Combination of 14 -3-3 binding signal and ER export motifs affect PM expression and channel properties

Graph summarizing the results obtained with clones modified with 14-3-3 binding site and ER export sequence from KAT1, in terms of PM expression and light-regulation

from 303 to 677, including the phosphomimetic mutation S676D) to the C-terminus of BLINK1. In this way, the relative positions of the DIDAE sequence and the 14-3-3 binding site from the native channel should be preserved. However, no current was detected in the HEK293T cells transfected with this channel (n=8). We know that the C terminus of KAT1 contains structural elements such as a cyclic nucleotide binding homologous domain (CNBHD) and a C-linker. From other biochemical

experiments, we know that the protein fragment does not properly fold and is prone to aggregate when it is detached from the TM portion. In the context of this behavior, it is possible that also a transplantation of the same C-terminus into another channel, as we did here, could lead to misfolding and aggregation.

It has been already mentioned that most of the modifications, which improves the surface expression of the synthetic channel, also cause a loss of channel regulation by light, whit the only exception of BLINK2. This seems to be a general trend, which is further supported by the data reported in the last chapter. The apparent correlation between surface expression and light regulation can be visualized in Fig. 40. Here we show the percentage of cells with a BLINK type current as a function of cells in which the respective channel was still showing a light sensitivity. The data reveal an obvious negative correlation.

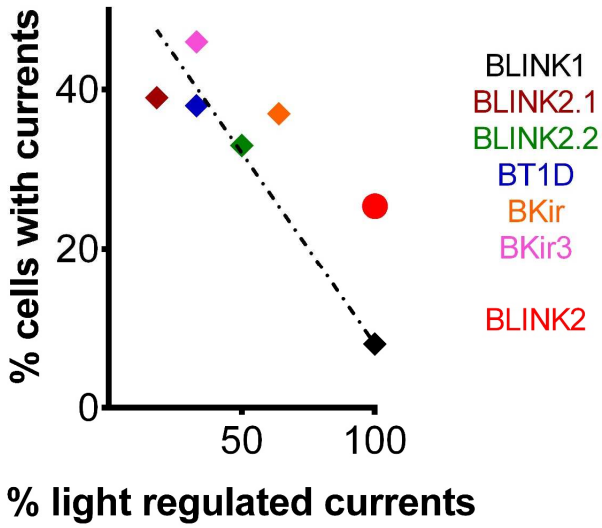

Fig. 40

Negative correlation between surface expression and light sensitivity of different BLINK1 constructs.

Graph shows the correlation observed between PM expression and degree of light regulation. Each color represents a different construct, according to the legend labelling.

The reason behind the relationship remains unknown. One possible explanation is that the trafficking pathway of proteins to the PM has to pass some rate limiting steps. Such rate limiting steps could be given by a limited availability of chaperons or adaptor proteins, which are necessary for the recognition of sorting signals and/or quality control. In such a scenario, more proteins might be sorted to the plasma membrane but the folding of these proteins may not be correct. We did not investigate this point further, given the good results obtained with BLINK2.

3.5.4 – Exchanging 14-3-3 binding motif of KAT1 with that of the proton pump

Another attempt to further increase the presence of BLINK2 in the PM was to replace the 14-3-3 binding motive in KAT1 with that of another well-known target of 14-3-3 proteins, namely the proton pump PMHA (Plasma membrane H^+-ATPase) [62].

PMHA has a very high affinity for 14-3-3 binding (K_D = 0.09µM) [78]. We therefore expected an increased PM expression of our chimeric construct, since the estimated K_D for the respective binding motive in KAT1 is only 0.7µM (A. Saponaro, personal communication). The phosphomimetic peptide QQNYDV from the core of the 14-3-3 binding motive in the ATPase was used to replace the respective motive from KAT1 in BLINK2. The new channel, named BLINK 2.3 (Fig 41), was again tested in HEK293T cells. BLINK2.3 gave rise to detectable currents in only 7% of transfected cells (n=29); in the cases in which the current could be measured, it did not exhibit light regulation. In all these cases the cell showed already in the dark BLINK type currents (Fig. 41).

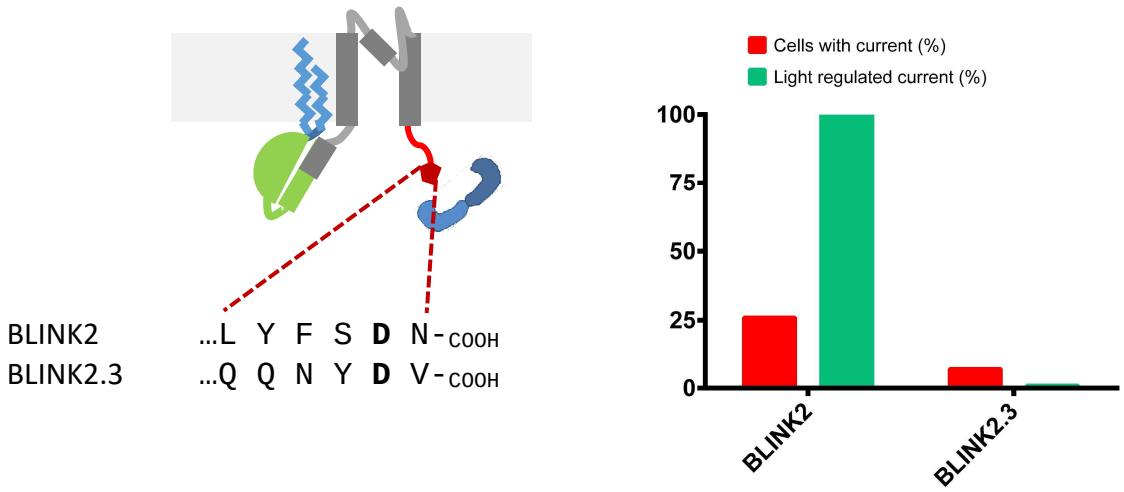

Fig. 41

BLINK2 and BLINK2.3 sequence and properties.

Left: Cartoon representing the channels monomer. Difference in sequences is highlighted; both clones have the phosphomimetic mutation of Serine in Aspartate in the last but one position (both in bold). Colours as in Fig. 23. Right: Graph summarizing the results obtained with BLINK2.3 compared to BLINK2.

Once again, we obtained a different behavior of the channel when it was fused with a 14-3-3 binding motif other than that of KAT1. This occurs even though the binding motive was in the latter embedded in the native context of the KAT1 C-terminus. In principle, the only difference between the constructs should be the affinity for the 14-3-3 proteins. This is higher in this case of the motive from the ATPase than in that from the KAT1 channel. In reality, we see that both constructs differ more profoundly.

Depending on the origin of the 14-3-3- binding motif the surface expression and the light regulation is different. There is a possibility that the two motifs recruit different isoforms of 14.3.3 and that they are connected to different trafficking pathways or modalities

3.6 – BLINK2 characterization

BLINK2 shows among all the constructs, which we tested, the best features including an improved surface expression and perfect light regulation. We therefore decided to further characterize its biophysical properties in patch clamp experiments on transfected HEK293T. Furthermore, we tested if BLINK2 can be used *in vivo* as a tool in optogenetic experiments. This was examined zebrafish (*Danio rerio*) embryos and mouse neurons. The latter was done in collaboration with Dr. Tonini (IIT, Genoa).

3.6.1 – Current kinetics in patch clamp recordings might be influenced by cytosolic content dilution

We routinely recorded BLINK2 currents in patch clamp experiment in HEK 293T cells in the whole cell configuration. Fig. 42A shows typical I/V curves of the BLINK2 current recorded at different times of exposure to dark and light. An experiment routinely started in the dark; we were usually waiting 6 minutes to allow the cell to reach a stable endogenous current level. Once the baseline was stable, the light was turned on.

Fig. 42B shows the values of the current at -60 mV re-plotted from Fig. 42A as a function of time; intermediate time points, which were not shown in Fig. 42A, have been added. It appears that the BLINK2 current is activated with a delay of about 1.5 to 2 minutes after start of the illumination. This delay is not present in BLINK1 and we can therefore conclude that it depends on the new structural feature of BLINK2, namely the binding site for 14-3-3 proteins on the C terminus.

The experiment shows another remarkable feature of BLINK2 in that the current continues to increase for another 3 minutes after the light was turned off (Fig. 42A). This is clearly visible also in Figure 42B. This continuous increase in BLINK current in the dark is quite remarkable and was not present in BLINK1.

To better understand the kinetics of this process we modified the experiment by reducing the time of illumination. In Fig. 42C and D are reported the light gated currents, which were measured in two other cells expressing the channel; these cells were exposed to blue light for 6 and 1.5 minutes. Also in these cells, we observed the same behaviour: BLINK2 starts opening about t=1.5 minutes after start of the illumination (t=0). The maximum current is reached about at t=10 minutes after start of the illumination. This kinetics is independent on whether the cell was exposed only for a short period of 1.5 min or constantly illuminated. About 15 to 20 minutes after reaching the maximum, the current declined back to the baseline. This was again independent on the history of illumination. The results

of these experiments suggest that a short illumination with blue light triggers an all or nothing mechanism, which transiently activates the channel. Illumination is only required to trigger this process; once elicited it follows an inherent kinetics, which is independent on the presence/absence of illumination. This interpretation is consistent with other experiments, which were performed in continuous light. As shown in Fig. 43A, also in this case the current increases briefly after onset of the illumination. It reaches the maximum after about 12 minutes and decreases towards the initial levels even in the presence of light.

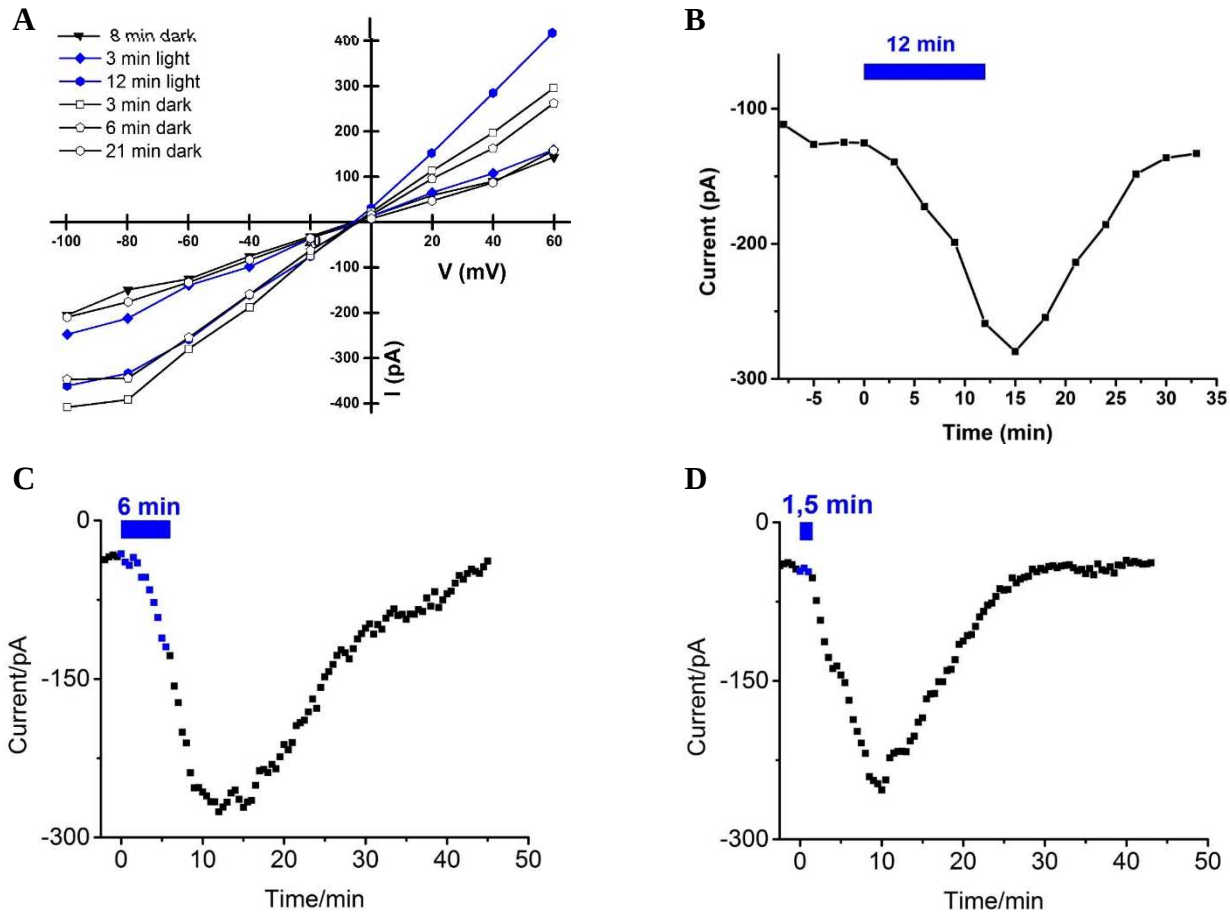

Fig. 42

Light induced BLINK2 currents have a transient activation kinetics

A: Steady state IV curves of HEK293T cells expressing BK6D – BLINK2. Data recorded recorded in different light/dark conditions at different time points.

B: Current amplitude at -60mV of BLINK2 expressing HEK293T cell at different light/dark conditions and time points. Values are taken from current traces recorded from the same cell shown in A. C and D: Representative currents recorded at -60 mV from two different HEK 293T cells expressing BLINK2 and exposed to blue light irradiation for different amounts of time.

Since we know that 14-3-3 binding to the C-terminus is required for channel regulation, we speculated that we might lose the binding of the 14-3-3 in the whole cell recordings. Notably in the whole cell configuration, mobile cytosolic components are diluted by perfusion of the cell with the pipette solution [79].

To test this hypothesis, we performed a competition experiment in which we added the synthetic peptide (LYFSpSN) corresponding to the 14-3-3 binding motif present in BLINK2 to the pipette solution. The peptide had a final concentration of 10 µM. Binding assays with the ITC method had shown that this was a saturating concentration for the binding of the peptide to purified 14-3-3 proteins from *Nicotiana tabacum* (A. Saponaro, personal communication).

The results of this first experiment, which was performed in the dark, are shown in Fig. 43B. The recordings show an increase in current, which is starting with a delay of approximately three minutes after the establishment of whole cell configuration e.g. the begin of the perfusion of the cell with the peptide. The current reached also in this case a maximum after 10 to 15 minutes before it decreases again. With time the current decays over 20 min back the current level to the initial value.

The kinetics of the channel recorded in the dark during perfusion with the phosphorylated peptide from the pipette is very similar to that seen in response to illumination (see Figure 43A and B).

The results obtained from this pilot experiment are in agreement with the hypothesis that a light-induced opening of the channel causes the removal of the 14-3-3 bound protein from the C-terminus. This might be the result of a conformational change in the protein, which is induced by light-triggered rearrangements of the LOV domain. The data obtained from this first experiment have to be confirmed by repeating the measurements, however these results taken together with the data collected so far, suggest that a loss of 14-3-3 binding during the experiment probably interferes with our recordings. It may mask the real activation/inactivation kinetics of the channel.

To avoid this problem, we adopted two different strategies: the first one was the addition of purified 14-3-3 proteins in the pipette solution during whole cell measurements, the second one was to record the currents either in cell-attached or in perforated-patch configuration.

In the first case, we added 10µM purified 14-3-3 proteins (isoform C) of tobacco in the pipette solution. We were choosing this isoform because it binds to the C terminus of KAT1 (A. Saponaro, personal communication). In these experiments, we could however not detect any difference in the behaviour of BLINK2 after the addition of the proteins. The entire 14-3-3 dimer (45kDa) may be too large for an efficient diffusion from the patch pipette. The protein could also be retained in the pipette and stick to the glass wall of the pipette. In both cases, it may not reach the cytosol during the measurements.

As for the second strategy, we tried the cell-attached configuration but we could not measure any current. This result was somehow expected, given that our previous immunostaining experiments had shown that the number of Kcv and BLINK channels on the cell membrane is still quite low and that they are distributed in clusters.

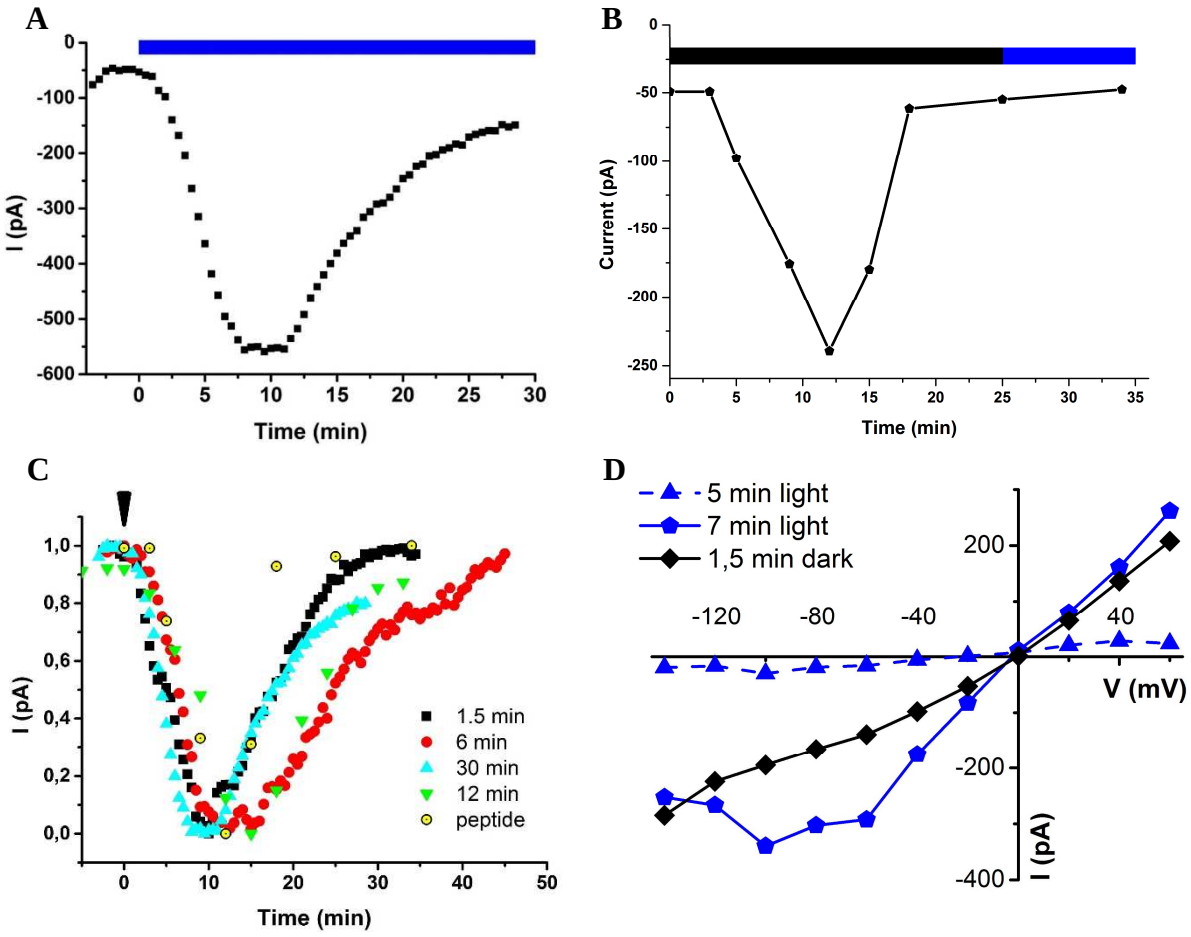

Fig. 43

Light induced BLINK2 currents show a transient activation kinetics

A: Current amplitude recorded at -60mV in different light/dark conditions and at different time points in a cell expressing BLINK2, following the addition of 10µM phosphorylated hexapeptide in the patch pipette.

B: Representative currents recorded at -60 mV from one HEK293T cells expressing BLINK2 and exposed to continuous blue light.

C: Superimposition of the current traces reported in figure 43A, B and 42B- D.

D: Steady state IV curves recorded with perforated patch technique at different time points following dark or light exposure in a cell expressing BLINK2 channel

We are currently try to measure the channel by using the perforated patch technique. This configuration allows, like the whole cell configuration, detection of the currents through all the

channels in the PM. Since the membrane in the tip of the patch electrode is not ruptured but only perforated, this method is interfering less with the cytosolic content of the cell.

We are currently using 25µM Escin in our pipette solution during measurements, because it inserts quickly in the membrane (we can record whole cell-like currents 5 to 8 minutes after the seal has been established) and is water soluble. With these properties, it has only a minimal effect on the pipette solution composition. With this approach, we can record stable currents from the same cell for no longer than 25 minutes. Given this limitation, we can only characterize either the activation or the inactivation kinetics (starting from light on) during a single experiment.

So far, we have been focusing on channel closure and we have successfully recorded one experiment. Starting from an open channel in blue light we observed a current reduction in the dark after 1.5 minutes, before the seal was lost (Fig. 43D). This data need to be repeated, but seems to indicate a faster deactivation kinetics, never recorded in whole cell.

3.6.2 – BLINK2 behavior *in vivo* confirm the applicability of the channel as an inhibitory optogenetics tool

In order to test the *in vivo* applicability of BLINK2 as an optogenetic tool, we repeated the experiment previously performed with BLINK1 in zebrafish embryos [31].

Embryos at the stage of 1-2 cells were injected with the cRNA coding for either BLINK2 or GFP. After 2 days, the larvae were tested for their ability to escape after a mechanical stimulus (touch response). Our hypothesis is that expression of the BLINK2 channel in either neurons and/or muscle cells, should prevent this escape response in blue light.

After exposure to light, the larvae injected with the channel showed an impaired response when compared to the GFP- injected larvae (Fig. 44B).

The percentage of larvae showing the affected phenotype (45%, n= 78) was slightly higher than that previously reported with BLINK1 (37%, n=230) (Fig. 44A and B).

The maximum number of affected embryos was reached after 45 to 60 minutes of light exposure (Fig. 42C and D), confirming that BLINK2 was still open and functional after this long exposure to light. This suggests that the channel closure observed in whole cell experiments with continuous light must be an artefact of the patch clamp recordings (Fig. 43A).

The experiment in Zebrafish with BLINK2 also showed a remarkable difference from those with BLINK1. The larvae expressing BLINK2 recovered in the dark much faster than those expressing BLINK1 (Fig. 44D). In BLINK1 injected larvae, more than 30 minutes of dark are required to completely revert the light effect and restore the normal escape behaviour (Fig. 44C). In larvae injected with BLINK2 only 15 minutes are needed for a full recovery.

This fast recovery allowed us to re-expose the larvae to light repetitively. The results of these experiments highlight the reproducible behaviour of the channel in this simple test system (Fig. 44D), confirming the *in vivo* applicability of the channel as an inhibitory optogenetic tool.

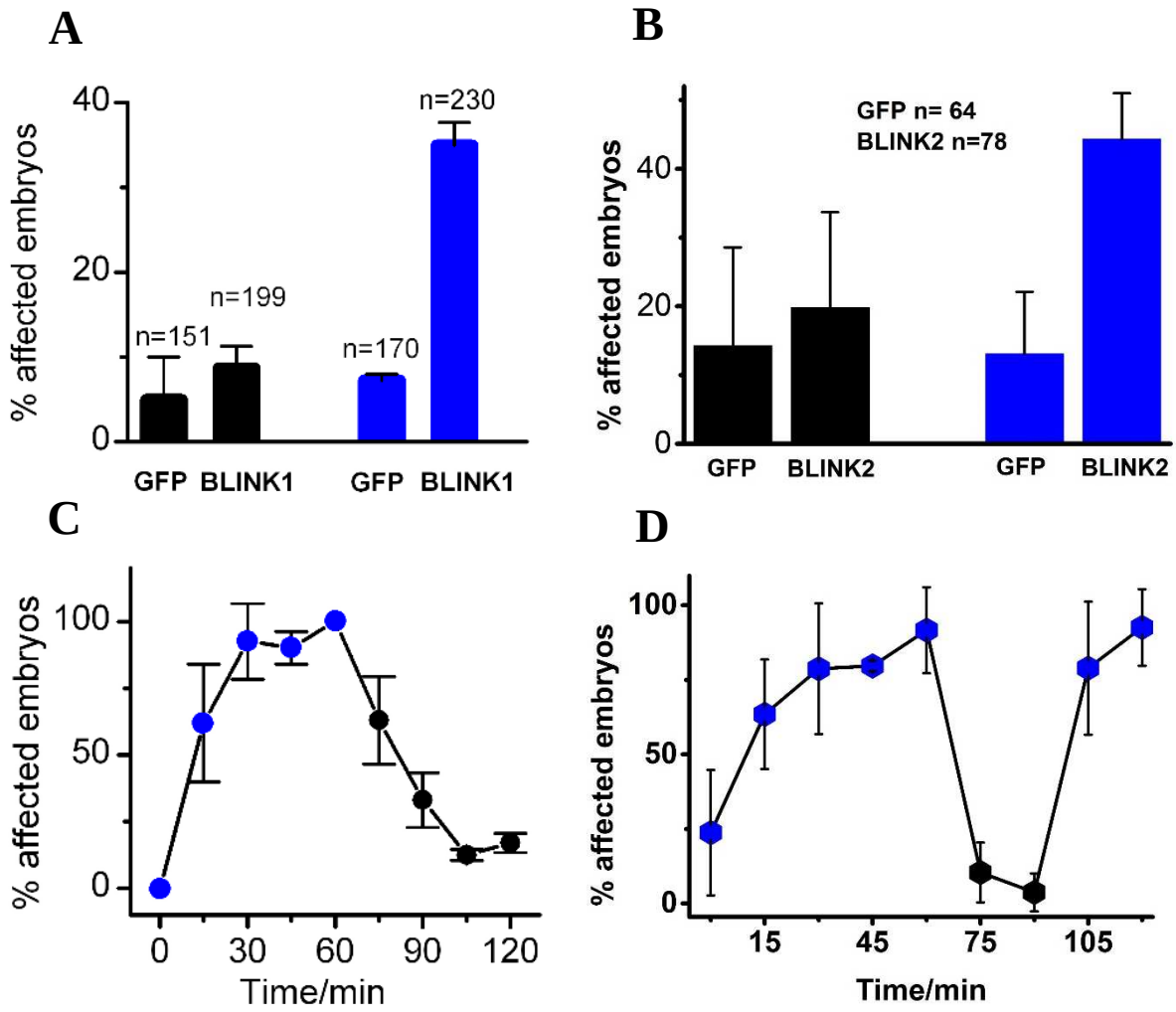

Fig. 44

Expression of BLINK1 and BLINK2 inhibits escape response of zebrafish larvae.

Results of touch response experiments performed on 2-days-old zebrafish larvae injected with BLINK1 (A, C, both modified from ref [31]*) or BLINK2 cRNA (B, D).*

A, B: Comparison between the number of embryos showing an altered escape response in BLINK- or GFP-expressing larvae. Fish were kept in dark or blue light during time marked by black and blue bars respectively. C, D: Kinetics of escape response inhibition in BLINK1 (C) or BLINK2 (D) expressing larvae. Blue data points collected in light black data point in dark. In both experiments, light was turned on at time 0 for 60 minutes. BLINK2 larvae were subjected to a second light irradiation for 30 minutes from t=90 min (D).

3.7 – Mutations in LOV domain affect channel kinetics and trafficking

In a parallel study, we investigated the possibility to increase the activation kinetics of BLINK channels, which is much slower than the photocycle of the LOV domain [31, 33]. This study was conducted before we realized that the kinetics of BLINK2 in patch clamp recordings in the whole cell configuration is determined by a dilution of the 14-3-3 protein. To this end, we introduced in the LOV domain of BLINK2 mutations, which were reported in the literature reported to affect the photocycle of isolated LOV2 domains [33]. The typical duration of the photocycle in the wild type LOV domain as an isolated protein has been estimated as 60 to 80s. The light-induced formation of the covalent adduct just requires few microseconds, while the disruption of the covalent adduct requires longer times, in the order of tens of seconds. All the mutations, which were identified as having an effect on the photocycle, are for this reason affecting the dark recovery step [33]. Guided by published data we inserted in the LOV domain of BLINK2 a whole set of mutations, which were reported to speed up the photocycle by up to an order of magnitude [33]. The five different mutants, which were created for this purpose, were BLINK2 V416T, BLINK2 I427V, BLINK2 Q513H, BLINK2 N414A+Q513H and BLINK2 Q513D. In addition, the BLINK2 N414A mutant was obtained and tested as a control. This single mutation has the opposite effect in that it increases the duration of the photocycle to up to 1400 seconds.

Six mutants were tested in patch clamp experiments and they provided some unexpected results. Some of the point mutation generated a very strong effect both, on light regulation and surface expression (Fig. 45A). The BLINK2 V416T (n=11), BLINK2 Q513H (n=16) and BLINK2 N414A (n=15) mutants did not generate any measurable currents when transfected in HEK293T cells. The BLINK2 I427V mutant (n=11) in contrast could reach the PM in 36% of cells, but totally lost the light regulation on channel gating (Fig. 45C). These mutations in the LOV domain presumably caused an instability in this domain structure. This in turn may have caused protein misfolding with the consequent loss of channel regulation. Cases of an even more severe misfolding may have caused degradation and hence a loss of channel proteins in the PM.

The BLINK2 N414A+Q513H double mutant showed no difference with the behavior of the wild type BLINK2 channel (n=9). The mutant exhibited light regulated currents in 25% of transfected cells (Fig. 45C). These data suggest that the combination of two mutations can have a huge impact on the PM expression of the channel. It seems as if the addition of the second mutation is balancing the negative effects of the two single mutants. The resulting mutant channel appears to be stable, reach the PM and respond to light.

A

Mutation	Reported time constant (s)
BLINK2 wt	60-80
I427V*	4
V416T	2.6
N414A	1427
Q513H	30
Q513D	5
N414A + Q513H	2

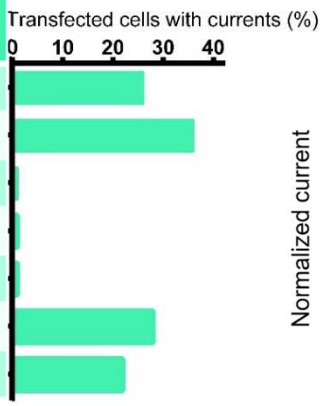

B

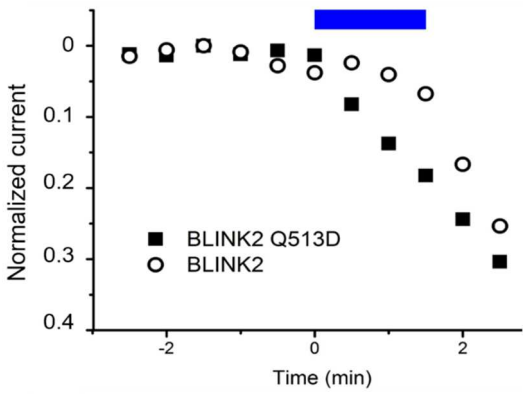

C

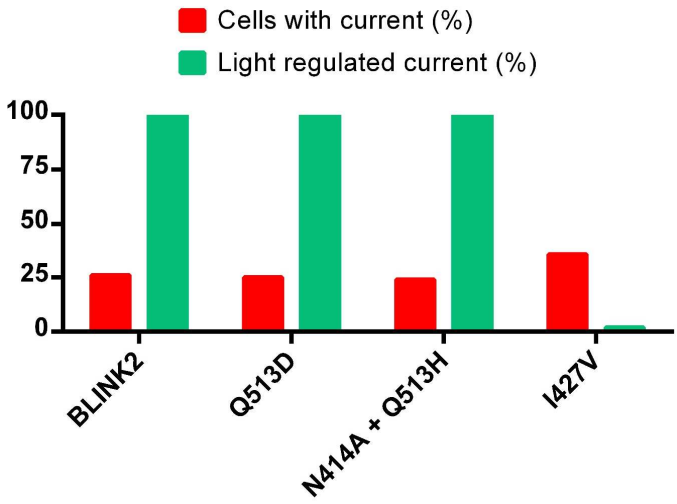

Fig. 45

Summary of effects of mutations on functional features of BLINK2

A: Table summarizing the results obtained testing clones with mutations in residues involved in the regulation of photocycle, compared to BLINK2 wild type channel. Among the three functional channels detected on PM, only BLINK2 I427V lost light regulation (*).

B: superimposition of representative currents recorded at -60 mV from two different HEK 293T expressing BLINK2 or BLINK2 Q513D and exposed to blue light irradiation for 1.5 minutes. Currents are normalized and 0 is the endogenous current level of HEK293T cells

C: Graph summarizing the results obtained on trafficking rate e light regulation inserting point mutations in the LOV domain of BLINK2.

As a last clone, we tested BLINK2 Q513D (QD mutant). This mutant showed some unexpected properties (Fig. 45B and C): it can reach the PM with the same efficiency as BLINK2 and shows some improved activation kinetics.

With this mutant, we recorded an increase in light stimulated current above the baseline already 30 seconds after light exposure. In the parental channel, the delay was 90 seconds (Fig. 45B). Unfortunately, due to the limit of the whole cell technique, diluting 14-3-3 proteins and affecting the channel behavior, we have not yet been able to examine the kinetics of channel closure. We are therefore not yet able to confirm if the mutant shows a faster dark recovery than the wild type, as we expect from reported data. We are currently investigating the *in vivo* properties of the QD mutant, performing the touch response test on Zebrafish larvae (see chapter 3.6.2). Preliminary data collected so far confirm that the QD mutant shows exactly the same percentage of affected embryos and the same kinetics as the wild type BLINK2. Larvae expressing the channel show an impaired escape response following light exposure, reaching a maximum of an altered phenotype in 45-60 minutes of irradiation. The shorter delay of the mutant for the onset of the light stimulated current seems to be irrelevant for the kinetics of the escape response inhibition. Notably, larvae expressing the QD mutant, which had an altered escape response in blue light, returned back in the dark to their normal behavior with the same kinetics as those expressing the parental channel. A close scrutiny of the data suggests that the QD mutant seems to induce in the injected larvae an even more severe phenotype after light exposure than the parental channel. While performing the experiments, we noticed that a high number of mechanical stimulations were required to elicit an escape response in larvae, which were expressing the QD mutant. This number of mechanical stimulations was higher than that required in larvae expressing BLINK1 or BLINK2 (Fig. 46).

In these experiments, the escape response of a fish is considered “affected” when the larvae requires three or more stimulations to elicit a proper escape response [31]. In experiments with BLINK2 expressing larvae, we noticed that some animals were already requiring more than 10 stimulations to exhibit a proper behavior. This was evident especially after 30 or more minutes in light (Fig 46). The same severe impairment was only rarely observed by BLINK1 expressing embryos. The results of these experiments foster the hypothesis that the increased PM expression of the BLINK2 channel could have exasperated this feature. Therefore, we were not surprised to find the same severe phenotype in embryos injected with the QD mutant. Also, this channel is like BLINK2 abundant in the PM. However, in experiments with larvae expressing the mutant channel we observed that even after only 15 minutes in light, some larvae were already showing the strong impaired phenotype. The number of larvae exhibiting this behavior was further increasing over time in the light (Fig. 46).

The results of these experiments suggest that the amplification of the impaired escape response, which is generated by the QD mutant, is not only the result of an increased PM expression of the channel. Also, the difference in kinetics of channel activation with a smaller delay in channel activation in the light could contribute to this phenotype. It is reasonable to assume that a faster opening of the channel can allow a much faster potassium efflux from the cells. This in turn could result in a stronger PM hyperpolarization. Such a scenario could explain why both, BLINK2 and the QD mutant channel augment the inhibition of the escape responds. It would also explain why the inhibition appears strong even after a short light exposure in QD mutant expressing larvae.

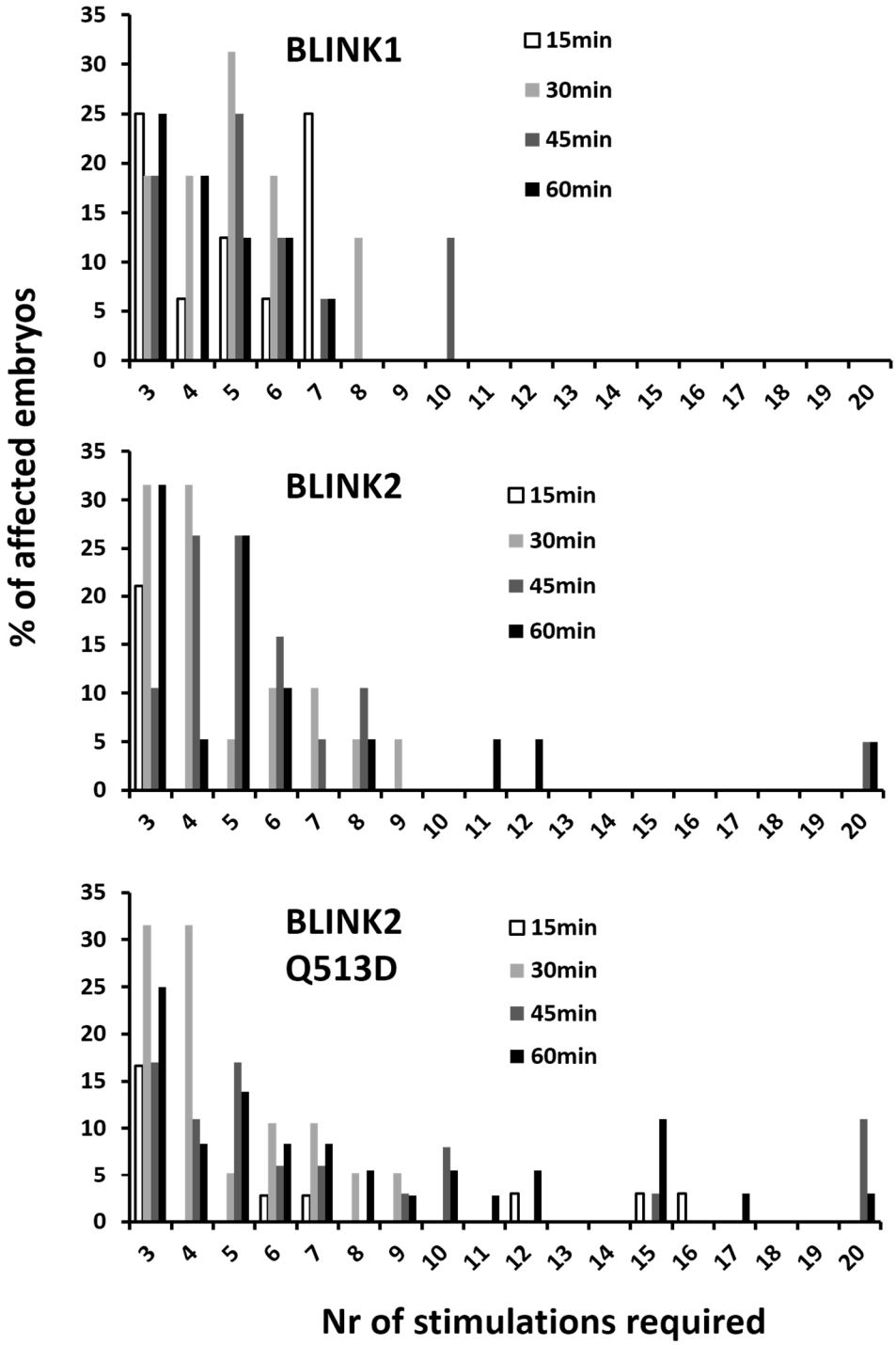

Fig. 46

Zebrafish larvae expressing BLINK2 or BLINK2 Q513D require more mechanical stimuli for an escape response than BLINK1.

Graphs showing the amount of stimulations required in a typical experiment to elicit an escape response in 2-days-old Zebrafish larvae injected with mRNA coding for BLINK1, BLINK2 or QD mutant. Fish were exposed to light for 15, 30, 45 or 60 minutes. Percentage of affected embryos is calculated on the total amount of embryos showing impaired escape response phenotype during the experiment.

Following the positive results obtained in the touch response tests in Zebrafish, the QD mutant has also been used for preliminary tests in cultured rat neurons and mouse brain slices. These experiments were performed by the group of Dr. Raffaella Tonini at IIT (Genova). The pilot experiments already show a clear light-dependent hyperpolarization and consequent inhibition of neuronal firing (Fig. 47B). The results of these recordings further confirming the applicability of the channel as an optogenetic tool. Following dark exposure, a population of neurons showed restored firing ability (Fig. 47 B), while in some other cases firing was not restored at least over the time of the recording (Fig. 47C).

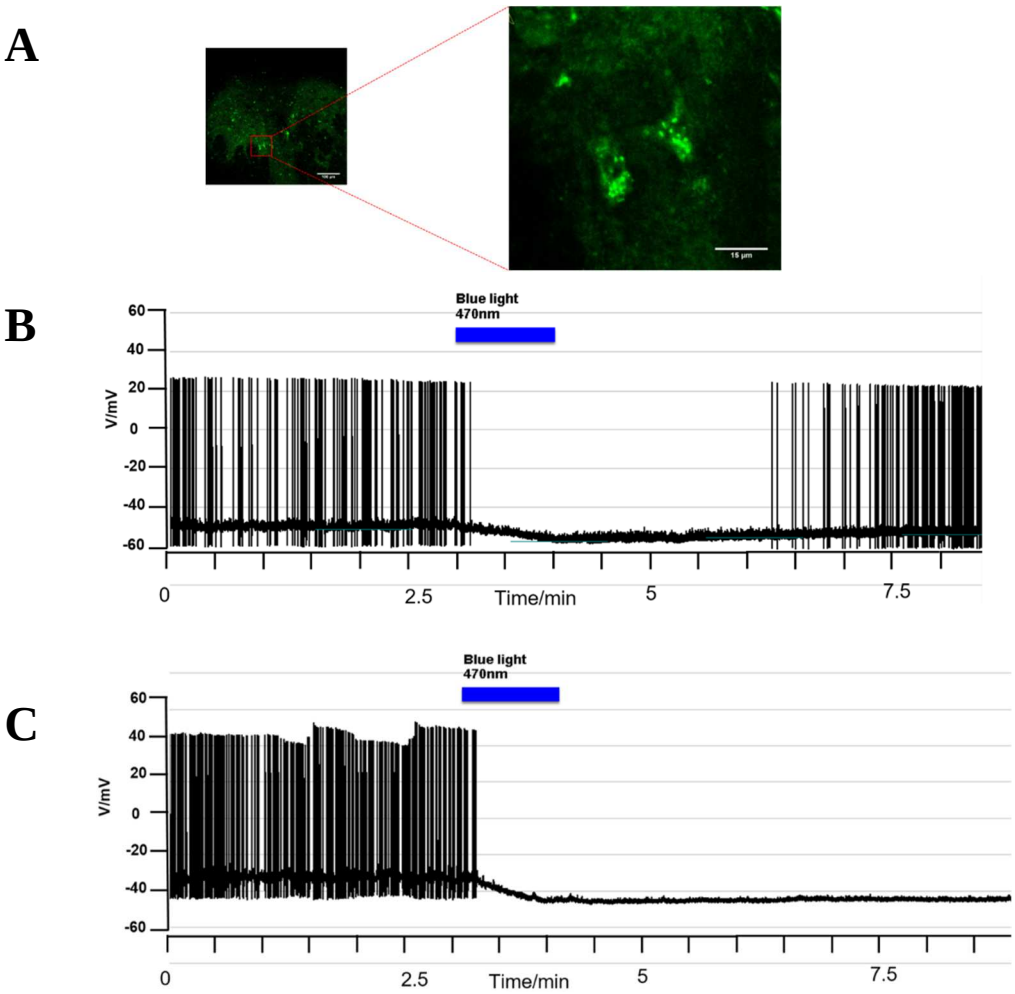

Fig. 47

Functional expression of BLINK2 Q513D in mouse neurons.

A: GFP expression allowed the identification of infected cells. White bar is 15 µm. B and C: current clamp recordings in two neurons from coronal brain slices expressing BLINK2Q513D. A light induced hyperpolarization and an inhibition of firing was detected after 1minute of blue light (470 nm) irradiation (blue bar). In A, the effect was reversible and cell reassumed firing. Experiments performed at IIT (Genova) by the group of Dr. Tonini. AAV-IRES-EGFP virus carrying BLINK2 Q513D under the control of CAG or hSyn promoters was used to infect primary cultured neurons and mice.

4 - CONCLUSIONS AND FUTURE PERSPECTIVES

In conclusion, the most successful strategy, among the several tested to improve BLINK1 expression in the plasma membrane, is the addition of trafficking signals to the channel C-terminus. Most of the chimeras obtained following this strategy showed improvement in their PM expression rate, increasing the amount of cells with a measurable K^+ current up to six times (i.e. BKir3). However, in most cases, increased surface expression was associated with the loss of light regulation, and the channel was already partly or completely open in the dark. Such a feature was clearly incompatible with *in vivo* optogenetics applications.

The apparent correlation between the amount of channels reaching the PM and the degree of light regulation of their currents, suggests the presence of an expression threshold after which the channels reaching the PM are no more properly working. This may be related to some limiting steps in the folding and trafficking of membrane proteins, i.e. availability of chaperons or adaptor proteins involved in signal recognition, and/or abundance of cofactors. However, as previously stated, our interest was not the trafficking mechanism *per se* but rather the result of obtaining an improved version of the channel with a higher PM expression. For this reason, we did not investigate this correlation further and we tested if even a moderate increase in trafficking as that one shown by BLINK2, would be sufficient to inhibit neuronal activity in vitro and in vivo.

BLINK2 characterization needs to be completed. Cell-attached and perforated patch experiment will give clear and definitive answers on the real channel kinetics. Interestingly, when we expressed BLINK2 in zebrafish larvae we did not observe any difference with BLINK1, as if the parental channel is already expressing at good levels in this organism. It is possible that the incubation temperature of the larvae (below 30°C) plays a role, since protein folding (and indirectly trafficking) is affected by temperature [45]. Notably, BLINK2 induced a faster recovery in the dark, if compared with BLINK1 expressing larvae. The reason for this might become clear once we will obtain full information on channel kinetics by cell-attached or perforated patch measurements.

Another unexpected finding was that point mutations expected to affect LOV photocycle and, in turn, channel kinetics, were clearly changing the expression level of the channel at the PM. A possible explanation is that these mutations had an effect on LOV domain folding and this, in turn, can affect quality control and prevent or promote protein forward trafficking.

Although these mutations affect the kinetics of LOV2 recovery in the dark, Q513D showed an unexpected effect also on the channel activation kinetics, reducing the delay in opening after light exposure. This property for some reasons affects the severity of the phenotype induced by the channel

in zebrafish: larvae injected with the Q513D mutant needed a higher number of stimulations than those expressing the wild type BLINK2 channel.

Finally, BLINK2 Q513D was successfully expressed *in vitro* in cultured neurons as well as *ex vivo* in mouse brain slices.

The experiments performed by the group of Dr. Tonini (IIT, Genoa) confirm the preliminary findings in zebrafish larvae: BLINK2 can hyperpolarize the neuronal membrane potential and prevent firing inhibition.

5 - REFERENCES

[1] K. Deisseroth, "Optogenetics," *Nat Methods.*, 2011.

[2] X. X. Zhou, M. Pan and M. Z. Lin, "Investigating neuronal function with optically controllable proteins," July 2015.

[3] Y. Mei and F. Zhang, "Molecular Tools and Approaches for Optogenetics," *Biol Psychiatry*, 2012.

[4] D. Tischer and O. D. Weiner, "Illuminating cell signalling with optogenetic tools," 2015.

[5] E. S. Boyden, F. Zhang, E. Bamberg, G. Nagel and K. Deisseroth, "Millisecond-timescale, genetically targeted optical control of neural activity," *nature neuroscience*, 2005.

[6] B. Y. Chow, X. Han, A. S. Dobry, X. Qian, A. S. Chuong, M. Li, M. A. Henninger, G. M. Belfort, Y. Lin, P. E. Monahan and E. S. Boyden, "High-performance genetically targetable optical neural silencing by light-driven proton pumps," *Nature*, 2010.

[7] V. Gradinaru, K. R. Thompson and K. Deisseroth, "eNpHR: a Natronomonas halorhodopsin enhanced for optogenetic applications," *Brain Cell Biol*, 2008.

[8] G. Nagel, T. Szellas, W. Huhn, S. Kateriya, N. Adeishvili, P. Berthold, D. Ollig, P. Hegemann and E. Bamberg, "Channelrhodopsin-2, a directly light-gated cation-selective membrane channel," *PNAS*, 2003.

[9] J. Mattis, K. M. Tye, E. A. Ferenczi, C. Ramakrishnan, D. J. O'Shea, R. Prakash, L. A. Gunaydin, M. Hyun, L. E. Fenno, V. Gradinaru, O. Yizhar and K. Deisseroth, "Principles for applying optogenetic tools derived from direct comparative analysis of microbial opsins," *Nature Methods*, 2012.

[10] F. Zhang, L.-P. Wang, M. Brauner, J. F. Liewald, K. Kay, N. Watzke, P. G. Wood, E. Bamberg, G. Nagel, A. Gottschalk and K. Deisseroth, "Multimodal fast optical interrogation of neural circuitry," *nature*, 2007.

[11] V. Gradinaru, F. Zhang, C. Ramakrishnan, J. Mattis, R. Prakash, I. Diester, I. Goshen, K. R. Thompson and K. Deisseroth, "Molecular and Cellular Approaches for Diversifying and Extending Optogenetics," *Cell*, 2010.

[12] M. Mahn, M. Prigge, S. Ron, R. Levy and O. Yizhar, "Biophysical constraints of optogenetic inhibition at presynaptic terminals," *Nature neuroscience*, 2016.

[13] A. Berndt, S. Y. Lee, J. Wietek, C. Ramakrishnan, E. E. Steinberg, A. J. Rashid, H. Kim, S. Park, A. Santoro, P. W. Frankland, S. M. Iyer, S. Pak, S. Ahrlund-Richter, S. L. Delp, R. C. Malenka, S. A. Josselyn, M. Carlén, P. Hegemann and K. Deisseroth, "Structural foundations of optogenetics: Determinants of channelrhodopsin ion selectivity," *PNAS*, 2016.

[14] J. Wietek, J. S. Wiegert, N. Adeishvili, F. Schneider, H. Watanabe, S. P. Tsunoda, A. Vogt, M. Elstner, T. G. Oertner and P. Hegemann, "Conversion of channelrhodopsin into a light-gated chloride channel," *Science*, 2014.

[15] A. Berndt, S. M. Lee, C. Ramakrishnan and K. Deisseroth, "Structure-guided transformation of channelrhodopsin into a light-activated chloride channel," *Science*, 2014.

[16] E. G. Govuronova, O. A. Sineshchekov, R. Janz, X. Liu and J. L. Spudich, "Natural light-gated anion channels: A family of microbial rhodopsins for advanced optogenetics," *Science*, 2015.

[17] J. S. Coombs, J. C. Eccles and P. Fatt, "The specific ionic conductance and the ionic movements across the motoneuronal membrane that produce the inhibitory post-synaptic potential," *J. Physiol.*, 1955.

[18] S. Naito and T. Ueda, “Characterization of Glutamate Uptake into Synaptic Vesicles,” *Journal of Neurochemistry*, 1985.

[19] S. Basavappa and J. C. Ellory, “The Role of Swelling-Induced Anion Channels During Neuronal Volume Regulation,” *Molecular Neurobiology,* 1996.

[20] Y. Ben-Ari, “Excitatory actions of GABA during development: the nature of nurture,” *Nature,* 2002.

[21] Y. Ben-Ari, E. Cherubini, R. Corradetti and J.-L. Gaiarsa, “Giant synaptic potentials in immature rat CA3 hippocampal neurons,” *Journal of physiology,* 1989.

[22] S. Wagner, M. Castel, H. Gainer and Y. Yarom, “GABA in the mammalian suprachiasmatic nucleus and its role in diurnal rhythmicity,” *Nature,* 1997.

[23] H. Alfonsa, E. M. Merricks, N. K. Codadu, M. O. Cunningham, K. Deisseroth, C. Racca and A. J. Trevelyan, “The Contribution of Raised Intraneuronal Chloride to Epileptic Network Activity,” *The Journal of Neuroscience,* 2015.

[24] J. V. Raimondo, L. Kay, T. J. Ellender and C. J. Akerman, “Optogenetic silencing strategies differ in their effects on inhibitory synaptic transmission,” *Nature Neuroscience,* 2012.

[25] J. Szabadics, C. Varga, G. Molnàr, S. Olah, P. Barzò and G. Tamas, “Excitatory Effect of GABAergic Axo-Axonic Cells in Cortical Microcircuits,” *Science,* 2006.

[26] M. Banghart, K. Borges, E. Isacoff, D. Trauner and R. H. Kramer, “Light-activated ion channels for remote control of neuronal firing,” *Nature neuroscience,* 2004.

[27] H. Janovjak, S. Szobota, C. Wyart, D. Trauner and E. Y. Isacoff, “A light-gated, potassium-selective glutamate receptor for the optical inhibition of neuronal firing,” *Nature neuroscience,* 2010.

[28] D. Schmidt, P. W. Tillberg, F. Chen and E. S. Boyden, “A fully genetically encoded protein architecture for optical control of peptide ligand concentration,” *Nature communications,* 2014.

[29] J.-Y. Kang, D. Kawaguchi, I. Coin, Z. Xiang, D. D. O'Leary and P. A. Slesinger, “In Vivo Expression of a Light-Activatable Potassium Channel Using Unnatural Amino Acids,” *Neuron,* 2013.

[30] D. Bichet, F. A. Haass and L. Y. Jan, “Merging functional studies with structures of inward-rectifier K+ channels,” *Nature Reviews Neuroscience,* 2003.

[31] C. Cosentino, L. Alberio, S. Gazzarrini, M. Aquila, E. Romano, S. Cermenati, P. Zuccolini, J. Petersen, M. Beltrame, J. L. Van Etten, J. M. Christie, G. Thiel and A. Moroni, “Engineering of a light-gated potassium channel,” *Science,* 2015.

[32] J. M. Christie, “Phototropin Blue-Light Receptors,” *Annu. Rev. Plant Biol,* 2007.

[33] A. Pudasaini, K. K. El-Araband and B. D. Zoltowski, “LOV-based optogenetic devices: light-driven modules to impart photoregulated control of cellular signaling,” *Frontiers in Molecular Biosciences,* 2015.

[34] B. Plugge, S. Gazzarrini, M. Nelson, R. Cerana, J. L. Van Etten, C. Derst, D. DiFrancesco, A. Moroni and G. Thiel, “A potassium channel protein encoded by chlorella virus PBCV-1,” *Science,* 2000.

[35] S. Gazzarrini, M. Severino, M. Lombardi, M. Morandi, D. DiFrancesco , J. L. Van Etten, G. Thiel and A. Moroni, “The viral potassium channel Kcv: structural and functional features,” *FEBS Letters,* 2003.

[36] D. Minor Jr, S. J. Masseling, Y. N. Jan and L. Y. Jan, “Transmembrane Structure of an Inwardly Rectifying Potassium Channel,” *Cell,* 1999.

[37] D. Strickland, X. Yao, G. Gawlak, M. K. Rosen, K. H. Gardner and T. R. Sosnick, "Rationally improving LOV domain-based photoswitches," *Nature Methods,* 2010.

[38] D. A. Towler, S. Adamns, S. R. Eubanks, D. S. Towery, E. Jackson-Machelski, L. Glaser and J. I. Gordon, "Myristoyl CoA:Protein N-Myristoyltransferase Activities from Rat Liver and Yeast Possess Overlapping Yet Distinct Peptide Substrate Specificities," *The Journal of Biolgical Chemistry,* 1988.

[39] B. Hertel, S. Tayefeh, T. Kloss, J. Hewing, M. Gebhardt, D. Baumeister, A. Moroni, G. Thiel and S. M. Kast, "Salt bridges in the miniature viral channel Kcv are important for function," *Eur Biophys J ,* 2010.

[40] C. Arrigoni, I. Schroeder, G. Romani, J. L. Van Etten, G. Thiel and A. Moroni, "The voltage-sensing domain of a phosphatase gates the pore of a potassium channel," *The Journal of general Physiology,* 2013.

[41] S. M. Harper, L. C. Neil and K. H. Gardner, "Structural Basis of a Phototropin Light Switch," *Science,* 2003.

[42] S. M. Harper, J. M. Christie and K. H. Gardner, "Disruption of the LOV-JR Helix Interaction Activates Phototropin Kinase Activity," *Biochemistry,* 2004.

[43] S. Gazzarrini, M. Kang, J. L. Van Etten, S. Tayefeh, S. M. Kast, D. DiFrancesco, G. Thiel and A. Moroni, "Long Distance Interactions within the Potassium Channel Pore Are Revealed by Molecular Diversity of Viral Proteins," *The Journal fo Biological Chemistry,* 2004.

[44] K. Sato, A. Norris, M. Sato and B. D. Grant, "C. elegans as a model for membrane traffic,," *Wormbook,* 2014.

[45] L. Ellgaard and A. Helenius, "Quality control in the endoplasmic reticulum," *Nature reviews,* 2003.

[46] M. Mikosch, A. C. Hurst, B. Hertel and U. Homann, "Diacidic Motif Is Required for Efficient Transport of the K+ Channel KAT1 to the Plasma Membrane," *Plant Physiology,* 2006.

[47] C. Stockklausner, J. Ludwig, J. P. Ruppersberg and N. Klocker, "A sequence motif responsible for ER export and surface expression of Kir2.0 inward rectifer K+ channels," *FEBS letters,* 2001.

[48] M. Aridor, J. Weissman, S. Bannykh, C. Nuoffer and W. E. Balch, "Cargo selection by the COPII budding machinery during export from the ER," *J Cell Biol.,* 1998.

[49] F. Adolf, M. Rhiel, I. Reckmann and F. T. Wieland, "Sec24C/D-isoform–specific sorting of the preassembled ER–Golgi Q-SNARE complex," *Mol Biol Cell,* 2016.

[50] Y. Suda and A. Nakano, "The yeast Golgi apparatus," *Traffic,* 2012.

[51] V. Gradinaru, K. R. Thompson, F. Zhang, M. Mogri, K. Kay, M. B. Schneider and K. Deisseroth, "Targeting and Readout Strategies for Fast Optical Neural Control In Vitro and In Vivo," *The Journal of Neuroscience,* 2007.

[52] Y. Zhang and R. M. Harris-Warrick, "An ER export signal accelerates the surface expression of shal potassium channels in pyloric neurons of the lobster stomatogastric ganglion," *Pflugers Arch - Eur J Physiol,* 2004.

[53] M. S. Marks, L. Woodruff, H. Ohno and J. S. Bonfacino, "Protein targeting by tyrosine- and di-leucine-based signals: evidence for distinct saturable components," *Journal of cell biology,* 1996.

[54] C. A. Chen and D. R. Manning, "Regulation of G proteins by covalent modification," *Oncogene,* 2001.

[55] A. Q. Gomes, B. R. Ali, J. S. Ramalho, R. F. Godfrey, D. C. Barral, A. N. Hume and M. C. Seabra, “Membrane Targeting of Rab GTPases Is Influenced by the Prenylation Motif,” *Mol Biol Cell*, 2003.

[56] T. A. Farazi, G. Waksman and J. I. Gordon, “Structures of Saccharomyces cereVisiae N-myristoyltransferase with Bound MyristoylCoA and Peptide Provide Insights about Substrate Recognition and Catalysis,” *Biochemistry*, 2001.

[57] N. Fukuda, M. Doi and S. Honda, “Yeast One-Hybrid Gc Recruitment System for Identification of Protein Lipidation Motifs,” *PlosOne*, 2013.

[58] S. M. Robbins, N. A. Quintrell and J. M. Bishop, “Myristoylation and differental palmitoylation of the HCK protein-tyrosine kinases govern their attachment to membranes and association with caveolae,” *Molecular and cellular biology*, 1995.

[59] M.-J. Bijlmakers and M. Marsh, “The on–off story of protein palmitoylation,” *Trends in Cell Biology*, 2003.

[60] B. Sottocornola, S. Visconti, S. Orsi, S. Gazzarrini, S. Giacometti, C. Olivari, L. Camoni, P. Aducci, M. Marra, A. Abenavoli, G. Thiel and A. Moroni, “The Potassium Channel KAT1 Is Activated by Plant and Animal 14-3-3 Proteins,” *The Journal of Biological Chemistry,* 2006.

[61] C. Anders, Y. Higuchi, K. Koschinsky, M. Bartel, B. Schumacher, P. Thiel, H. Nitta, R. Preisig-Mueller, G. Schlichtoerl, V. Renigunta, J. Ohkanda, J. Daut, N. Kato and C. Ottmann, “A Semisynthetic Fusicoccane Stabilizes a Protein-Protein Interaction and Enhances the Expression of K+ Channels at the Cell Surface,” *Chemistry and Biology,* 2013.

[62] G. Duby and M. Boutry, “The plant plasma membrane proton pump ATPase: a highly regulated P-type ATPase with multiple physiological roles,” *European Journal of Physiology,* 2009.

[63] V. Cotelle and N. Leonhardt, “14-3-3 Proteins in Guard Cell Signaling,” *Frontieres in plant science*, 2016.

[64] X. Lianga, A. C. Da Paula, Z. Bozòkyb, H. Zhang, C. A. Bertrand, K. W. Peters, J. D. Forman-Kay and R. A. Frizzel, “Phosphorylation-dependent 14-3-3 protein interactions regulate CFTR biogenesis,” *Molecular Biology of the Cell,* 2012.

[65] H. Fu, R. Subramanian and S. Marsters, “14-3-3 PROTEINS: Structure, Function, and Regulation,” *Annu. Rev. Pharmacol. Toxicol.,* 2000.

[66] Y. Aghazadeh and V. Papadopoulos, “The role of the 14-3-3 protein family in health, disease, and drug development,” *Drug Discovery Today,* 2016.

[67] M. Rosenquist, P. Sehnke, R. J. Ferl and C. Larsson, “Evolution of the 14-3-3 protein family: does the large number of isoforms in multicellular organisms reflect functional specificity?,” *J Mol Evol.,* 2000.

[68] A. Hofherr, B. Fakler and N. Klocker, “Selective Golgi export of Kir2.1 controls the stoichiometry of functional Kir2.x channel heteromers,” *Journal of Cell Science,* 2005.

[69] F. Zhang, L.-P. Wang, M. Brauner, J. F. Liewald, K. Kay, N. Watzke, P. G. Wood, E. Bamberg, G. Nagel, A. Gottschalk and K. Deisseroth, “Multimodal fast optical interrogation of neural circuitry,” *Nature,* 2007.

[70] D. Ma, N. Zerangue, Y.-F. Lin, A. Collins, M. Yu, Y. N. Jan and L. Y. Jan, “Role of ER Export Signals in Controlling Surface Potassium Channel Numbers,” *Science,* 2001.

[71] H. Farhan, V. Reiterer, A. Kriz, H.-P. Hauri, M. Pavelka, H. H. Sitte and M. Freissmuth, “Signal-dependent export of GABA transporter 1 from the ER-Golgi intermediate compartment is specified by a C-terminal motif,” *Journal of cell science*, 2008.

[72] G. Romani, A. Piotrowski, S. Hillmer, J. Gurnon, J. L. Van Etten, A. Moroni, G. Thiel and B. Hertel, "A virus-encoded potassium ion channel is a structural protein in the chlorovirus Paramecium bursaria chlorella virus 1 virion.," *J. Gen. Virol,* 2013.

[73] S. Kashojiya, K. Okajima, T. Shimada and S. Tokutomi, "Essential Role of the A'α/Aβ Gap in the N-Terminal Upstream of LOV2 for the Blue Light Signaling from LOV2 to Kinase in Arabidopsis Phototropin1, a Plant Blue Light Receptor," *PlosOne,* 2015.

[74] A. S. Halavity and K. Moffat, "N- and C-Terminal Flanking Regions Modulate Light-Induced Signal Transduction in the LOV2 Domain of the Blue Light Sensor Phototropin 1 from AVena satiVa," *Biochemistry,* 2007.

[75] F. Brandizzi, N. Frangne, S. Marc-Martin, C. Hawes, J.-M. Neuhaus and N. Paris, "The Destination for Single-Pass Membrane Proteins Is Influenced Markedly by the Length of the Hydrophobic Domain," *The Plant Cell,* 2002.

[76] M. J. Adjobo-Hermans, J. Goedhart and J. Theodorus W. J. Gadella, "Plant G protein heterotrimers require dual lipidation motifs of Galpha and Ggamma and do not dissociate upon activation," *Journal of Cell Science,* 2006.

[77] G. Duby and M. Boutry, "The plant plasma membrane proton pump ATPase: a highly regulated P-type ATPase with multiple physiological roles," *European Journal of Physiology,* 2009.

[78] A. Paiardini, P. Aducci, L. Cervoni, F. Cutruzzulà, C. Di Lucente , G. Janson, S. Pascarella, S. Rinaldo, S. Visconti and L. Camoni, "The Phytotoxin Fusicoccin Differently Regulates 14-3-3 Proteins Association to Mode III Targets," *International Union of Biochemistry and Molecular Biology Life,* 2014.

[79] P. Thomas and T. G. Smart, "HEK293 cell line: A vehicle for the expression of recombinant proteins," *Journal of Pharmacological and toxicological methods,* 2005.

[80] A. V. Bryskin and I. Matsumura, "Overlap extension PCR cloning: a simple and reliable way to create recombinant plasmids," *Biotechniques,* 2010.

[81] D. L. Minor Jr, S. J. Masseling, Y. N. Jan and L. Y. Jan, "Transmembrane Structure of an Inwardly Rectifying Potassium Channel," *Cell,* 1999.

PART II

CONTENT

I. Cosentino, C., Alberio, L., Gazzarrini, S., Aquila, M., Romano, E., Cermenati, S., Zuccolini, P., Beltrame, M., Van Etten, J. L., Christie, J. M., Thiel, G. and Moroni, A. (2015) **Engineering of a light-gated potassium channel**. *Science*. 348 (6235):707-10. doi: 10.1126/science.aaa2787

II. Cosentino, C., Alberio, L., Thiel, G. and Moroni, A. (2016) **Yeast-based screening system for the selection of functional light-driven K^+ channels**. *Methods in Molecular Biology, Synthetic Protein Switches: Methods and Protocols.* Submitted.

may also stimulate the design of new antiviral drugs, because it reveals key regions interfering with nucleoprotein oligomerization and/or genome encapsidation. Finally, because MeV shares many common features with other *Paramyxoviridae* and with nsNSVs in general, this near-atomic structure of the helical MeV N_{core}-RNA nucleocapsid may be valuable for the whole *Mononegavirales* field.

REFERENCES AND NOTES

1. www.who.int/mediacentre/factsheets/fs286/en/.
2. R. W. H. Ruigrok, T. Crépin, D. Kolakofsky, *Curr. Opin. Microbiol.* **14**, 504–510 (2011).
3. D. Bhella, A. Ralph, R. P. Yeo, *J. Mol. Biol.* **340**, 319–331 (2004).
4. A. Desfosses, G. Goret, L. Farias Estrozi, R. W. H. Ruigrok, I. Gutsche, *J. Virol.* **85**, 1391–1395 (2011).
5. G. Schoehn *et al.*, *J. Mol. Biol.* **339**, 301–312 (2004).
6. E. H. Egelman, S. S. Wu, M. Amrein, A. Portner, G. Murti, *J. Virol.* **63**, 2233–2243 (1989).
7. R. G. Tawar *et al.*, *Science* **326**, 1279–1283 (2009).
8. P. Ge *et al.*, *Science* **327**, 689–693 (2010).
9. R. Cox *et al.*, *Proc. Natl. Acad. Sci. U.S.A.* **111**, 15208–15213 (2014).
10. A. A. V. Albertini *et al.*, *Science* **313**, 360–363 (2006).
11. T. J. Green, X. Zhang, G. W. Wertz, M. Luo, *Science* **313**, 357–360 (2006).
12. F. Yabukarski *et al.*, *Nat. Struct. Mol. Biol.* **21**, 754–759 (2014).
13. A. Desfosses, R. Ciuffa, I. Gutsche, C. Sachse, *J. Struct. Biol.* **185**, 15–26 (2014).
14. See supplementary materials on *Science* Online.
15. S. E. Bakker *et al.*, *J. Gen. Virol.* **94**, 1734–1738 (2013).
16. T. J. Green *et al.*, *J. Virol.* **88**, 3766–3775 (2014).
17. R. Buckland, P. Giraudon, F. Wild, *J. Gen. Virol.* **70**, 435–441 (1989).
18. P. Calain, L. Roux, *J. Virol.* **67**, 4822–4830 (1993).
19. F. Iseni *et al.*, *RNA* **8**, 1056–1067 (2002).
20. M. R. Jensen *et al.*, *Proc. Natl. Acad. Sci. U.S.A.* **108**, 9839–9844 (2011).
21. R. L. Kingston, W. A. Baase, L. S. Gay, *J. Virol.* **78**, 8630–8640 (2004).
22. S. Longhi *et al.*, *J. Biol. Chem.* **278**, 18638–18648 (2003).
23. S. A. Krumm, M. Takeda, R. K. Plemper, *J. Biol. Chem.* **288**, 29943–29953 (2013).

ACKNOWLEDGMENTS

We thank A. Jakobi for assistance in real-space coordinate refinement using PHENIX, and M. Jamin for discussions and comments on the manuscript. This work used the platforms of the Grenoble Instruct Center (ISBG: UMS 3518 CNRS-CEA-UJF-EMBL) with support from FRISBI (ANR-10-INSB-05-02) and GRAL (ANR-10-LABX-49-01) within the Grenoble Partnership for Structural Biology (PSB); the electron microscope facility is supported by the Rhône-Alpes Region and by the Fondation pour la Recherche Medicale. A.D. received support from EMBL Interdisciplinary Postdoc (EIPOD) fellowships under Marie Curie Actions (PCOFUND-GA-2008-229597). The data reported in this manuscript are tabulated in the main paper and in the supplementary materials. The cryo-EM map of the helical MeV N_{core}-RNA nucleocapsid and the atomic model are deposited in the Electron Microscopy Data Bank and in the Protein Data Bank with accession codes EMDB-2867 and 4uft. The authors declare no competing financial interests. I.G., R.W.H.R., and G.S. designed the study; M.H. purified biological material; I.G., A.D., W.L.L., C.S., and G.S. performed research and analyzed data; R.W.H.R. and G.E. contributed to data interpretation; and I.G. wrote the paper with input from G.E.

SUPPLEMENTARY MATERIALS

www.sciencemag.org/content/348/6235/704/suppl/DC1
Materials and Methods
Figs. S1 to S4
Table S1
References (*24*–*35*)

23 December 2014; accepted 6 April 2015
Published online 16 April 2015;
10.1126/science.aaa5137

OPTOGENETICS

Engineering of a light-gated potassium channel

Cristian Cosentino,[1]* Laura Alberio,[1] Sabrina Gazzarrini,[1] Marco Aquila,[1] Edoardo Romano,[1] Solei Cermenati,[1] Paolo Zuccolini,[1] Jan Petersen,[2] Monica Beltrame,[1] James L. Van Etten,[3] John M. Christie,[2] Gerhard Thiel,[4] Anna Moroni[1]†

The present palette of opsin-based optogenetic tools lacks a light-gated potassium (K^+) channel desirable for silencing of excitable cells. Here, we describe the construction of a blue-light–induced K^+ channel 1 (BLINK1) engineered by fusing the plant LOV2-Jα photosensory module to the small viral K^+ channel Kcv. BLINK1 exhibits biophysical features of Kcv, including K^+ selectivity and high single-channel conductance, but reversibly photoactivates in blue light. Opening of BLINK1 channels hyperpolarizes the cell to the K^+ equilibrium potential. Ectopic expression of BLINK1 reversibly inhibits the escape response in light-exposed zebrafish larvae. BLINK1 therefore provides a single-component optogenetic tool that can establish prolonged, physiological hyperpolarization of cells at low light intensities.

Potassium ion (K^+) channels have a modular structure with sensor domains connected to a central ion-conducting pore (*1*). The pore integrates signals coming from the sensors and translates them into opening or closing the channel (*2*). This allows K^+ channels to alter the membrane potential of cells in response to a variety of physiological stimuli. Extending the range of signal inputs recognized by K^+ channels can be achieved by grafting exogenous sensor domains onto the pore module (*3*, *4*). With this modular interplay between sensor and pore, it is possible to engineer synthetic channels that respond to any signal by *ex novo* coupling of sensors to pores. This strategy provides new tools for the investigation and manipulation of biological functions (*5*). An attractive synthetic channel in this context is a light-gated K^+ channel, which is important because of the ability of K^+ to terminate excitatory currents within cells. This device would allow remote manipulation of the membrane potential with high temporal and spatial resolution and would represent an efficient control mechanism for many cellular processes, including neuronal firing and hormone release.

Several attempts have been made to create synthetic light-gated K^+ channels (*6*–*9*); however, these systems suffer from several shortcomings in that they require the addition of cofactors (*6*, *7*), are irreversible (*8*), or rely on multiple components (*9*). To overcome these obstacles, we engineered a single-component light-gated K^+ channel by fusing the LOV2-Jα photosensory region of a plant blue-light receptor (*10*) to the miniature K^+ channel pore Kcv (*11*). Rational design and directed evolution were employed to ultimately generate a blue-light–inducible K^+ channel that functions reversibly to drive cell membrane potentials to K^+ equilibrium in the absence of exogenous cofactors. The LOV2-Jα photoswitch from *Avena sativa* phototropin 1 (hereafter LOV) can be used to control protein activity by light-induced conformational changes (*12*). We therefore adopted this strategy to place Kcv under light control. LOV was fused to various regions of Kcv known to be mechanically important for channel gating (fig. S1A and constructs 3 to 12 in table S1).

A functional complementation approach based on the growth rescue of Δ*trk1* Δ*trk2* potassium transport–deficient yeast (strain SGY1528) (*13*) was adapted to screen for light-gated channel activity after replica plating (fig. S1B). One Kcv variant with LOV fused at the N terminus (LK) showed light-induced growth on selective agar (4 mM K^+) and liquid culture (fig. S1, B and C). LK was expressed in *Xenopus* oocytes and tested by a two-electrode voltage clamp. LK currents showed modest but reproducible increases in conductance after transfer from darkness to blue light (455 nm, 80 $\mu W/mm^2$) (fig. S2A). However, photostimulation of LK currents required tens of minutes to develop and appeared to be irreversible. In an attempt to enhance coupling of LOV to Kcv, the soluble photosensory region of LK was tethered to the plasma membrane. Introducing a putative myristoylation/palmitoylation sequence (MGCTVSAE) (*14*) at the N terminus of LK resulted in improved, but unexpected, properties. The new variant myLK (Fig. 1A and fig. S2B) showed an enhanced response to light compared with LK, but, in this case, light was found to inhibit rather than activate the channel conductance (fig. S2B). Moreover, the effect of light was reversible and it did not decrease after repetitive exposures. The light sensitivity of the channel was wavelength-specific, elicited by blue but not by red light (fig. S2B). The dynamic range of the light effect (DR), i.e., the ratio between light and dark current, was approximately 1.3. To improve the performance of myLK, three point

[1]Department of Biosciences, University of Milano, Italy. [2]Institute of Molecular, Cell and Systems Biology, University of Glasgow, UK. [3]Department of Plant Pathology and Nebraska Center for Virology, University of Nebraska-Lincoln, Lincoln, NE 68583-0900, USA. [4]Membrane Biophysics, Technical University of Darmstadt, Darmstadt, Germany.
*Present address: Illumina Italy, Via Senigallia 18/2, Milano 20161, Italy. †Corresponding author. E-mail: anna.moroni@unimi.it

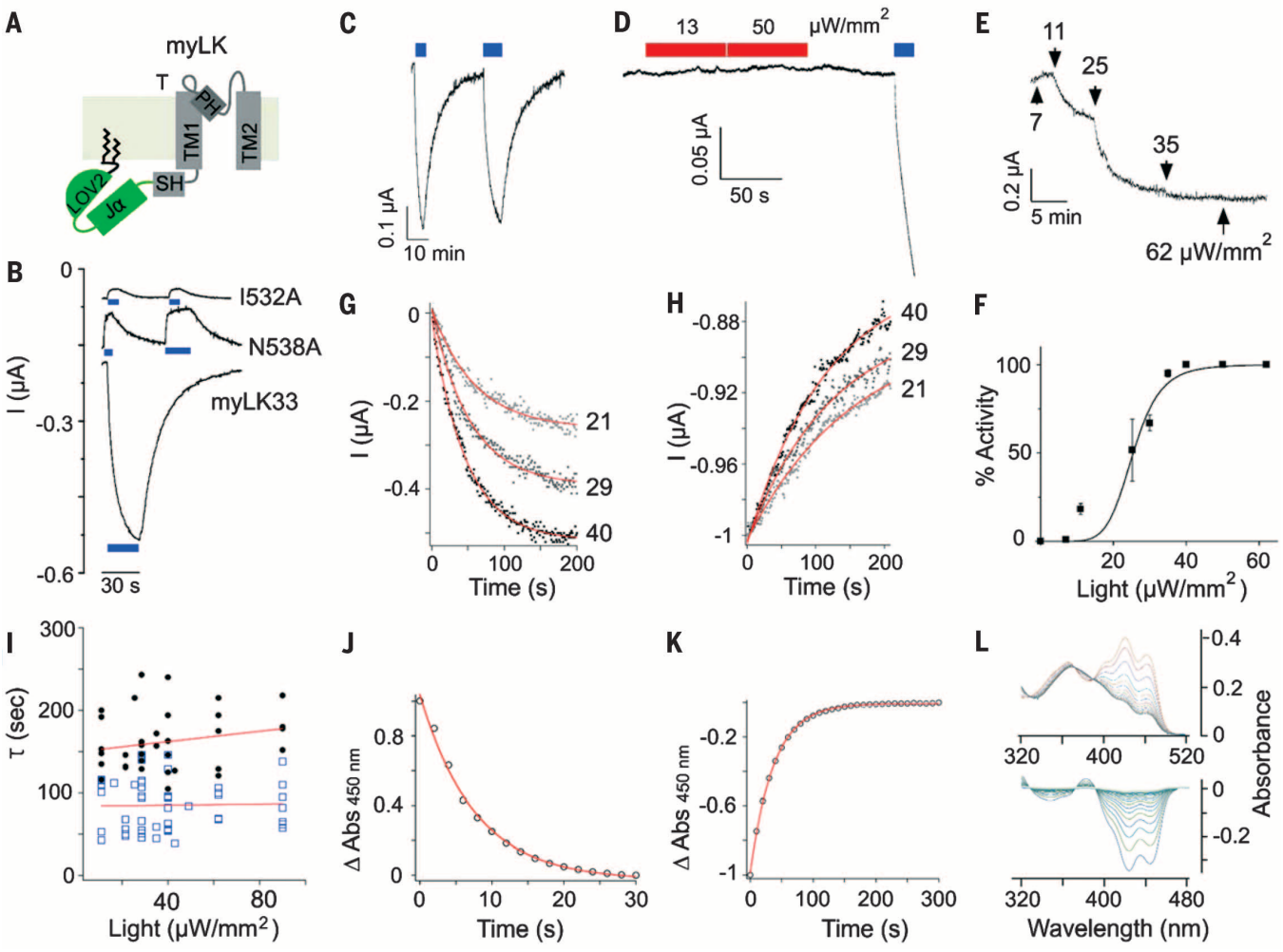

Fig. 1. Engineering and functional characterization of light-gated myLK channels. (**A**) Cartoon representation of myLK engineered by fusing LOV to Kcv with an additional N terminal myristoylation/palmitoylation sequence; myLK is shown as a monomer in the membrane. Kcv comprises slide helix (SH), pore-helix (PH), turret (T), and transmembrane domains (TM1 and TM2) (*23*). The LOV domain includes LOV2 and Jα (*10*). Jagged lines indicate lipid anchoring to the membrane. (**B**) Currents recorded at −60 mV in 100 mM $[K^+]_{out}$, from oocytes expressing myLK mutants: I532A, N538A, and myLK33. Note that myLK I532A and N538A conductances are inhibited by blue light (blue bars, 455 nm), whereas that of myLK33 is activated. (**C**) Repetitive photoactivation of myLK33 shows the reproducibility of the effect. (**D**) Red light (red bars, 617 nm) at two light intensities, 13 and 50 μW/mm^2, does not activate myLK33 current, whereas blue light does. (**E**) Current response of myLK33 to increasing light intensities recorded at −80 mV showing threshold (>7 μW/mm^2) and saturating (35 μW/mm^2) values of light intensity. (**F**) Dose-response curve obtained from $n = 4$ oocytes. Line indicates data fitting by a Hill-type equation, yielding a dissociation constant $k = 25$ μW/mm^2 and a Hill coefficient $n = 6$. (**G**) Kinetics of myLK33 activation by different intensities of blue light and (**H**) subsequent inactivation in the dark. An oocyte expressing myLK33 was exposed to a repetitive light/dark regime with increasing light intensities ranging from low (21 μW/mm^2) to medium (29 μW/mm^2) to saturating (40 μW/mm^2) intensities. The current responses to the three light treatments are normalized to common starting values $I = 0$ for the onset of channel activation and $I = -1$ for the start of current decay in the dark; numbers on current traces indicate the light intensities in μW/mm^2. Fitting of data with single exponential equation (red lines) yields similar τ_{on} values for low (21 μW/mm^2, $\tau = 49$ s), medium (29 μW/mm^2, $\tau = 52$ s), and high (40 μW/mm^2, $\tau = 59$ s) light intensity. Currents decay in the dark with the same velocity, irrespective of pretreatment with a high ($\tau = 148$ s), medium ($\tau = 137$ s), or low ($\tau = 158$ s) light. (**I**) τ_{on} (blue symbols) and τ_{off} (black symbols) from a large number of independent experiments plotted as a function of light intensity. (**J**) Photoadduct formation kinetics for myL (construct 13, table S1) expressed and purified from *Escherichia coli*. Light-induced absorption changes were recorded at 450 nm ($\Delta Abs_{450\ nm}$) in response to blue-light irradiation (455 nm, 90 μW/mm^2) and show exponential kinetics ($\tau_{on} = 7.6$ s). (**K**) Dark recovery of $Abs_{450\ nm}$ after light excitation shows exponential kinetics ($\tau_{off} = 38$ s). (**L**) Representative light-induced absorption spectra of myL recorded at 2-s intervals (upper panel) and light-minus-dark difference spectra recorded every 10 s (lower panel).

mutations (G528A, I532A, and N538A) known to augment LOV-effector protein interactions (*15*) were introduced into the construct, singly or in combination (constructs 15 to 21, table S1). Several of these variants exhibited robust differential growth over a range of selective conditions (fig. S3). Notably, two mutants, myLKI532A and myLKN538A, had increased DR values, 1.5 and 1.9, respectively (Fig. 1B), confirming that myLK architecture enables rational protein design.

To screen for additional DR improvements, random mutagenesis was performed using myLKN538A to generate a library of myLK-encoding sequences. Potassium transport–deficient yeasts, transformed with this mutant library, were grown initially on nonselective agar plates and then replica-plated onto selective medium before exposure to darkness or light. Yeast expressing the parental myLKN538A channel did not grow on media with $[K^+]_{out}$ below 4 mM. Thus, variants growing below this concentration were selected for further characterization. Thirty-five variants were obtained showing strong differential growth in the light (either

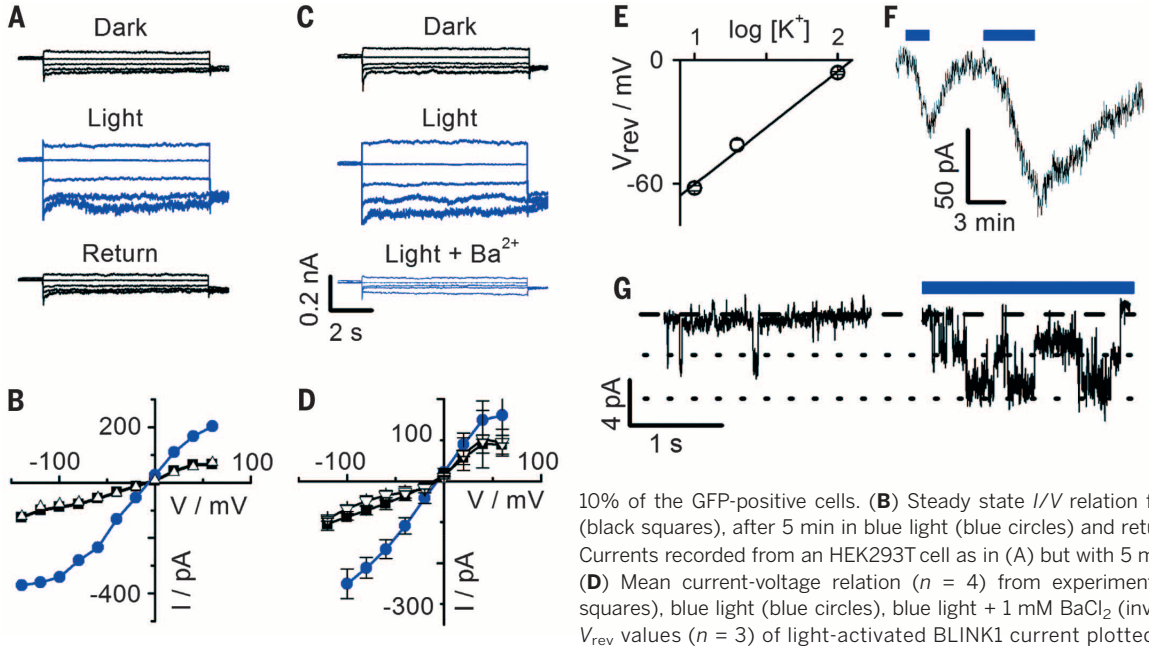

Fig. 2. Properties of BLINK1 in HEK293T cells. (**A**) Whole-cell currents recorded in HEK293T cells expressing myLJSK (BLINK1), in dark, blue light (455 nm, 40 μW/mm^2) and after returning to the dark. Voltage steps from +60 to –120 mV, tails at –80 mV (selected traces are shown every 40 mV). A measurable current, above the background, was found in about 8 to 10% of the GFP-positive cells. (**B**) Steady state *I/V* relation from currents in (A): dark (black squares), after 5 min in blue light (blue circles) and return in dark (triangles). (**C**) Currents recorded from an HEK293T cell as in (A) but with 5 mM of $BaCl_2$ added in light. (**D**) Mean current-voltage relation (n = 4) from experiments as in (B): dark (black squares), blue light (blue circles), blue light + 1 mM $BaCl_2$ (inverted triangles). (**E**) Mean V_{rev} values (n = 3) of light-activated BLINK1 current plotted as a function of $[K^+]_{out}$; slope = 58 mV/log $[K^+]$. Pipette solution contained 130 mM K^+. (**F**) Repetitive activation/deactivation of BLINK1 current at –70 mV by blue light/dark transitions. (**G**) Single-channel fluctuations recorded at –70 mV from the same BLINK1-expressing cell in dark (left) and in blue light (right). Dashed line indicates zero current level; dotted lines indicate apparent single-channel opening levels. Calculated single-channel conductance is 70 pS.

activation or inhibition), 13 of which survived a second round of selection (to eliminate false positives) and were sequenced. The recovered mutations mapped throughout the randomized portion of myLK, but a subset clustered around proline 13 of Kcv (fig. S4), a residue known to affect channel gating (*16*). Notably, one particular variant, myLK33 (construct 33, fig. S4), harboring a mutation in P13 (P13L) and in the myristoylation/palmitoylation sequence (A7T), was activated rather than inhibited by light, with a relatively large DR value (DR = 3) (Fig. 1B). MyLK33 was therefore chosen for extensive functional characterization.

The channel could be repeatedly activated by light when expressed in oocytes without undergoing apparent inactivation (Fig. 1C). Activation was blue-light specific because red light had no perceivable effect on channel activity (Fig. 1D). By exposing the oocyte to increasing light intensities (Fig. 1E), we obtained a sigmoidal current response with a distinct activation threshold (Fig. 1F). The mean dose-response curve was best fitted with a Hill function yielding a value for half-activation, k = 25 μW/mm^2, and a Hill coefficient n = 6. This operational light sensitivity of the cell is less by a factor of about 500 than that of cells expressing light-sensitive pumps such as NpHR (*17*).

To obtain information on the kinetics of channel activation/deactivation in light/dark, cells were irradiated with different intensities of blue light and transferred back into darkness. Activation and deactivation kinetics could be fitted with a single exponential function (Fig. 1, G and H). The time constants did not change over a wide range of light intensities, from suboptimal to saturating (Fig. 1I). Activation (τ_{on}, 87 ± 28 s, n = 52) was about twice as fast as deactivation (τ_{off} 168 ± 31 s, n = 43). To further examine the relationship between channel gating and the photocycle of the sensor, we performed spectroscopic measurements on the sensor portion of the protein (myL), which was used to construct the channel. Global photoadduct formation at saturating light intensity (90 μW/mm^2) and its recovery in the dark (Fig. 1, J to L) show exponential kinetics with values of 7.6 s for τ_{on} and 38 s for τ_{off}. Hence, myL activates, under the same light conditions, about 10 times as fast as the channel, whereas photoadduct decay is about 4.5 times as fast as channel deactivation in the dark. Thus, the primary light sensing by the photosensor seems to be only loosely correlated with channel gating. This agrees with the observation that other constructs harboring the same photoswitch as myLK33 (see, for example, I532A and N538A) responded to light with a different kinetics (Fig. 1B). Together, these findings suggest that light-regulated channel activity is mostly dominated by slow conformational changes that follow LOV2-Jα photoactivation.

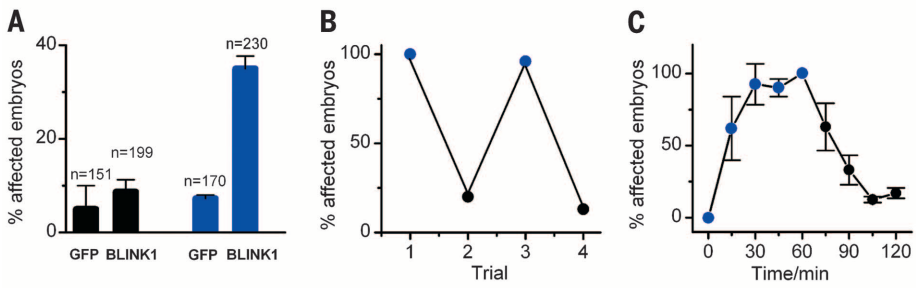

Fig. 3. Light controls the behavior of zebrafish expressing BLINK1. (**A**) Altered escape response in 2-day-old zebrafish, expressing BLINK1 or GFP. The embryos were injected at t_0, kept 24 hours in the dark, and then either exposed to blue light (80 μW/mm^2) (blue) or kept in the dark (black). The escape response was tested by gentle mechanical stimulation with a pipette tip (see movie S1). Number of embryos (n) is indicated. (**B**) Reversibility of the effect of blue light on the escape response. Each data point represents the response of a batch of 2-day-old BLINK1-injected embryos, preselected for positive light response (n = 15). The embryos were repetitively exposed to blue light (blue circles) and dark (black circles) treatments (30 to 45 min each). (**C**) Kinetics of the light effect on the escape response of 2-day-old embryos. At time zero, blue light was turned on and the response to mechanical stimulation was checked every 15 min. After 60 min, the effect reached the maximum and the light was turned off to monitor the deactivation kinetics. Data are from three experiments in which the n of responding embryos was 62 over a total number of 163 (38%). Data were normalized to the maximum number of responding embryos at plateau in each experiment (after 60 min of light).

Experimental evidence that myLK33 retains the pore properties of the parental K^+-selective channel Kcv is summarized in fig. S5. Barium, a known Kcv channel blocker, completely inhibited both dark- and light-induced currents of myLK33 (fig. S5A). The current-voltage (*I-V*) curve (fig. S5B) shows that light activation of myLK33 is voltage-independent. The reversal potentials (V_{rev}) of myLK33 photocurrent shifted according to the Nernst equation by 51 mV for a 10-fold increase in external K^+ concentration, a value similar to that of Kcv (*11*) (fig. S5C). Moreover, exchanging 100 mM external K^+ with Na^+ shifted V_{rev} to the left by 110 mV, indicating a very low Na^+ permeability (P_{Na}/P_K = 0.015 ± 0.001 (n = 4) (fig. S5D).

Despite these desirable features, in vivo application of myLK33 is hampered by its high dark activity. We have previously shown in other synthetic channels that the linker between the sensor and the effector module influences the coupling of the two (*4*). We therefore progressively reduced the linker region within myLK in an attempt to improve the control of the photosensor over the channel pore (constructs 23 to 37 in table S1 and fig. S6). Best results were obtained with myLJSK, which lacks the final nine amino acid residues within the Jα helix (fig. S7A). This variant showed stringent differential growth in the yeast complementation assay (fig. S7B) but was poorly expressed in oocytes. Immunolabeling showed that this channel is present on the membrane of human embryonic kidney 293T (HEK293T) cells, albeit at a moderate level, when compared with the parental channel Kcv (fig. S7C). Subsequent electrophysiological characterization in HEK293T cells demonstrated that myLJSK is activated by blue light (Fig. 2, A and B). Light activation is fully reversible in the dark (Fig. 2, A and B) and inhibited by Ba^{2+} (Fig. 2, C and D). Importantly, myLJSK lacks any channel activity in darkness, as evident from the comparison of the amount of current in the dark and in the presence of Ba^{2+} (fig. S7D). Channel opening moves the reversal potential of the cell with E_K, the K^+ equilibrium voltage (Fig. 2E). The light sensitivity of myLJSK occurs in the same range as that of myLK33, being saturated at ~60 $\mu W/mm^2$ (fig. S7E).

Light gating of myLJSK is best appreciated in gap-free recordings. Repetitive exposure to blue light caused rapid activation followed by deactivation in darkness (Fig. 2F). Data recorded from single-channel fluctuations (Fig. 2G) showed a light-induced increase in channel activity and indicated a unitary conductance of about 70 pS, consistent with the high conductance of Kcv and its synthetic variant Kv_{Synth1} (*4*). The high single-channel conductance and the relatively low macroscopic currents (≤400 pA at −100 mV) are consistent with the low number of channels, which were detectable by immunolocalization (fig. S7C). A low number of channel proteins with a large unitary conductance offers the advantage of an efficient control over the membrane voltage with minimal disturbance of the cell. These properties of myLJSK ultimately fulfilled our criteria for successful light gating of Kcv. Hence, we renamed this variant BLINK1, blue-light–induced K^+ channel 1. Expression of BLINK1 in Sf9 insect cells (fig. S8A) produced fluorescence properties that are characteristic for LOV-containing proteins (fig. S8, B and C). Photoadduct formation and decay for BLINK1 was therefore analyzed by fluorescence spectroscopy and showed kinetics similar to those obtained for myLOV in vitro (14.5 s for τ_{on} and 51s for τ_{off}) (fig. S8, D and E).

To determine the in vivo applicability of BLINK1 for optogenetics, we examined its ability to regulate the escape response of zebrafish embryos. Two-day old embryos respond to touch with a burst of swimming (*18*). We reasoned that BLINK1 photoactivation in zebrafish neurons (either somatosensory or motor) and/or in myocytes would prevent or drastically impair this behavior. Embryos injected with either BLINK1 or green fluorescent protein (GFP) RNA showed robust escape motions when kept in darkness [over 90% of embryos in both cases (BLINK1, n = 199; GFP, n = 151)]. By contrast, when embryos were exposed to blue light, 37% of BLINK1-expressing embryos exhibited a reduced escape response (n = 230) compared with just 9% in control larvae (n = 170) (Fig. 3A and movie S1). The blue-light effect was fully and repetitively reverted in darkness (Fig. 3B), as expected for a BLINK1-driven effect. The light-driven effect on embryonic escape motion developed with a half-time of 15 to 20 min and was reverted by dark with a similar kinetics (Fig. 3C).

Several additional observations underscored that BLINK1 was expressed in zebrafish and that altered behavior of the larvae was driven directly by its activation in blue light. First, the presence of the channel is detectable by Western blotting in BLINK1-injected embryos (fig. S9A). Second, the success of eliciting escape behavior was highly dependent on the wavelength of light with red light (617 nm) being ineffective at evoking altered behavior (fig. S9B). Third, in the dark, viability and morphology were similar in embryos expressing BLINK1 or GFP (wild-type embryos at 2dpf BLINK1 = 77%, n = 81; GFP = 69%, n = 59), confirming that BLINK1 is tightly closed in the absence of light. Taken together, these data demonstrate the ability of BLINK1 to modulate behavioral responses in vivo.

In conclusion, we have created a light-activated K^+ selective channel by combining a blue-light sensor and a simple K^+ channel pore. The resulting BLINK1 channel is fully genetically encoded and does not depend on external factors for its light regulation, as the flavin mononucleotide chromophore is ubiquitously present in cells. BLINK1 is therefore a promising tool in optogenetics and has several desirable properties relative to other light-gated pumps (*17*, *19*, *20*) and channels (*21*, *22*) used for inhibiting the functions of excitable cells. First, in contrast to light-gated pumps, which move H^+ or Cl^- ions, it moves K^+, a physiological ion, down its electrochemical equilibrium. Thus, BLINK1 does not expose the cell to unphysiological hyperpolarizations or ion gradients. Second, its large unitary conductance guarantees that a small number of channels can efficiently decrease the input resistance of cells and hyperpolarize the membrane. In addition, the channel does not inactivate in light, which allows long-term control of channel activity by light. The apparent sensitivity of BLINK1 to light, combined with its slow kinetics, makes it a powerful tool for long-term inhibition of cells at low light intensities. Our pilot experiments in zebrafish demonstrate that BLINK1 can be successfully used as an in vivo optogenetic tool. Besides an obvious application for inhibiting neuronal activity, this channel will also find applications in the control of cellular processes, which require long-term stabilization of the membrane voltage such as cell cycle regulation or the control of hormone secretion.

REFERENCES AND NOTES

1. S. B. Long, E. B. Campbell, R. Mackinnon, *Science* **309**, 897–903 (2005).
2. R. Latorre, F. J. Morera, C. Zaelzer, *J. Physiol.* **588**, 3141–3148 (2010).
3. U. M. Ohndorf, R. MacKinnon, *J. Mol. Biol.* **350**, 857–865 (2005).
4. C. Arrigoni *et al.*, *J. Gen. Physiol.* **141**, 389–395 (2013).
5. M. R. Banghart, M. Volgraf, D. Trauner, *Biochemistry* **45**, 15129–15141 (2006).
6. M. Banghart, K. Borges, E. Isacoff, D. Trauner, R. H. Kramer, *Nat. Neurosci.* **7**, 1381–1386 (2004).
7. H. Janovjak, S. Szobota, C. Wyart, D. Trauner, E. Y. Isacoff, *Nat. Neurosci.* **13**, 1027–1032 (2010).
8. J. Y. Kang *et al.*, *Neuron* **80**, 358–370 (2013).
9. D. Schmidt, P. W. Tillberg, F. Chen, E. S. Boyden, *Nat. Commun.* **5**, 3019 (2014).
10. J. M. Christie, *Annu. Rev. Plant Biol.* **58**, 21–45 (2007).
11. B. Plugge *et al.*, *Science* **287**, 1641–1644 (2000).
12. J. M. Christie, J. Gawthorne, G. Young, N. J. Fraser, A. J. Roe, *Mol. Plant* **5**, 533–544 (2012).
13. F. C. Chatelain *et al.*, *PLOS ONE* **4**, e7496 (2009).
14. C. Aicart-Ramos, R. A. Valero, I. Rodriguez-Crespo, *Biochim. Biophys. Acta* **1808**, 2981–2994 (2011).
15. D. Strickland *et al.*, *Nat. Methods* **7**, 623–626 (2010).
16. B. Hertel *et al.*, *Eur. Biophys. J.* **39**, 1057–1068 (2010).
17. J. Mattis *et al.*, *Nat. Methods* **9**, 159–172 (2011).
18. R. M. Colwill, R. Creton, *Rev. Neurosci.* **22**, 63–73 (2011).
19. F. Zhang *et al.*, *Nature* **446**, 633–639 (2007).
20. X. Han, E. S. Boyden, *PLOS ONE* **2**, e299 (2007).
21. A. Berndt, S. Y. Lee, C. Ramakrishnan, K. Deisseroth, *Science* **344**, 420–424 (2014).
22. J. Wietek *et al.*, *Science* **344**, 409–412 (2014).
23. S. Tayefeh *et al.*, *Biophys. J.* **96**, 485–498 (2009).

ACKNOWLEDGMENTS

We thank G. Romani for providing the antibody to Kcv; D. Minor for the *Saccharomyces cerevisiae* SGY1528 strain; U. P. Hansen, I. Schroeder, and A. Bertl for helpful discussion; and M. Ascagni for technical help with confocal microscopy. This work was supported by Fondazione Cariplo grant 2009-3519, PRIN (Programmi di Ricerca di Rilevante Interesse Nazionale) 2010CSJX4F, and MAE (Ministero Affari Esteri) 01467532013-06-27 to A.M.; by the UK Biotechnology and Biological Sciences Research Council (BB/J016047/1 and BB/M002128) to J.M.C.; and by the Landes-Offensive zur Entwicklung Wissenschaftlich-ökonomischer Exzellenz (LOEWE) initiative Soft Control to G.T.

SUPPLEMENTARY MATERIALS

www.sciencemag.org/content/348/6235/707/suppl/DC1
Materials and Methods
Figs. S1 to S9
Table S1
Movie S1
References (*24–31*)

11 November 2014; accepted 7 April 2015
10.1126/science.aaa2787

Engineering of a light-gated potassium channel
Cristian Cosentino *et al.*
Science **348**, 707 (2015);
DOI: 10.1126/science.aaa2787

Supplementary Materials for

Engineering of a light-gated potassium channel

Cristian Cosentino, Laura Alberio, Sabrina Gazzarrini, Marco Aquila, Edoardo Romano, Solei Cermenati, Paolo Zuccolini, Jan Petersen, Monica Beltrame, James L. Van Etten, John M. Christie, Gerhard Thiel, Anna Moroni*

*Corresponding author. E-mail: anna.moroni@unimi.it

Published 8 May 2015, *Science* **348**, 707 (2015)
DOI: 10.1126/science.aaa2787

This PDF file includes:

Materials and Methods
Figs. S1 to S9
Table S1
References

Other Supplementary Material for this manuscript includes the following:
(available at www.sciencemag.org/cgi/content/full/348/6235/707/DC1)

Movie S1

Supplementary Materials for

Engineering of a light-gated potassium channel

Cristian Cosentino, Laura Alberio, Sabrina Gazzarrini, Marco Aquila, Edoardo Romano, Solei Cermenati, Paolo Zuccolini, Jan Petersen, Monica Beltrame, James L. Van Etten, John M. Christie, Gerhard Thiel and Anna Moroni

This section includes:

Materials and Methods
Figures S1-S9
Tables S1
Movie S1
Supplementary References

Materials and Methods:

Cloning procedures and plasmids

All constructs were prepared by adding the LOV2 domain, aa 404-546 of *Avena sativa* Phototropin 1 (NPH1-1 GenBank: AAC05083.1) (*24*) to Kcv, aa 2-94 of chlorovirus PBCV-1-Kcv (NP_048599.1) (*11*) by overlapping PCR. The complete list of mutations, deletions and insertions, which were introduced in each construct, is reported in Table S1. Mutations introduced either in the LOV domain or in Kcv are numbered on the original sequences of phototropin and Kcv. Overlapping PCR was used to add the N-terminal myristoylation and palmitoylation sequence (MGCTVSAE) (*14*) to the N terminus of the construct and QuikChange XL II (Agilent Technologies) was used to introduce point mutations. Coding sequences were cloned in pYES2-Met25 vector (*25*) for *S.*

cerevisiae expression; in pSGEM (a modified version of pGEM-HE vector) for expression in *Xenopus laevis* oocytes; in pCDNA3.1+ for HEK293T cells expression; in a modified version of pET-21d containing a 7His-Strep II-SUMO tag (*26*) for expression in *E. coli* and in pCS2+ for zebrafish expression. The plasmid for expression in SF9 *Spodoptera frugiperda* cells was built by Gibson assembly (*27*) using pAcHLT-A digested with *Sph*I and *Sac*I as backbone, a fragment amplified from pAcHLT-A (base pairs 215-2203) and the BLINK1 coding sequence amplified with a 3' primer creating a C-terminal 6His-tag.

Yeast functional complementation assays

Functional complementation assays were performed using the *S. cerevisiae* strain SGY1528 (*MATa ade2–1 can1–100 his3–11,15 leu2–3,112 trp1–1 ura3–1 trk1::HIS3 trk2::TRP1* (*25, 28*) This strain lacks the endogenous K^+ uptake system and it is not able to grow on media supplemented with K^+ lower than 100 mM.

To test the functionality of the clones, yeast colonies were inoculated in non-selective medium (SD -Ura, 100 mM KCl) and grown overnight to stationary phase. Cultures were then diluted to OD_{600} = 0.8 and 10-fold serial dilutions were spotted (7µl) onto selective plates (SEL -Ura -Met with 0.5, 1, 4 mM KCl). Twin plates were prepared for each K^+ concentration and were either exposed to blue light or grown in the dark. After 3 and 4 days at 30°C images were taken and plates were screened for colonies with differential growth between Blue light and dark in the presence of low KCl concentration. To confirm functional complementation, cultures from overnight stationary phase were also inoculated in liquid selective media (SEL -Ura -Met with 4, 7, 10, 100 mM KCl) and grown for up to 117 h in presence of blue light or in the dark. OD_{600} of the cultures were measured to determine the growth ratio between the two conditions at 21, 45, 52 and 117 h after inducing protein expression. Positive clones were selected for plasmid isolation and DNA amplification in *E. coli* for sequencing. Non-selective and selective media were prepared as previously described (*25*). Solid media were obtained adding 15g/l agar.

Yeast random library screening

Randomization was performed on the sequence coding the myristoylation and palmitoylation domain, the whole LOV domain and the Kcv channel up to the first transmembrane region, where the channel DNA sequence has an endogenous *Sma*I restriction site. Random mutagenized libraries were generated using the Gene Morph II random mutagenesis kit (Agilent Technologies) in three steps: two samples with 50 ng of myLK N538A were amplified by PCR (30 cycles) with PAGE-purified 60-mer primers (IDT-Tema Ricerca). The forward primer is complementary to the upstream plasmid sequence while the reverse primer is complementary to the Kcv sequence downstream of the *Sma*I restriction site (corresponding to the first transmembrane region). Two µl of each PCR reaction were used as template for a subsequent amplification reaction (30 cycles). This was repeated twice. The end products of the final six reactions were gel-purified, grouped and gap-repaired in yeast SGY1528 strain with *Sma*I linearized pYES2-Met25 plasmid containing wild- type myLK N538A. Co-transformation was performed with a Frozen-EZ yeast transformation II kit (Zymo Research). The library was first plated on non-selective medium (SD –Ura with 100 mM KCl) and grown for 3 days at 30 °C, in dark, yielding roughly 20000 transformed colonies. Non-selective plates were then replica-plated twice onto selective plates (SEL –Ura -Met with 0.5 mM KCl) and grown for 3 days at 30 °C under blue light or dark conditions. Colonies showing differential growth between the two conditions were selected for subsequent functional complementation assays.

Electrophysiology

***Xenopus* oocytes -** cRNAs were transcribed in vitro using T7 RNA polymerase (Promega) as described (*11*). Oocytes were prepared according to standard methods and injected with 50 nl of water or 50 nl of cRNA (0.8 µg/µl) and incubated in the dark at 19°C in ND96 solution : 96 mM NaCl, 2 mM KCl, 1.8 mM $CaCl_2$, 1mM $MgCl_2$, 5 mM HEPES–NaOH buffer (pH 7.5), 5 mM sodium pyruvate, 50 µg /ml gentamicin). Measurements were performed 2-5 days after injection. Currents

were recorded by two-electrode voltage clamp, using the Gene-Clamp 500 amplifier (Axon Instruments) under control of pCLAMP7. Oocytes were perfused at room temperature with a solution containing: 100 mM KCl, 1.8 mM $CaCl_2$, 1 mM $MgCl_2$, and 5 mM HEPES-KOH buffer (pH 7.4). When different KCl concentrations were used, the osmolarity was adjusted to 215 mOsm with mannitol. The voltage protocols applied consisted in a step protocol of 20 mV steps from + 60 to -180 mV or in a gap free protocol at -60 or -80 mV. The channel blocker $BaCl_2$ was applied to the external solution at a concentration of 1 or 5 mM, as indicated.

HEK293T cells - HEK293T cells were cultured in Dulbecco's modified Eagle's medium (Euroclone) supplemented with 10% fetal bovine serum (Euroclone), 100 IU/mL of penicillin and 100 µg/ml of streptomycin, and stored in a 37 °C humidified incubator with 5% CO_2. BLINK1 and myLK33 cDNAs were co-transfected in HEK293T with a plasmid containing green fluorescent protein (GFP). Transfections were performed with TurboFect Transfection Reagent (Thermo Scientific). One to two days after transfection, HEK293T cells were dispersed by trypsin treatment and placed on 35-mm plastic petri dishes. Cells showing a clear fluorescence signal were selected for patch clamp analysis. Membrane currents were recorded in whole cell configuration using a Dagan 3900A patch-clamp amplifier and digitized using a Digidata 1322A controlled by pCLAMP 9.2. The pipette solution contained: 10 mM NaCl, 130 mM KCl, 2 mM $MgCl_2$, and 5 mM HEPES–KOH buffer (pH 7.2). The extracellular bath's solution contained: 100 mM KCl, 80 mM D-Mannitol, 1.8 mM $CaCl_2$, 1 mM $MgCl_2$ and 5 mM HEPES–KOH buffer (pH 7.4). When different KCl concentrations were used, the osmolarity was adjusted to 290 mOsm with mannitol. The channel blocker $BaCl_2$ was applied to the external solution at a concentration of 1 or 5 mM.

Light stimulation

Yeast functional complementation assays were performed by means of a custom-made array of light emitting diodes (LEDs) (Royal-Blue LED, λ 447 ± 10 nm, LUXEON Rebel LED) for homogeneous

illumination of the samples (2 ± 0.2 μW/mm^2) in a controlled temperature chamber. The same system was used for illumination of zebrafish embryos at 80 μW/mm^2. Red light was also provided at 80 μW/mm^2 by means of Red-Orange LED, λ 617 nm (MR-H2060-20T, LUXEON Rebel LEDs). Transfected HEK293T cells and injected oocytes were protected from ambient light to prevent receptor activation prior to the assays and all manipulations were performed under red light (MR-H2060-20T, LUXEON Rebel LEDs Red-Orange (617 nm)) in the Faraday cage shielded with a 580 nm cutoff filter (Rosco Supergel, Deep Amber #22). Blue light was provided by a light-emitting diode (Royal Blue, 455 nm, High-Power LED; Thorlabs) at intensity indicated in figure legends. Light power was measured using a handheld light power meter (Thorlabs).

Protein expression and spectroscopic analysis

For protein expression and purification, *E. coli* RosettaBL21(DE3)pLysS (Novagen) cells were grown in LB medium to an OD_{600} of 0.6, induced with 0.5 mM IPTG and incubated overnight at 24 °C. Cells were harvested and tandem affinity purified with subsequent SUMO protease cleavage of the tag as described (*26*).

Sf9 insect cells were grown in a monolayer with TC100 medium containing 10% FBS at 27 °C. For the construction of recombinant virus the transfer vector was co-transfected into cells with linearized baculovirus DNA using the BacMagic DNA Kit (Novagen). Transfected cells were incubated for 5 days to raise the primary viral stock. Two additional rounds of virus propagation (each for 3 days) were performed. High titer virus was used for protein expression. Cells were incubated in medium supplemented with 20 μM riboflavin for 3 days in darkness prior to harvest. For fluorescence emission and excitation measurements, the cells were washed to remove residual riboflavin and resuspended in Dulbecco's PBS at a density of 1.5 x 10^7 cells/ml.

Absorption spectra of purified protein from *E. coli* were collected with a Shimadzu MultiSpec-1501 diode array spectrophotometer at room temperature. *In vivo* fluorescence emission and excitation spectra of insect cells were recorded using a Perkin-Elmer LS-55 luminescence spectrometer. Fluorescence excitation spectra were recorded by monitoring the emission at 520 nm. Fluorescence emission spectra were obtained using an excitation wavelength of 450 nm. For absorbance and fluorescence measurements, a blue-light emitting diode (λ 455 nm) provided the excitation pulse.

Immunocytochemistry

HEK293T cells transfected with BLINK1 and Kcv-GFP (*29*) channels were treated with blocking solution containing 2% BSA in PBS. Cells were incubated 1 hour with anti-Kcv monoclonal antibody (*30*) washed briefly with blocking solution and incubated 1 hour with Alexa Fluor® 594 AffiniPure secondary antibody and Hoechst dye. Confocal microscopy analyses were performed using Leica SP2 (http://www.leica-microsystems.com) laser scanning confocal imaging system.

Microinjections and touch response assays in zebrafish

pCS2+BLINK1 and pCS2+GFP constructs were linearized with *Not*I and transcribed with Sp6 RNA polymerase, using the mMESSAGE mMACHINE® SP6 Transcription Kit (Ambion) and following manufacturer's instructions. Embryos were injected at the 1- to 2-cell stage with 200pg/embryo of RNA in water (W3500, Sigma-Aldrich), supplemented with rhodamine-dextran (D1817, Molecular Probes) as a tracer. Injected embryos were raised in E3 medium (5 mM NaCl, 0.17 mM KCl, 0.33 mM $MgSO_4$, 0.33 mM $CaCl_2$) at 28.5 °C and manually dechorionated at 1 day post-fertilization (1 dpf). The screening for touch-evoked escape response was performed at 2 days post-fertilization (unless differently specified), following standardized procedures. Using a hand-broken microloader tip, a gentle stimulus was applied to the tail of the embryos and their reaction observed. Wild-type embryos at this developmental stage swim away from the source of the stimulus (*31*).

Western blot

Yeast microsome preparation-Yeast cells grown in liquid culture in selective medium for 3 days at 30 °C were pelleted (1,500 x *g*, 20 min). Pellet was resuspended in Breaking Buffer (50 mM NaH2PO4*H2O, 1 mM EDTA, 5 % (w/v) glycerol, 5µM Leupeptin, 1µM Pepstatin, 0.1mM PMSF, 5mM DTT). Cells were broken by vortexing with glass beads (425-600 µm, Sigma-Aldrich) and centrifugated (4000 x *g*, 5 min) to remove cell debris. Then, the Eppendorf tube was centrifuged (15,000 x *g*, 1 hour) at 4°C and the supernatant was discarded. The microsomes were resuspended in Breaking Buffer and stored at -80 °C.

Preparation of zebrafish lysates- Deyolked embryos were resuspended in modified RIPA buffer (50mM Tris, 150mM KCl, 0.1%SDS, 5%DOC, 0.1% NP-40, filter sterilized) and homogenized using IKA T10 basic homogenizer. Lysates were quantified and stored at -80°C.

Insect cell protein extract - Cells were harvested (1,000 x *g*, 1min) and resuspended in Dulbecco's phosphate buffered saline supplemented with cOmplete EDTA-free protease inhibitor (Roche). Lysis of cells was performed by sonication with subsequent centrifugation (14,000 x *g*, 5 min) to remove cell debris.

Western blot analysis- 60 µg (zebrafish) or 13µg (yeast) /lane of total protein were separated on 4-20% tris-glycine denaturating gel (Novex). Proteins were blotted on a PVDF membrane and blots were blocked in 5% dry milk in TBST solution for 2 hours and incubated with primary anti-Kcv monoclonal antibody (*30*) at 4 °C overnight. Then the blots were rinsed in TBST for 3 X 10 min and incubated with alkaline phosphatase-conjugated secondary antibody for 1 hour. Antibody binding was detected using SIGMAFAST BCIP/NBT tablet (Sigma).

For immunodetection of BLINK1 protein expressed in insect cells, 20 µg of total protein were separated by SDS-PAGE on a 4-20% gradient gel (BioRad) and transferred to a nitrocellulose membrane. The membrane was blocked for 1 h with TBST containing 4% milk powder, followed by 1 h incubation with the first antibody (anti-Kcv). Afterwards the membrane was washed 3 x TBST

for 10 min each, incubated with the secondary HRP conjugated antibody for 45 min and then washed again as described before. Detection of immune complexes was made with ECL (Pierce) according to manufacturer's instructions and a Fusion Fx imager (peqlab) used to record the signal.

Table S1. List of constructs and details on their sequences. L= LOV domain (LOV2 and Jα); K= Kcv; my= myristoylaytion and palmytoylation sequence MGCTVSAE; GIN= mutations G528A, I532A and N538A (NPH1.1 numbering); M = methionine residue inserted N terminal to L. All constructs have been functionally characterized in yeast or/and in oocytes.

	NR	NAME	DETAILS
CONTROLS	1	Kcv	Kcv PBCV-1 (1-94)
	2	L	AsPhotI (404-546) NPH1.1, GenBank: AAC05083.1
LOV COUPLING TO KCV	3	KL	PBCV-1 (1-94) ::LOV2 (404-546)
	4	KldL	PBCV-1 (1-94) ::D ::LOV2 (404-546)
	5	KPPL	PBCV-1 (1-32) ::LOV2 (404-546) ::PBCV-1 (44-94)
	6	KGGL	PBCV-1 (1-34) ::LOV2 (404-546) ::PBCV-1 (33-94)
	7	KLK	PBCV-1 (1-94) ::LOV2 (404-546) ::PBCV-1 (3-94)
	8	LK	M ::LOV2 (404-546) ::PBCV-1 (3-94)
	9	LK SΔ2	M ::LOV2 (404-544) ::PBCV-1 (3-94)
	10	LK SΔ6	M ::LOV2 (404-544) ::PBCV-1 (7-94)
	11	LK SΔ10	M ::LOV2 (404-544) ::PBCV-1 (11-94)
	12	LSK	M ::LOV2 (404-522) ::PBCV-1 (3-94)
my CONTROLS	13	myL	my(1-8) ::LOV2 (404-546)
	14	myLK	my(1-8) ::LOV2 (404-546) ::PBCV-1 (3-94)
RATIONAL MUTAGENESIS	15	myLK I	my(1-8) ::LOV2 (404-546) I532A ::PBCV-1 (3-94)
	16	myLK G	my(1-8) ::LOV2 (404-546) G528A ::PBCV-1 (3-94)
	17	myLK N	my(1-8) ::LOV2 (404-546) N538A/E ::PBCV-1 (3-94)
	18	myLK GN	my(1-8) ::LOV2 (404-546) G528A N538A/E ::PBCV-1 (3-94)
	19	myLK IN	my(1-8) ::LOV2 (404-546) I532A N538A ::PBCV-1 (3-94)
	20	myLK GI	my(1-8) ::LOV2 (404-546) G528A I532A ::PBCV-1 (3-94)
	21	myLK GIN	my(1-8) ::LOV2 (404-546) G528A I532A N538A ::PBCV-1 (3-94)
RANDOM MUTAGENESIS	22	myLK33	my(1-8) A7T ::LOV2 (404-546) N538A ::PBCV-1 (3-94) P13L
LINKER MODIFICATIONS	23	myLK33 Δ6	my(1-8) A7T ::LOV2 (404-546) N538A ::PBCV-1 (9-94) P13l
	24	myLK33 Δ9	my(1-8) A7T ::LOV2 (404-543) N538A ::PBCV-1 (9-94) P13l
	25	myLK33 Δ28	my(1-8) A7T ::LOV2 (404-522) N538A ::PBCV-1 (7-94) P13l
	26	myLK33 Δ(KEL)	my(1-8) A7T ::LOV2 (404-543) N538A ::PBCV-1 (3-94) P13l
	27	myLK Δ9	my(1-8) ::LOV2 (404-541) ::PBCV-1 (7-94)
	28	myLSK	my(1-8) ::LOV2 (404-522) ::PBCV-1 (3-94)
	29	myLJ21SK	my(1-8) ::LOV2 (404-543) ::PBCV-1 (6-94)
	30	myLJ18SK	my(1-8) ::LOV2 (404-540) ::PBCV-1 (6-94)
	31	myLTKdp	my(1-8) ::LOV2 (404-522) ::PBCV-1 (13-94)
	32	myLTKep	my(1-8) ::LOV2 (404-517) ::PBCV-1 (12-94)
	33	myLTKdr	my(1-8) ::LOV2 (404-522) ::PBCV-1 (10-94)
	34	myLJK	my(1-8) ::LOV2 (404-544) ::PBCV-1 (11-94)
	35	myLJSK	my(1-8) ::LOV2 (404-537) ::PBCV-1 (3-94)
	36	myLK Δ(KEL)	my(1-8) ::LOV2 (404-543) ::PBCV-1 (3-94)
	37	myLK N Δ(KEL)	my(1-8) ::LOV2 (404-543) N538A ::PBCV-1 (3-94)

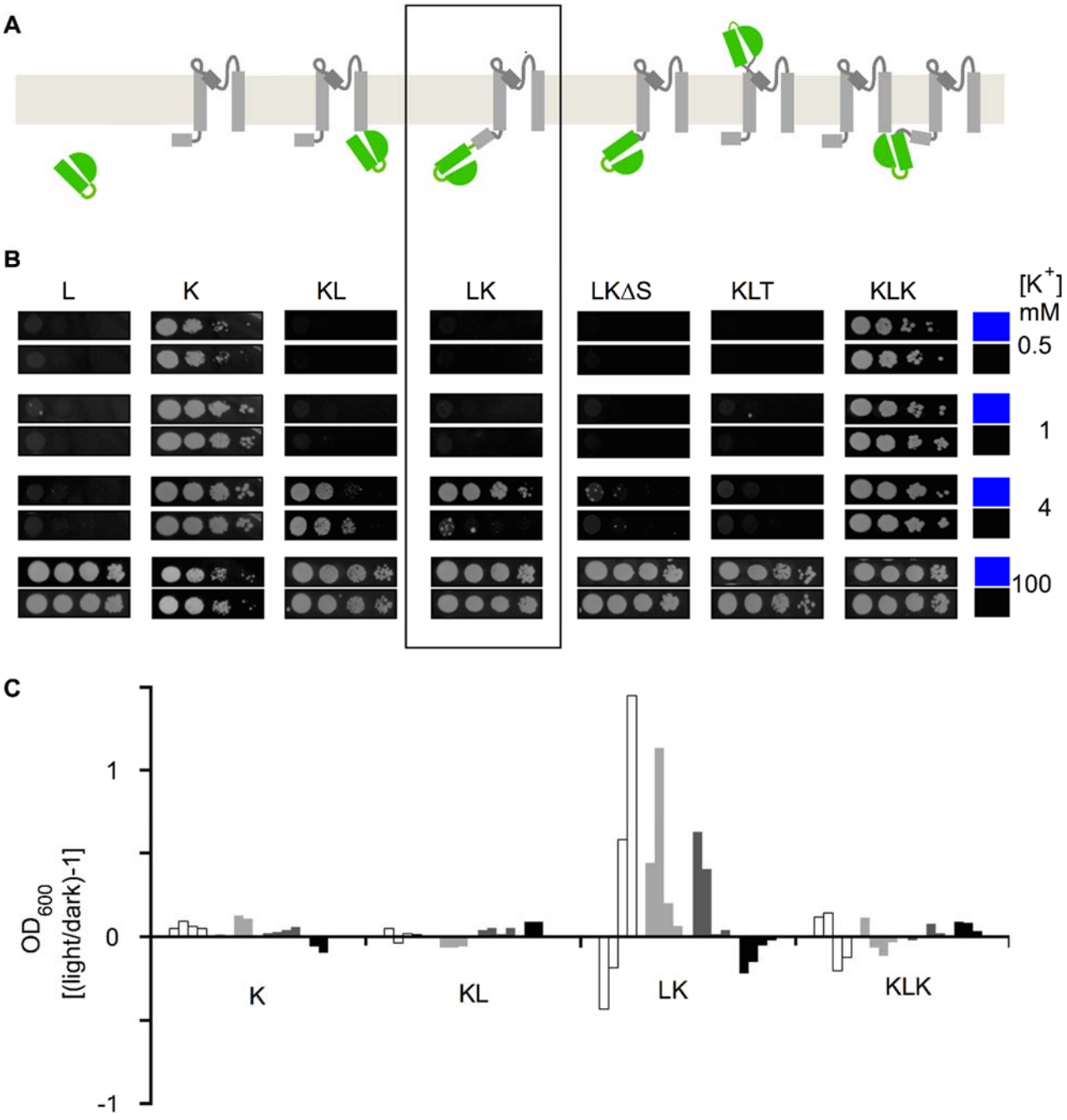

Figure S1. Steps to developing rudimental light sensitivity in the K^+ channel Kcv
(A) Cartoon representation of the constructs engineered by fusing the light sensor to several positions. LOV domain is in green; Kcv in grey. The constructs are shown as monomers inserted into the lipid bilayer. (B) Functional complementation of *Δtrk1 Δtrk2* potassium transport deficient yeast growth in solid medium with the above constructs named as follow: L, LOV domain; K, Kcv; ΔS, deletion of the N terminal slide helix (S) of Kcv; T, turret. Serial dilutions of overnight cultures were spotted onto solid medium plates containing 0.5, 1, 4 and 100 mM K^+ and exposed either to dark (black square) or blue light (447 ± 10 nm, 2 ± 0.2 µW/mm^2) (blue square). Images were taken after 3 days. Boxed is the LK construct, which was selected for further improvement. (C) Yeast growth complementation with light-gated channel candidates in liquid medium. *Δtrk1 Δtrk2* potassium transport deficient yeast transformed with a selection of the constructs above (K, KL, LK and KLK) was grown in liquid medium in dark and blue light. The medium contained 4, 7, 10 and 100 mM KCl, shown by increasing grey-levels. The four bars of the same color indicate, from left to right, the values of the OD_{600} ratio [(light/dark)-1] measured after 21 h, 45 h, 52 h and 117 h.

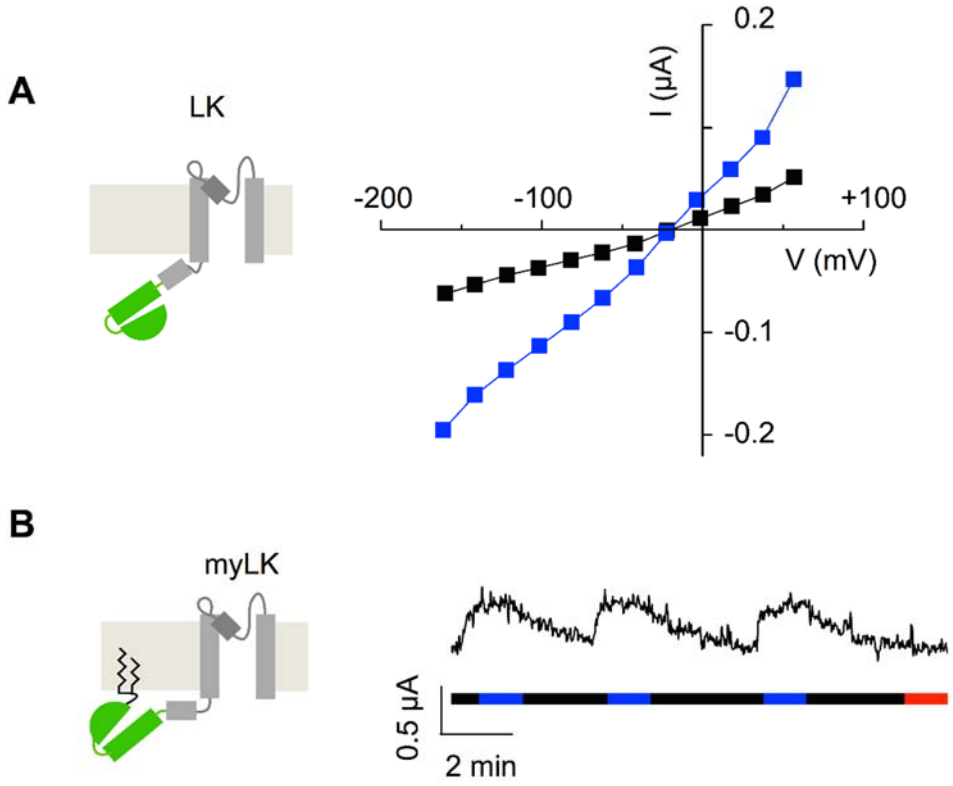

Figure S2. Current recordings from LK and myLK channels in dark and light.
(A) Cartoon representation and current-voltage relationship of LK recorded in *Xenopus* oocyte in the dark (■) and after 10 min of blue light (455 nm, 80 µW/mm^2) (■). External solution contained 50 mM [K^+]. (B) Cartoon of myLK with the N-terminal myristoylation and palmitoylation sequence. Continuous current recording at -60 mV in 50 mM $[K^+]_{out}$ from one oocyte expressing myLK. The oocyte was exposed to dark/light cycles, including blue light (455 nm) and red light (617 nm).

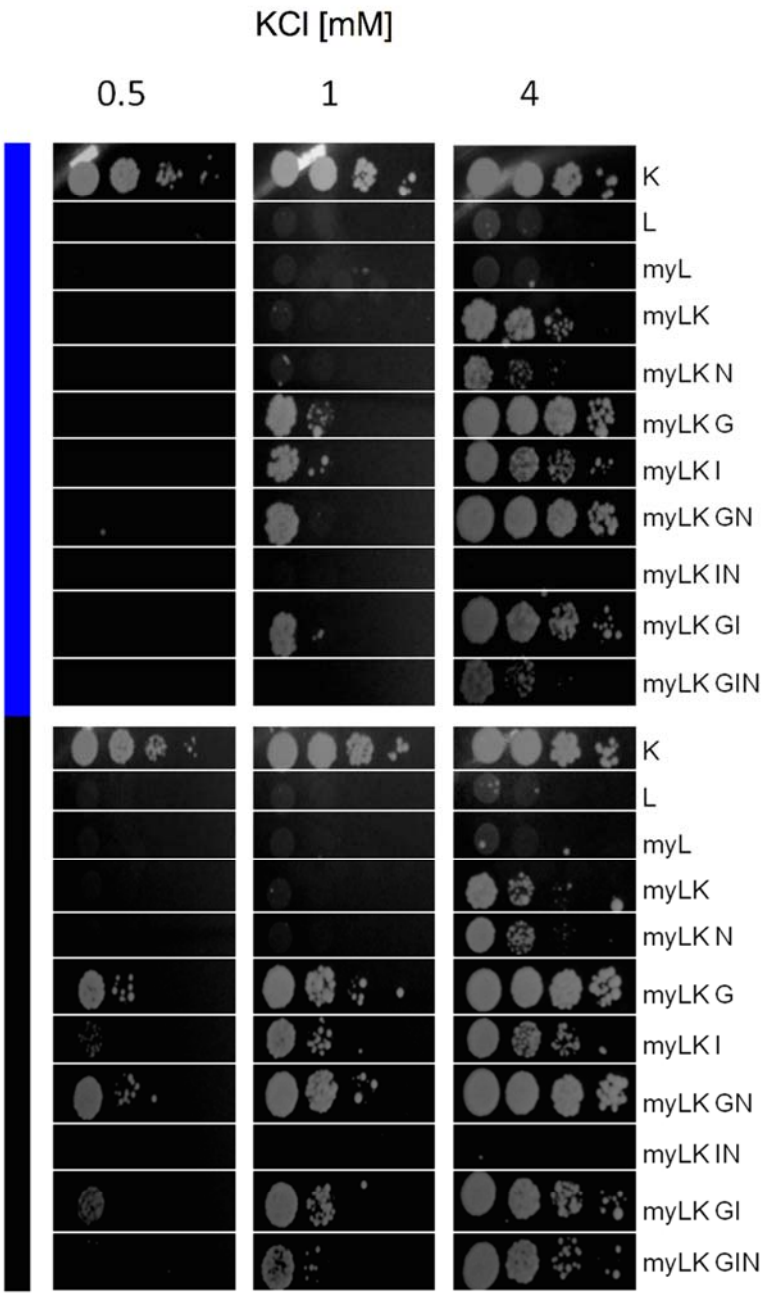

Figure S3. Impact of mutations introduced in myLK on functional complementation of yeast. Mutations introduced in the Jα region of myLK were: G528A, I532A and N538A (in short GIN). For functional complementation details see fig. S1B.

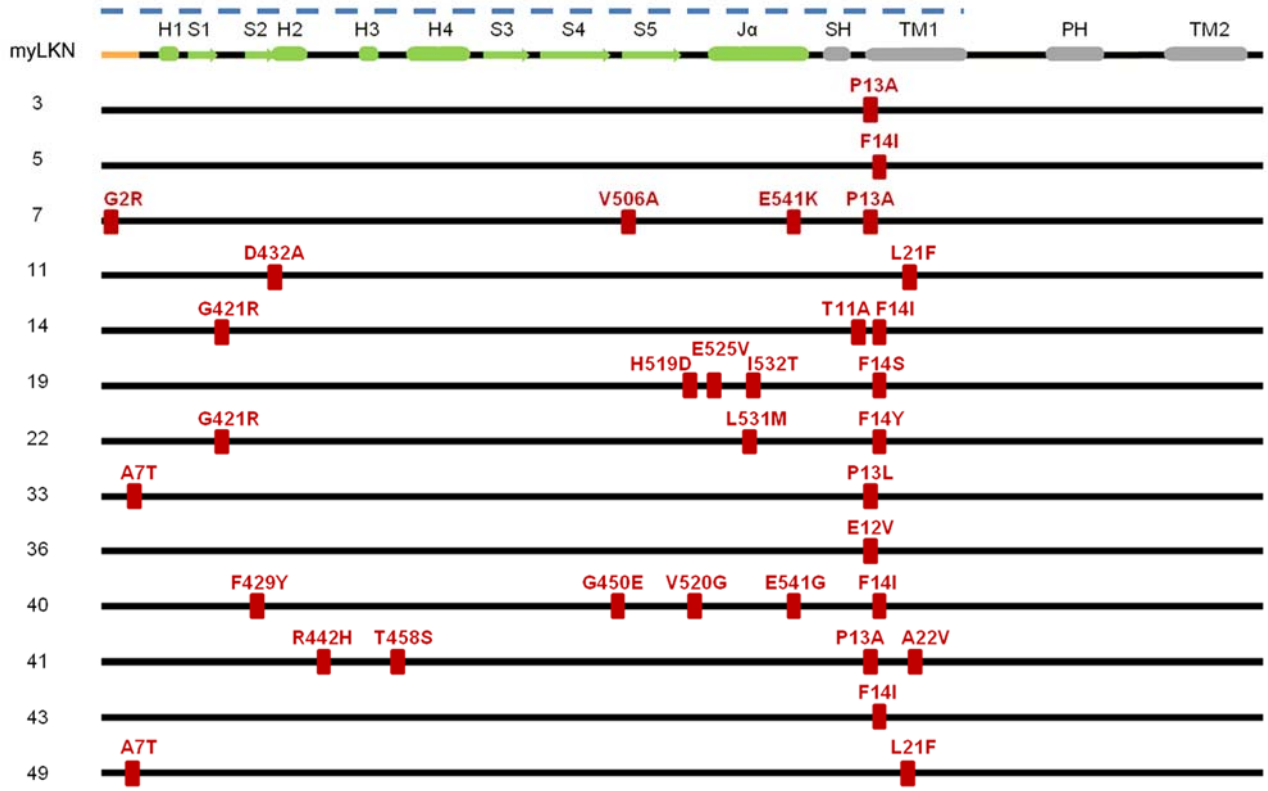

Figure S4. List of clones retrieved from library screening

List of 13 clones selected from a library of myLKN538A (myLKN) mutants and schematic representation of the mutations found and of their position in the sequence, represented by a black line. Colored elements, indicated on the myLKN sequence, are as follow: orange, myristoylation and palmytoylation sequence; green, secondary structures of LOV domain (H1-H4, α helices; S1-S5, beta sheets and Jα); grey, secondary structures of Kcv (SH, TM1, PH, TM2, see fig. 1A). Dotted line marks the randomized portion of the channel. LOV mutations are numbered on NPH1.1 sequence (AAC05083.1), while those on Kcv are numbered on PBCV-1-Kcv sequence (NP_048599.1).

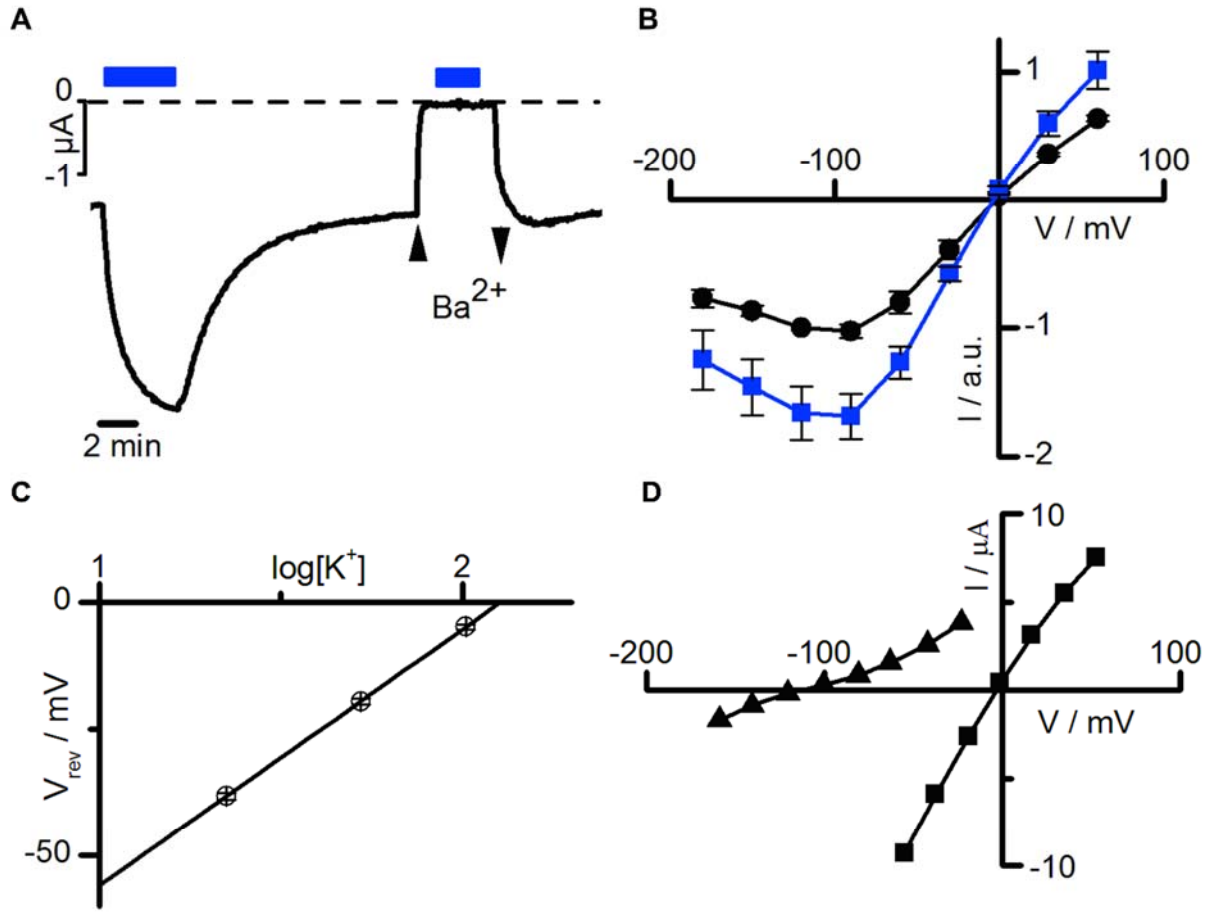

Figure S5. Electrophysiological properties of myLK33 in *Xenopus* oocytes
(A) Effect of blue light on the inward current recorded from one oocyte expressing myLK33, at -80 mV in 50 mM $[K^+]_{out}$. Dotted line indicates zero current level. Bars indicate illumination with blue light (40 µW/mm^2). Arrowheads indicate addition and removal of 1 mM $BaCl_2$ from the solution. (B) Mean I/V relationship obtained from n= 5 oocytes: (●) dark, (■) light. Values normalized to the dark current at – 120 mV are expressed in arbitrary units (a.u.). (C) Nernst plot with V_{rev} shown as a function of $[K^+]_{out}$ calculated assuming $[K^+]_{in}$ = 110 mM (*11*). Regression line has a slope of -51mV per log unit $[K^+]_{out}$. (D) I/V curves around V_{rev} of the photocurrent recorded either in 100 mM $[KCl]_{out}$ (■) or $[NaCl]_{out}$ (▲).

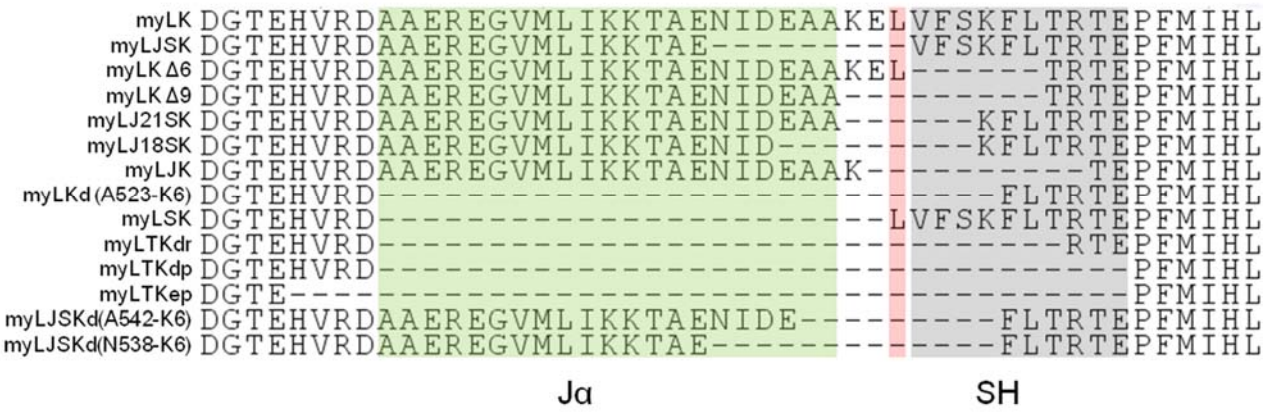

Figure S6. Modification of the linker sequence connecting the myL domain to Kcv
List of myLK clones and their amino acid sequences showing the modifications introduced in the linker region connecting Jα (residues 523-543 of LOV) (green) to the slide helix (SH, residues 3-12 of Kcv) (grey). The three central residues lysine, glutamate and leucine (KEL), belong to a short loop that follows Jα in LOV. Leucine (pink) is also the starting amino acid of Kcv sequence, after removal of the initial methionine.

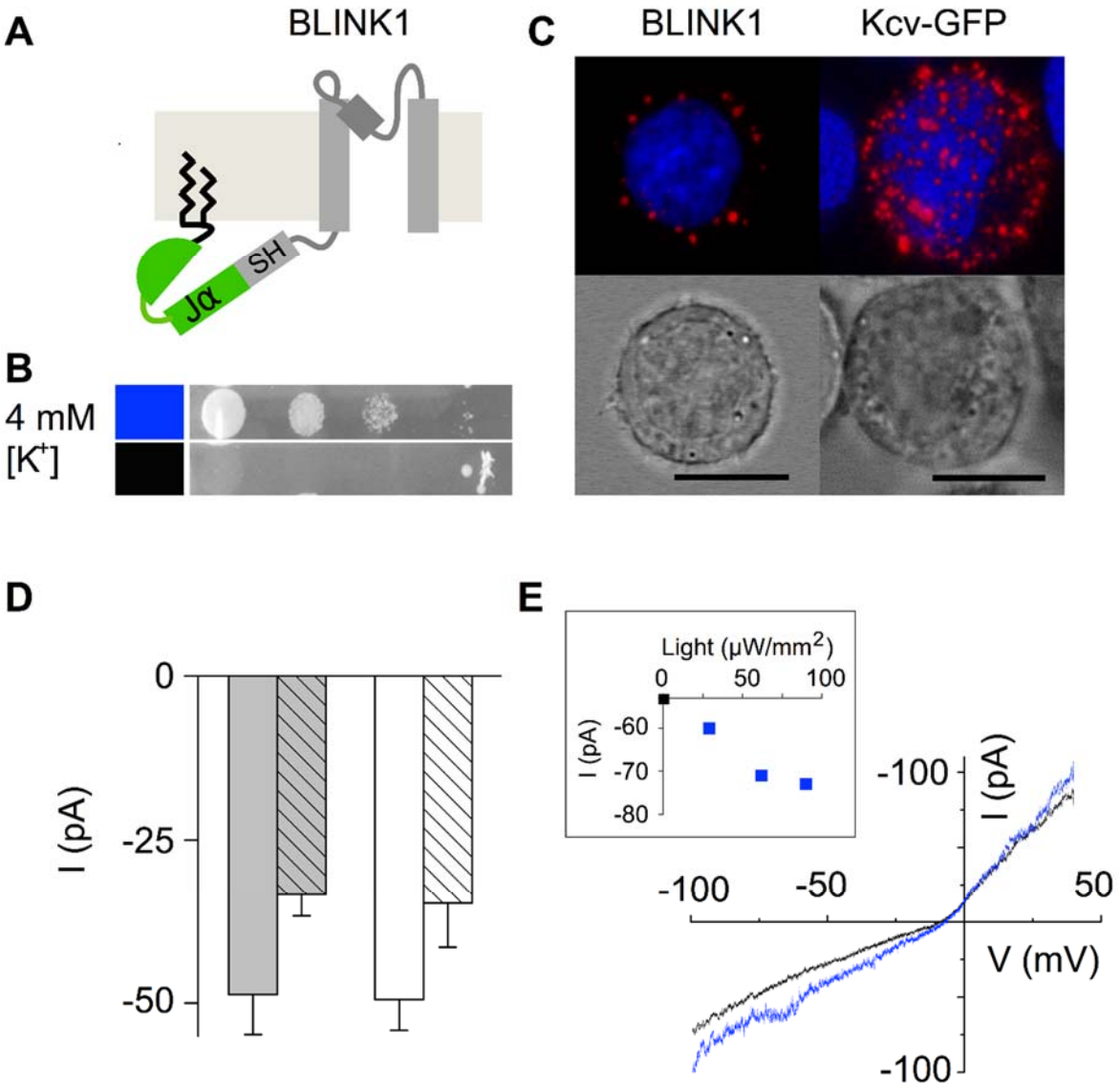

Figure S7. BLINK1 expression in yeast and in HEK293T cells
(A) Cartoon representation (for details see fig. S6) of myLJSK= BLINK1 showing Jα connected to the slide helix (SH) of Kcv; (B) yeast functional complementation by BLINK1 performed as described in fig. S1B. The phenotype shown was observed in 50% of 10 independent experiments. (C) Immunolocalization performed on non-permeabilized HEK293T cells with anti-Kcv monoclonal antibody recognizing specifically the tetrameric form of the channel (*30*). Left, cells transfected with BLINK1; right: cells transfected with Kcv-GFP. Calibration bar: 10μm. Fluorescent images show secondary antibody (conjugated to Alexa 594) in red and Hoechst staining of nuclei in blue. Lower panels show corresponding bright field images. (D) Currents recorded in the dark from HEK293T cells (n = 4) transfected with BLINK1 + GFP (white) or GFP alone (n = 8) (grey). Black diagonal pattern indicates the addition of 1 mM $BaCl_2$ to the external solution. Measurements were performed at -80 mV in 100 mM $[K^+]_{out}$. (E) I/V recorded from a HEK293T cell expressing BLINK1 in dark (black line, average of three subsequent ramps) and blue light (blue line, 455 nm, 90 μW/mm^2). Inset: increase in BLINK1 current recorded at -80 mV, as a function of increasing blue light intensity.

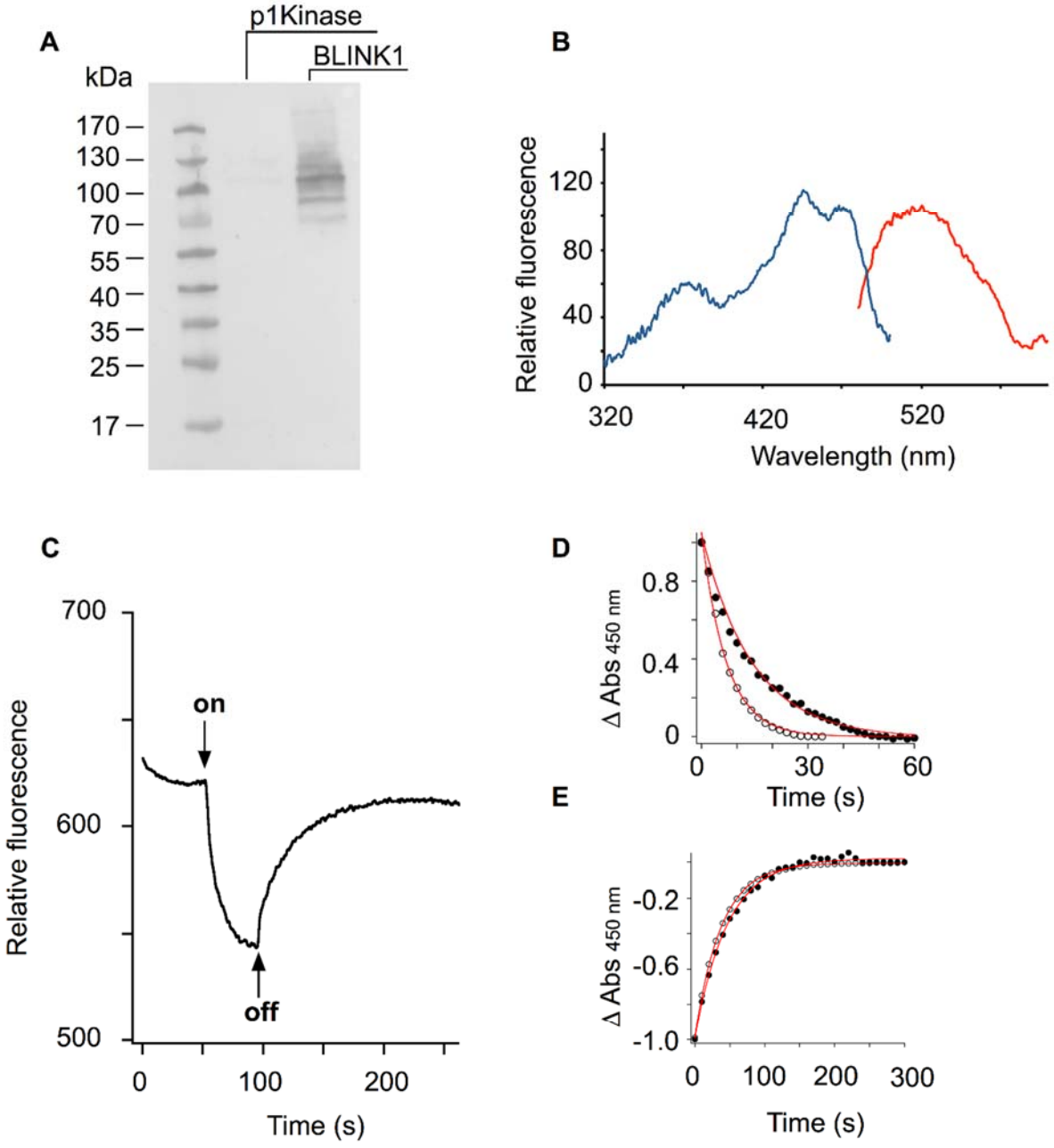

Figure S8. Expression and photochemical characterization of BLINK1 in insect cells.
(A) Immnunoblot analysis on Sf9 insect cells infected with either recombinant baculovirus expressing BLINK1 or the kinase domain of Arabidopsis phototropin 1 (p1Kinase) as a negative control. Molecular weight obtained for BLINK1 is consistent with the tetrameric form of the protein (106.5 kDa). (B) Corrected fluorescence excitation (blue line) and emission (red line) spectra for insect cells expressing BLINK1. Spectra were obtained by subtracting control spectra (from cells expressing p1Kinase). (C) Representative light-induced changes in fluorescence emission (520 nm) observed for insect cells expressing BLINK1 following blue light irradiation (on; 455 nm, 90 $\mu W/mm^2$) and after irradiation (off). (D) Photoadduct formation for BLINK1 (black circles) shows exponential kinetics (τ =14.5 s) similar to that obtained for myL (open circles). (E) Photoadduct decay for BLINK1 (black circles) shows exponential kinetics (τ = 51 s) similar to that of for myL (open circles). Data of myL are redrawn from Fig. 1.

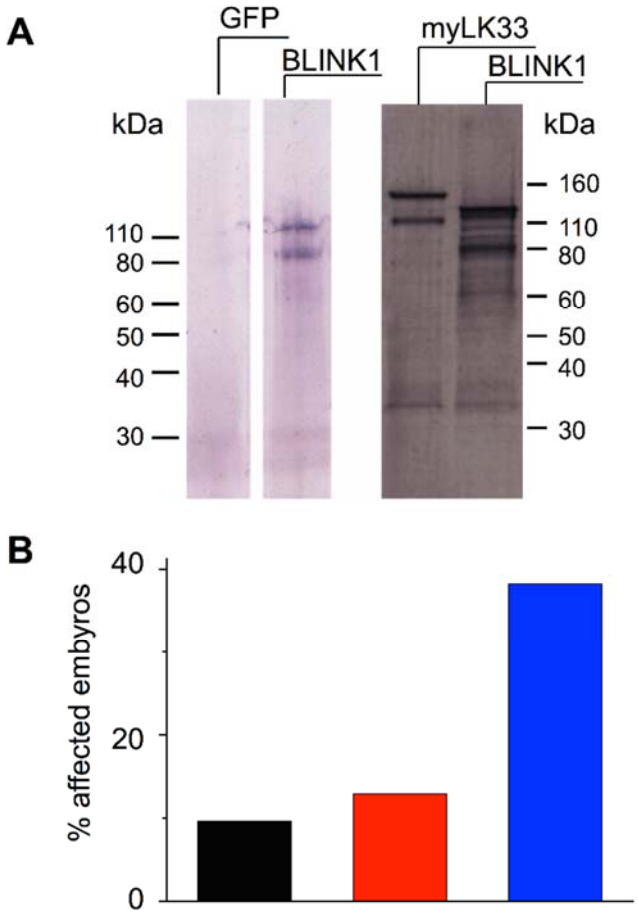

Figure S9. BLINK1 protein expression and absence of red light effect on zebrafish embryos

(A) Western blot analysis performed with an anti-Kcv antibody that recognizes the tetrameric conformation only of the channel (*30*). Left blot, zebrafish lysates expressing GFP or BLINK1; right blot, yeast microsomes expressing myLK33 or BLINK1. Numbers on the side indicate molecular weights in kDa. Expected m.w of BLINK1 is 106.5 kDa and of myLK33 is 110.5 kDa.

(B) Altered escape response in 3 day-old zebrafish, expressing BLINK1. The embryos (n=34) were tested for escape response with the following protocol: the fish were first kept for 1h in the dark (black) then illuminated for 45 min with red light (617 nm, 80 $\mu W/mm^2$) (red) and finally for 45 min with blue light (80 $\mu W/mm^2$) (blue). The escape response was tested at the end of each illumination period by gentle mechanical stimulation with a pipette tip (see Movie S1).

Movie S1. Touch response of zebrafish embryos expressing BLINK1.
(GFP) 2 day-old control embryo (GFP-injected), exposed to blue light for 1 h and then tested by mechanical stimulation with the tip of a pipette. (BLINK1) BLINK1-injected embryo, same treatment as the GFP-injected one.

References and Notes

1. S. B. Long, E. B. Campbell, R. Mackinnon, Crystal structure of a mammalian voltage-dependent Shaker family K+ channel. *Science* **309**, 897–903 (2005). Medline doi:10.1126/science.1116269

2. R. Latorre, F. J. Morera, C. Zaelzer, Allosteric interactions and the modular nature of the voltage- and Ca2+-activated (BK) channel. *J. Physiol.* **588**, 3141–3148 (2010). Medline doi:10.1113/jphysiol.2010.191999

3. U. M. Ohndorf, R. MacKinnon, Construction of a cyclic nucleotide-gated KcsA K+ channel. *J. Mol. Biol.* **350**, 857–865 (2005). Medline doi:10.1016/j.jmb.2005.05.050

4. C. Arrigoni, I. Schroeder, G. Romani, J. L. Van Etten, G. Thiel, A. Moroni, The voltage-sensing domain of a phosphatase gates the pore of a potassium channel. *J. Gen. Physiol.* **141**, 389–395 (2013). Medline doi:10.1085/jgp.201210940

5. M. R. Banghart, M. Volgraf, D. Trauner, Engineering light-gated ion channels. *Biochemistry* **45**, 15129–15141 (2006). Medline doi:10.1021/bi0618058

6. M. Banghart, K. Borges, E. Isacoff, D. Trauner, R. H. Kramer, Light-activated ion channels for remote control of neuronal firing. *Nat. Neurosci.* **7**, 1381–1386 (2004). Medline doi:10.1038/nn1356

7. H. Janovjak, S. Szobota, C. Wyart, D. Trauner, E. Y. Isacoff, A light-gated, potassium-selective glutamate receptor for the optical inhibition of neuronal firing. *Nat. Neurosci.* **13**, 1027–1032 (2010). Medline doi:10.1038/nn.2589

8. J. Y. Kang, D. Kawaguchi, I. Coin, Z. Xiang, D. D. O'Leary, P. A. Slesinger, L. Wang, In vivo expression of a light-activatable potassium channel using unnatural amino acids. *Neuron* **80**, 358–370 (2013). Medline doi:10.1016/j.neuron.2013.08.016

9. D. Schmidt, P. W. Tillberg, F. Chen, E. S. Boyden, A fully genetically encoded protein architecture for optical control of peptide ligand concentration. *Nat. Commun.* **5**, 3019 (2014). Medline doi:10.1038/ncomms4019

10. J. M. Christie, Phototropin blue-light receptors. *Annu. Rev. Plant Biol.* **58**, 21–45 (2007). Medline doi:10.1146/annurev.arplant.58.032806.103951

11. B. Plugge, S. Gazzarrini, M. Nelson, R. Cerana, J. L. Van Etten, C. Derst, D. DiFrancesco, A. Moroni, G. Thiel, A potassium channel protein encoded by chlorella virus PBCV-1. *Science* **287**, 1641–1644 (2000). Medline doi:10.1126/science.287.5458.1641

12. J. M. Christie, J. Gawthorne, G. Young, N. J. Fraser, A. J. Roe, LOV to BLUF: Flavoprotein contributions to the optogenetic toolkit. *Mol. Plant* **5**, 533–544 (2012). Medline doi:10.1093/mp/sss020

13. F. C. Chatelain, S. Gazzarrini, Y. Fujiwara, C. Arrigoni, C. Domigan, G. Ferrara, C. Pantoja, G. Thiel, A. Moroni, D. L. Minor Jr., Selection of inhibitor-resistant viral potassium channels identifies a selectivity filter site that affects barium and amantadine block. *PLOS ONE* **4**, e7496 (2009). Medline doi:10.1371/journal.pone.0007496

14. C. Aicart-Ramos, R. A. Valero, I. Rodriguez-Crespo, Protein palmitoylation and subcellular trafficking. *Biochim. Biophys. Acta* **1808**, 2981–2994 (2011). Medline doi:10.1016/j.bbamem.2011.07.009

15. D. Strickland, X. Yao, G. Gawlak, M. K. Rosen, K. H. Gardner, T. R. Sosnick, Rationally improving LOV domain-based photoswitches. *Nat. Methods* **7**, 623–626 (2010). Medline doi:10.1038/nmeth.1473

16. B. Hertel, S. Tayefeh, T. Kloss, J. Hewing, M. Gebhardt, D. Baumeister, A. Moroni, G. Thiel, S. M. Kast, Salt bridges in the miniature viral channel Kcv are important for function. *Eur. Biophys. J.* **39**, 1057–1068 (2010). Medline doi:10.1007/s00249-009-0451-z

17. J. Mattis, K. M. Tye, E. A. Ferenczi, C. Ramakrishnan, D. J. O'Shea, R. Prakash, L. A. Gunaydin, M. Hyun, L. E. Fenno, V. Gradinaru, O. Yizhar, K. Deisseroth, Principles for applying optogenetic tools derived from direct comparative analysis of microbial opsins. *Nat. Methods* **9**, 159–172 (2011). Medline doi:10.1038/nmeth.1808

18. R. M. Colwill, R. Creton, Imaging escape and avoidance behavior in zebrafish larvae. *Rev. Neurosci.* **22**, 63–73 (2011). Medline doi:10.1515/rns.2011.008

19. F. Zhang, L. P. Wang, M. Brauner, J. F. Liewald, K. Kay, N. Watzke, P. G. Wood, E. Bamberg, G. Nagel, A. Gottschalk, K. Deisseroth, Multimodal fast optical interrogation of neural circuitry. *Nature* **446**, 633–639 (2007). Medline doi:10.1038/nature05744

20. X. Han, E. S. Boyden, Multiple-color optical activation, silencing, and desynchronization of neural activity, with single-spike temporal resolution. *PLOS ONE* **2**, e299 (2007). Medline doi:10.1371/journal.pone.0000299

21. A. Berndt, S. Y. Lee, C. Ramakrishnan, K. Deisseroth, Structure-guided transformation of channelrhodopsin into a light-activated chloride channel. *Science* **344**, 420–424 (2014). Medline doi:10.1126/science.1252367

22. J. Wietek, J. S. Wiegert, N. Adeishvili, F. Schneider, H. Watanabe, S. P. Tsunoda, A. Vogt, M. Elstner, T. G. Oertner, P. Hegemann, Conversion of channelrhodopsin into a light-gated chloride channel. *Science* **344**, 409–412 (2014). Medline doi:10.1126/science.1249375

23. S. Tayefeh, T. Kloss, M. Kreim, M. Gebhardt, D. Baumeister, B. Hertel, C. Richter, H. Schwalbe, A. Moroni, G. Thiel, S. M. Kast, Model development for the viral Kcv potassium channel. *Biophys. J.* **96**, 485–498 (2009). Medline doi:10.1016/j.bpj.2008.09.050

24. E. Huala, P. W. Oeller, E. Liscum, I. S. Han, E. Larsen, W. R. Briggs, *Arabidopsis* NPH1: A protein kinase with a putative redox-sensing domain. *Science* **278**, 2120–2123 (1997). Medline doi:10.1126/science.278.5346.2120

25. D. L. Minor Jr., S. J. Masseling, Y. N. Jan, L. Y. Jan, Transmembrane structure of an inwardly rectifying potassium channel. *Cell* **96**, 879–891 (1999). Medline doi:10.1016/S0092-8674(00)80597-8

26. J. M. Christie, A. S. Arvai, K. J. Baxter, M. Heilmann, A. J. Pratt, A. O'Hara, S. M. Kelly, M. Hothorn, B. O. Smith, K. Hitomi, G. I. Jenkins, E. D. Getzoff, Plant UVR8

photoreceptor senses UV-B by tryptophan-mediated disruption of cross-dimer salt bridges. *Science* **335**, 1492–1496 (2012). Medline doi:10.1126/science.1218091

27. D. G. Gibson, L. Young, R. Y. Chuang, J. C. Venter, C. A. Hutchison 3rd, H. O. Smith, Enzymatic assembly of DNA molecules up to several hundred kilobases. *Nat. Methods* **6**, 343–345 (2009). Medline doi:10.1038/nmeth.1318

28. W. Tang, A. Ruknudin, W. P. Yang, S. Y. Shaw, A. Knickerbocker, S. Kurtz, Functional expression of a vertebrate inwardly rectifying K+ channel in yeast. *Mol. Biol. Cell* **6**, 1231–1240 (1995). Medline doi:10.1091/mbc.6.9.1231

29. A. Moroni, C. Viscomi, V. Sangiorgio, C. Pagliuca, T. Meckel, F. Horvath, S. Gazzarrini, P. Valbuzzi, J. L. Van Etten, D. DiFrancesco, G. Thiel, The short N-terminus is required for functional expression of the virus-encoded miniature K^+ channel Kcv. *FEBS Lett.* **530**, 65–69 (2002). Medline doi:10.1016/S0014-5793(02)03397-5

30. G. Romani, A. Piotrowski, S. Hillmer, J. Gurnon, J. L. Van Etten, A. Moroni, G. Thiel, B. Hertel, A virus-encoded potassium ion channel is a structural protein in the chlorovirus *Paramecium bursaria* chlorella virus 1 virion. *J. Gen. Virol.* **94**, 2549–2556 (2013). Medline doi:10.1099/vir.0.055251-0

31. M. Granato, F. J. van Eeden, U. Schach, T. Trowe, M. Brand, M. Furutani-Seiki, P. Haffter, M. Hammerschmidt, C. P. Heisenberg, Y. J. Jiang, D. A. Kane, R. N. Kelsh, M. C. Mullins, J. Odenthal, C. Nüsslein-Volhard, Genes controlling and mediating locomotion behavior of the zebrafish embryo and larva. *Development* **123**, 399–413 (1996). Medline

Yeast-based screening system for the selection of functional light-driven K^+ channels

Cristian Cosentino[1], Laura Alberio[1], Gerhard Thiel[2] and Anna Moroni[1]

Author affiliations

[1]Department of Biosciences, University of Milan and Biophysics Institute, National Research Council (CNR), Italy

[2]Plant Membrane Biophysics, Technical University Darmstadt, Darmstadt, Germany

Corresponding Author: Anna Moroni, Department of Biosciences, University of Milano, Via Celoria 26, 201333 Milano, Italy, email: anna.moroni@unimi.it; tel. +39 02 50314826, fax +39 02 50314815

Summary

Ion channels control the electrical properties of cells by opening and closing (gating) in response to a wide palette of environmental and physiological stimuli. Endowing ion channels with the possibility to be gated by remotely applied stimuli, such as light, provides a tool for *in vivo* control of cellular functions in behaving animals. We have engineered a synthetic light-gated potassium (K^+) channel by connecting an exogenous plant photoreceptor LOV2 domain to the K^+ channel pore Kcv. Here we describe the experimental strategy that we have used to evolve the properties of the channel towards full control of light on pore gating. Our method combines rational and random mutagenesis of the channel followed by a yeast-based screening system for light-activated K^+ conductance.

Key Words

Functional complementation, protein evolution, rational and random mutagenesis, light, screening, *S. cerevisiae*, optogenetics, ion channels, potassium (K^+), gating

Running Title

Engineering Light-Regulated K^+ Channels

1. Introduction

Potassium (K^+) channels are membrane proteins ubiquitous in living organisms. They drive the flux of K^+ ions across the ion-impermeant lipid membrane. In higher organisms, they play a fundamental role in controlling cell excitability and intercellular communication, particularly between neurons. Potassium channels are tetrameric proteins in which each monomer contributes to the formation of a central ion conductive pore surrounded by regulatory or sensor domains. All K^+ channels operate according to a common principle: upon perception of the stimuli, the peripheral sensors convey the information to the pore that opens or closes in response (gating). Given their common modular architecture, K^+ channels tolerate swapping of pore and sensor modules between members of different families without losing functionality (1,2). More surprising is the evidence that exogenous sensors found in proteins unrelated to the K^+ channel superfamily can be grafted on the pore to control gating. In the past, we have engineered a functional voltage-gated K^+ channel by connecting the voltage sensor of CiVSP, a phosphatase found in the ascidian *Ciona intestinalis*, to the pore of a Kcv, a K^+ channel found in the algae virus PBCV-1 (3). An exciting perspective is the expansion of signals perceived by K^+ channels beyond the realm of those already sensed by native channels. Regulation of K^+ channels by infrared light, magnetic fields or ultrasounds that freely penetrate mammalian tissues, will offer the unprecedented possibility to control cellular functions in freely moving and behaving organisms.

We recently succeeded in engineering BLINK1, a blue light (475 nm)-gated K^+ channel that can be used to inhibit the electrical activity of neurons in optogenetics (4). BLINK1 was engineered by connecting the light sensor module LOV2 of *Avena sativa* phototropin (5) to the N-terminus of Kcv (Fig. 1A). Crucial for the project was the development of a yeast-based screening system that allowed fast screening for functional K^+ channels. We had previously shown that Kcv expression rescues growth of *S. cerevisiae* Δtrk1 Δtrk2 mutants in low external K^+ (6,7). In this project, we were further screening for the ability of the engineered channels to promote differential growth in light and dark. A prototype channel retrieved from the first round of screening was further improved through a random mutagenesis approach that generated a library of mutants. In a second round of screening, about

30000 clones from the library were transformed in yeast and the colonies tested for differential yeast growth in light/dark. Channel variants showing improved complementation ability, compared to the parental channel, were selected for further electrophysiological characterization of the channel currents.

2. Materials

2.1 Coding Sequences for the LOV2 domain and the Kcv Channel

1. LOV2 domain: aminoacids 404 - 546 of *Avena sativa* Phototropin 1 (NPH1-1) (GenBank: AAC05083.1)
2. Kcv: aminoacids 2 - 94 of Paramecium bursaria Chlorella virus 1 potassium ion channel protein (PBCV-1-Kcv) (NP_048599.1)

2.2 Expression Vector

1. The pYES2-Met25 expression vector (4) was used for protein expression in *Saccharomyces cerevisiae.*

2.3 Cloning and Expression Organisms

1. *Escherichia coli* (DH5α) for cloning procedures and plasmid DNA amplification
2. *Saccharomyces cerevisiae* Δtrk1 Δtrk2 mutants (SGY1528) for functional complementation by light-driven K^+ ion channels.

2.4 *E. coli* Growth Media

1. LB medium: add 10 g Tryptone, 5 g Yeast Extract, 10 g NaCl to 800 ml ultrapure water. Mix and adjust pH to 7.0 with 1 M NaOH. Make up to 1 L with water. Autoclave and store at RT. Before use, add selective antibiotics. For solid LB medium proceed as previous step and add 15 g/L agar. After sterilization allow the medium to cool down, add selective antibiotics, and

then pour medium into petri dishes. Seal solid plates with parafilm and store in the dark at +4°C (*see* **Note 1**).

2. Ampicillin: 50 mg/ml stock solution. Weigh 500 mg Ampicillin sodium salt and dissolve in 10 ml ultrapure water. Make aliquots and store in the dark at -20°C (*see* **Note 2**).
3. Gentamycin: 20 mg/ml stock solution. Weight 200 mg Gentamycin sulphate; prepare 10 ml solution and aliquot as in previous step (*see* **Note 2**).

2.5. Yeast Growth Media

1. Complete Yeast Medium supplemented with 100 mM KCl (YPDA+100 KCl): weigh 20 g Peptone, 20 g D-Glucose, 10 g Yeast Extract, 50 mg Adenine hemisulfate, 7.4 g KCl and add to 800 ml ultrapure water. Mix and adjust pH to 5.6 with 1 M HCl; make up to 1 L with water and autoclave. To obtain solid medium, add 20 g Agar (Plant cell culture tested, Sigma-Aldrich) before autoclaving. Pour agar-containing medium into petri dishes while still molten and seal with parafilm when cooled. Store liquid medium at RT and plates at +4°C.
2. Minimal SD medium without Uracil and supplemented with Adenine and 100 mM KCl (SD-U+100 KCl): Weigh 26.7 g Minimal SD base (Clontech), 765 mg CSM dropout Uracil (CSM-Ura; Formedium), 100 mg Adenine hemisulfate, 7.4 g KCl and dissolve in water as described in previous step. Mix and adjust pH to 5.5 with 1M KOH. Make up to 1 L with water. To obtain solid medium, add 20 g Agar (Plant cell culture tested, Sigma-Aldrich). Autoclave and store liquid medium at RT, pour agar plates as previously described and store at + 4°C.
3. Selective medium without Uracil and Methionine, supplemented with Adenine and KCl (SEL-U-M+KCl): weight 725 mg L-Arginine, 100 mg Adenine hemisulfate, 1.5 g CSM dropout Uracil and Methionine (CSM-Ura-Met; Formedium), 10 g D-Glucose and add to 800 ml of water. Add 2 ml of 500 mM $MgSO_4$ and 200 µl of 500 mM $CaCl_2$. Supplement with KCl at the desired final concentration diluting a 2 M stock solution (*see* **Note 3**). Mix and adjust pH to 6.0 with Phosphoric acid. Make up to 1 L with water. Autoclave and store liquid

medium at RT. Before use, add 1 µl Vitamin solution and 1 µl Trace Elements per each ml of media. For solid medium, add 15 g Low Potassium Agar (Sigma-Aldrich #P9338). After sterilization, allow the medium to cool down and add Trace Elements and Vitamins as previously described; pour medium into petri dishes. Seal solid plates and store at +4°C in the dark (*see* **Note 4**).

4. Vitamin solution: weight and add in a 50 ml tube 10 mg Biotin, 20 mg D-Panthotene acid calcium salt, 20 mg Nicotinic acid, 20 mg Pyridoxine HCl, 20 mg Thiamine and 10 mg Myo-inositol. Add ultrapure grade water up to 50 ml, mix and filter the solution through 0.2 µm syringe filter. Store at +4°C, in the dark (*see* **Note 5**).
5. Trace elements: weight 25 mg Boric acid, 2 mg CuSO4, 5 mg KI, 25 mg FeCl3, 20 mg MnSO4, 45 mg Molybdic acid, 20 mg $ZnSO_4$, 500 µl HCl 37% and dissolve in 50 ml of water. Sterilize the solution as described in previous step. Store at +4°C, in the dark (*see* **Note 5**).

2.6 Mutation Strategies

2.6.1. Enzymes and Reagents

1. High-fidelity PCR Amplification System (e.g. Pfu DNA polymerase)
2. QuikChange II XL Site-Directed Mutagenesis Kit
3. GeneMorph II Random Mutagenesis Kit
4. Restriction Enzymes
5. Commercial PCR purification kit (e.g. QIAquik PCR Purification Kit)
6. Commercial DNA gel extraction kit (e.g. Wizard SV Gel and PCR Purification Kit)
7. Commercial DNA plasmid purification kit (e.g. QIAprep Spin Miniprep Kit)
8. Commercial yeast transformation kit: e.g. the Frozen-EZ yeast transformation II kit (Zymo Research).

2.6.2. PCR Primers

Primer characteristics for each application:

9. Overlap extension PCR (OE-PCR): presence of G or C at 5' end; T_m between 64-66°C; the overlapping region with the target sequence has to be 15-22 bp long.
10. Terminal Extension PCR (TE-PCR): 5' extension can be up to 35 bp long; T_m of region annealing to target sequence has to be between 64-66°C.
11. Site directed mutagenesis PCR (SDM-PCR): primer length should be between 42-45 bp; the desired mutation has to be close to the centre of the primer sequence; the T_m (calculated as per QuikChange II XL Site-Directed Mutagenesis Kit) has to be greater than 78°C.
12. Restriction free PCR (RF-PCR): 5'end is a 22-24 bp long region annealing to target sequence with T_m greater than 70°C; 3'end region has to anneal to target region with T_m between 64-66°C.
13. Error prone PCR (EP-PCR): the primer binding sites are located on the vector sequence at a distance greater than 70 bp from desired restriction sites. T_m is between 64 and 66°C. In Error Prone PCR reactions, the required primers stocks concentration is 250 ng/µl.

2.7. Light Irradiation

1. Functionally effective Blue light: Tri-Star Rebel LED (Luxeon #MR-R0500-20T) containing three Royal-Blue LEDs, mounted on 20 mm Tri-Star Saber base: 2730 mW at recommended operating current 700 mA; λ= 447.5 nm (440-460 nm); beam angle 125°
2. LED Heat Sink: Alpha Heat Sink (Luxeon #N80-20B) with convection thermal resistance rating of 2.85 °C/W and 80 x 80 x 20 mm footprint.
3. LED adhesive tape: thermally conductive, electrically isolating and adhesive Bond-Ply 100 pad (Luxeon #LXT-T-12) cut to fit the 20 mm Luxeon LED's Tri-Star base. Operational temperature from -30°C to 120°C; thermal performance 4.5°C/W

4. Functionally ineffective Red light: Tri-Start Rebel LED (Luxeon #MR-H2060-20T) containing three Red-Orange LEDs, mounted on 20 mm Tri-Star Saber base: 366 mW at recommended operating current 700 mA; λ= 617 nm (610-620 nm); beam angle 125°
5. Safety light: Deep-Orange co-extruded polycarbonate film (Rosco Supergel #22) applied to main room light source: RGB 240:80:0; transmittance ~0% at λ <540 nm

2.8. Light/Dark Differential Screening Chamber

The screening is performed in a temperature-controlled chamber where culture plates can be either exposed to homogeneous light irradiation or kept in the dark. Figure 2 shows a schematic drawing of the chamber, from the side view (Fig. 2A) and from the top (Fig. 2B).

1. Homogenous light irradiation is provided as follows: a metal scaffold is built around a 1 square meter surface, in order to place 9 LED assemblies 70 cm above cellular cultures (*see* **Note 6**). Each LED assembly is composed of a heat sink mounted on top of a Tri-star LED, through thermal conductive adhesive tape. The thermal sink allows an adequate passive cooling system that ensures long time LED functionality (Fig. 2A). LED assemblies are mounted on three metal bars to allow homogenous radiation distribution over the table surface. LED assemblies are grouped in series and groups are in parallel with each other, accordingly to power supply specifications. This connection system allows easy removal of a single LED in case of technical maintenance. (Fig. 2B). White panels reflecting irradiated light are placed around the table, in order to homogeneously distribute light over the plate surface. A space between the panels and the table was left to allow air circulation. Moreover, the open conformation of the scaffold ensures homogenous temperature conditions all over the chamber.
2. Dark condition is obtained by means of a dark cardboard and a black cloth covering the plates and allowing air circulation.

3. Methods

The selection assay is based on a *S. cerevisiae* mutant Δtrk1 Δtrk2 (SGY1528) that cannot grow in low external K^+. Expression of heterologous K^+ transport proteins restore growth in low K^+. Functional synthetic channels were identified by their ability to complement the yeast growth phenotype in low external K^+.

3.1. Preparation of *S. cerevisiae* Competent Cells

1. Grow SGY1528 cells on YPDA + 100 mM KCl solid medium up to 3 days at 30°C.
2. Inoculate a single colony in 3 ml YPDA + 100 mM KCl broth and grow overnight in 30°C shaking incubator (*see* **Note 7**).
3. Dilute cell culture 1:50 in YPDA + 100 mM KCl broth and grow in 30°C shaking incubator until OD_{600} is between 0.8 and 1.0 (*see* **Note 8**).
4. Centrifuge cells at 500 g for 4 min, then discard supernatant.
5. Commercially available kit such as the Frozen-EZ yeast transformation II provide reagents and protocols to obtain competent yeast cells with high transformation efficiency.
6. Aliquot cells in small volumes and store at -80°C (*see* **Note 9**).

3.2. Transformation of *S. cerevisiae* cells

Commercially available kit such as the Frozen-EZ yeast transformation II allow for a high yield in yeast transformation procedures.

1. Follow manufacturer's instruction to transform cells (*see* **Note** Error! Reference source not found.**0**)
2. Plate up to 5 µl cells over 1/3 of a minimal SD medium plate
3. Incubate plates up to 3-4 days at 30°C

3.3. Rational and Random Mutagenesis Strategies

Two main strategies were followed to build a synthetic light-driven ion channel: First, a rational approach was pursued, which consisted in connecting the sensor to the pore module in different positions guided by what is known on the gating mechanism of the channel. This was followed by a random mutagenesis approach aiming to improve the properties of a promising candidate retrieved from the previous approach. Rational mutagenesis was performed using a combination of different PCR amplification methods. The standard thermal cycler program in combination with Pfu DNA polymerase is as follows: step 1, 30 sec at 95°C; step 2 (15 to 35 cycles), 10 sec at 95°C, 20 sec at T_m, 1 min per kb of amplicon at 72°C; step 3, 5 to 7 min at 72 °C; step 4, 7°C for unlimited time.

3.3.1. Rational Mutagenesis: Terminal Extension PCR (TE-PCR)

TE-PCR extends both termini of a target sequence for further sequence manipulation (e.g. restriction enzyme cloning; OE-PCR; motif addiction; see Fig. 3A). To set up PCR parameters, only the primer region annealing to the target sequence has to be taken into account. The reaction is based on a standard PCR protocol based on Pfu DNA polymerase, following the standard reagent concentration and the standard thermal cycler program as per manufacturer's instructions.

3.3.2. Rational Mutagenesis: Overlap Extension PCR (OE-PCR)

The OE-PCR allows joining of regions originally separated in the native sequence (see Fig. 3B). Two partially overlapping amplicons are generated through terminal extension PCR.

OE-PCR occurs with an initial step using a mixture of these amplicons as reciprocal primers; following this step, a standard PCR protocol enriches the newly generated construct.

1. Generate partially overlapping amplicons through TE-PCR (see paragraph 3.3.1) using a combination of one TE-PCR primer and one OE-PCR primer: the resulting fragments will have a common annealing region.

2. Isolate amplicons running the PCR reaction on 1% Agarose gel and purify the desired fragment with any commercially available DNA gel extraction kit.
3. First OE-PCR reaction: mix within a PCR tube 0.75 U Pfu DNA polymerase, 1x Pfu polymerase buffer, 200 μM dNTPs, 40 ng of the longest and partially overlapping amplicon; 1:1 molar ratio of the shorter overlapping amplicon; make final volume up to 50 μl with ultrapure water.
4. Setup standard PCR protocol, with following modifications: Step 2, 15 cycles and T_m at 55°C; skip step 3, move directly to step 4 (7°C).
5. Second OE-PCR reaction: add 0.5 μl of 10 μM primers (forward and reverse) to allow full amplification of the newly generated construct.
6. Setup standard PCR protocol, with following modifications: T_m 55°C.
7. Isolate amplicons running the reaction on 1% agarose gel and purify the desired fragment with a commercially available DNA gel extraction kit.

3.3.3. Rational Mutagenesis: Directed Mutagenesis PCR (SDM-PCR)

This procedure introduces amino acid substitutions, insertions or deletions into a target sequence (see Fig. 3C). To this purpose, commercial products as QuikChange site directed mutagenesis kit are available.

1. Perform SMD-PCR as per manufacturer's guide, with minor adaptations: T_m value and elongation time regulation, based on the target sequence.
2. Transform PCR product into *E. coli* cells, extract and purify the obtained plasmid
3. Verify the presence of the desired mutation by sequencing

3.3.*4*. Random Mutagenesis: Error prone PCR (EP-PCR)

EP-PCR randomly mutates a target region by using an error prone DNA polymerase. Commercially available kits such as GeneMorph II random mutagenesis are specifically designed for this purpose. EP-PCR primers used in this reaction were designed to perfectly match the target plasmid sequence, in order to allow subsequent recombination in gap repair (Fig. 4).

1. The following setup was designed to generate 10-15 random point mutations per 1 Kb of target DNA as per instructions of the GeneMorph II random mutagenesis kit. Use 50 ng target DNA (e.g. 510 ng of 5.5 Kb plasmid containing a 560 bp long target sequence) and run the amplification reaction as follows: step 1, 95°C for 2 min; step 2, 95°C for 30 seconds, 64°C for 30 seconds, 72°C for 1 per 1Kb amplified, repeated for 30 cycles; step 3, 72°C for 10 min.
2. Use 2 µl of the PCR product as a template for another EP-PCR. Repeat this step twice.
3. Isolate amplicons running the reaction on 1% agarose gel and purify the desired fragment with a commercially available DNA gel extraction kit.
4. Proceed to yeast transformation and gap repair.

3.3.5. Random Mutagenesis: Gap Repair

Gap repair allows the generation of libraries of a randomly mutated clone within the same non-mutagenized vector background (see Fig. 4). High efficiency yeast transformation is recommended. Gap repair transformation requires an open plasmid, with terminal regions annealing to the terminal regions of the mutagenized fragment that has to be inserted in (*see* **Note 11**).

1. To prepare the vector for a gap repair reaction, prepare a restriction digest of the plasmid by mixing in a tube 10 µg of circular pYES2-Met25 expression plasmid, 50 U of each restriction enzyme, 1x reaction buffer according to restriction enzyme manufacturer's instructions. Make final volume up to 50 µl with water (*see* **Note 12**).
2. Incubate at the appropriate temperature following restriction enzyme manufacturer's instructions for more than 1h 30 min.
3. Isolate digested fragments running the reaction on 1% Agarose gel and purify the linearized plasmid with any commercially available DNA gel extraction kit.
4. To perform a gap repair reaction, prepare into a 2 ml tube a mixture of 500 ng EP-PCR randomly mutated amplicons with 1 µg of cut yeast expression vector.

5. Transform the mixture into 50 µl SGY1528 competent cells using any commercially available yeast transformation kit, providing high transforming rate. When transforming yeast cells with Frozen-EZ yeast transformation II kit, eight transformation reactions are enough to plate cells onto 36 ∅ 150 mm petri dishes (*see* **Note 13**).
6. Dilute transformed cells with MilliQ water up to 6.5 ml and mix.
7. Plate 180 µl of diluted cells on 36 ∅ 150 mm petri dishes containing SD-U+100 mM KCl
8. Number the plates and provide each with a mark reporting the orientation for the following replica plating step.
9. Incubate at 30°C in the dark up to 4 days.

3.4 Light-Driven Functional Complementation

The yeast mutant strain SGY1528 (*see* **Note 14**) is suitable for functional complementation tests of light-gated synthetic potassium channels inserted in pYES2-Met25 vector. Functional complementation is performed on SEL-U-M medium supplemented with KCl at a selective concentration. The differential growth between light and dark exposed colonies determines which clones are functional. Light-driven functional complementation can either be performed in low throughput by means of a drop-test assay or in high-throughput:

3.4.1. Low Throughput Screening by Drop-Test

The drop test method allows fine screening of tens of colonies on a single plate by functional complementation. Ten-fold serial dilutions of liquid cell culture are spotted onto solid selective medium and grown under light irradiation or in the dark. The differential growth rate of the same colony, at the same dilution, at the two different conditions, reflects a different ability in complementing the defective yeast phenotype.

1. Pick-up the desired colony from solid non-selective medium (SD-U+A + 100 mM KCl) and inoculate it in 3 ml of liquid non-selective medium. Grow cells overnight in 30°C shaking incubator in the dark.
2. Centrifuge 2 ml of the overnight cell culture at 2700 g for 2 min and discard supernatant
3. Resuspend pellet with 2 ml sterile water to wash cells
4. Centrifuge cells at 2700 g for 2 min and discard the supernatant
5. Add 1 ml sterile water and resuspend cells
6. In a different tube, transfer 50 µl resuspended cells and add 950 µl water (1:20 dilution)
7. Measure OD_{600} of the 1:20 dilution and calculate the OD_{600} of the resuspended cells
8. Dilute the resuspended cells to OD_{600} = 0.8 with water.
9. Prepare tenfold serial dilutions in 2 ml tubes: transfer 100 µl cell from OD_{600} =0.8 preparation in a new tube and add 900 µl water (1:10 dilution). After mixing, repeat the same procedure starting from 1:10 dilution to obtain 1:100 dilution and from the 1:100 dilution to obtain 1:1000 dilution.
10. Spot 7 µl drops of each dilution onto plates of SEL-A-M+U medium, supplemented with KCl at the desired selective concentration. Prepare each plate in duplicate to test simultaneously two functional conditions.
11. Seal plates with parafilm and incubate inverted for 3 days at 30°C under light or dark conditions in the chamber described at paragraph 2.8.
12. To purify the plasmid from selected colonies, pick the desired colony from solid non-selective medium and inoculate in 3 ml of liquid non-selective medium.
13. Grow cells overnight in a shaking incubator at 30°C in the dark.
14. Purify yeast plasmid with any commercially available plasmid extraction kit (*see* **Note 15**).
15. In a new 2 ml tube transform 10 µl DH5α *E. coli* competent cells with 1 µl of the yeast extracted plasmid.
16. Plate 90 µl transformed cells on LB agar plate supplemented with selective antibiotics and incubate overnight at 37°C

17. Inoculate colonies in a 50 ml tube containing 7 ml LB broth, supplemented with selective antibiotics; grow cells overnight at 37°C in a shaking incubator.
18. Proceed as per any commercially available DNA plasmid purification kit workflow

3.4.2. High-throughput Screening by Replica Plating

This step allows the replication of the same colony over two plates with selective medium. The replica plates are then incubated under different growing condition and differentially growing colonies identified and selected for further analysis.

1. With a sterile velvet cloth, replicate colonies grown onto each non-selective plate onto two different Ø150 mm plates containing SEL-U-M+A supplemented with the desired selective KCl concentration.
2. Seal and number the two selective plates according to mother plate number and selection condition and mark each to report the orientation as for the non-selective plate (*see* **Note 16**).
3. Incubate plates at 30°C in the growth chamber. One subset of plates must be placed under effective light irradiation, the second subset must be grown in the dark (*see* **Note 17**).
4. After three days, light irradiated and dark grown plates are compared to find differentially grown yeast colonies (*see* **Note 18**). Colonies that have been identified by differential growth in replica plating must be validated to eliminate fake positives.
5. To validate the phenotype, identify the colonies that show differential growth between light and dark condition following replica plating.
6. Inoculate the selected colonies in liquid non-selective medium (SD-U+A + 100 mM KCl) and purify plasmid from the liquid growth.
7. Transform *S. cerevisiae* competent cells and confirm the phenotype (dark/light differential growth) by drop test.

4. Notes

1. Cover plates with aluminium foil to keep LB agar supplemented with ampicillin in the dark. Ampicillin is light sensitive and degrades under high temperature and light exposure. Moreover, storing plates in an inverted position (with their lid down) allows the condensed water to accumulate on the plastic lid instead of on the medium.
2. Aliquot 1 ml of antibiotics stock solution into 1.5 ml Eppendorf tubes. When preparing aliquots of Ampicillin, cover tube with aluminium foil to keep solution in dark. Stock solutions are 1000x, when supplemented to LB media add 1µl antibiotic to each ml of medium.
3. Dissolve 14.9 g KCl in 100 ml ultrapure water to have a 2 M stock solution. Add 250 µl, 500 µl or 2 µl of the obtained stock solution to supplement 1 L medium with 0.5 mM, 1 mM or 4 mM KCl, respectively. Weight 7.4 g of KCl powder to prepare 1 L of 100 mM KCl containing medium.
4. Low Potassium Agar from Sigma-Aldrich (#P9338) allows the preparation of media supplemented with very low potassium concentrations (e.g. 0.5 mM).
5. Filtering vitamins and trace elements through 0.2 µm syringe filters ensure sterilization of the solution. Filter under laminar airflow hood directly into sterile 50 ml falcon tubes. Cover the tubes with aluminium foil to protect from light irradiation. Open tubes only in sterile environment.
6. Nine assemblies of Royal-blue Tri-Star Rebel LED, at 2730 mW each, are able to irradiate 1 sq m table at an average light distribution (λ= 447 nm) of 160-230 µW/cm^2.
7. Inoculate 3 ml of cell culture in a 15 ml tube.
8. This process typically requires about 4 h when applying 1:50 dilution and about 3 h when working with 1:25 dilution.
9. Allow cells to cool down slowly by placing tubes into a polystyrene box, within the -80°C refrigerator. This procedure allows gradual freezing of the cells and improves their transformation efficiency.

10. Frozen-EZ Yeast Transformation II kit workflow adaptation: prepare in a 2 ml tube a mixture of 1 ul (> 200 ng/ul) expression vector, 5 ul SGY1528 competent cells, 50 ul EZ3 solution. Incubate cells at 30°C for 45 minutes and mix the solution every 15 minutes.
11. The product of three consecutive EP-PCR reactions is typically enough to perform a gap repair transformation plated on up to 18 petri dishes (Ø150 mm).
12. Cut the plasmid by restriction digestion leaving sticky and blunt end opposite each other to avoid plasmid re-circularization. Lacking restriction sites can be inserted by SDM-PCR.
13. This number of plates occupies roughly $1m^2$ of an irradiated area during functional complementation tests. Depending on the cell density per plate, it can provide about 20000 growing colonies per functional screening.

14. SGY1528 is a K^+ uptake defective yeast strain: Mata Ade2-1 can1-100 his3-11,15 leu2-3,112 trp1-1 ura3-1 trk1::HIS3 trk2::TRP1 (10).
15. When using Zymoprep Yeast plasmid Miniprep II kit a typical purification from 2 ml cell culture has an average yield between 20 and 120 ng/µl. However, the purity of this extraction is not suitable for sequencing, for this reason a further cloning step in *E. coli* cells and subsequent plasmid purification are necessary.
16. Seal plates with parafilm to protect cell culture from contamination and drying. Orientation mark will help to identify the original colony on the mother plate.
17. Effective irradiation to allow yeast functional complementation of BLINK light-driven potassium channel (4): 210 ± 20 $\mu W/cm^2$ using Royal Blue Light (λ = 447 nm).
18. The average yield of differentially growing colonies obtained is up to 20 per plate.

5. Acknowledgments

This work was supported by MAE (Ministero Affari Esteri) grant n. 01467532013-06-27 and ERC 2015 AdG n. 695078 noMAGIC to A.M.

6. References

1. Ohndorf, U.M., and MacKinnon, R. (2005) Construction of a cyclic nucleotide-gated KcsA K+ channel. *J. Mol. Biol.*, 350, 857–865
2. McCoy JG1, Rusinova R, Kim DM, Kowal J, Banerjee S, Jaramillo Cartagena A, Thompson AN, Kolmakova-Partensky L, Stahlberg H, Andersen OS, Nimigean CM. (20014). A KcsA/MloK1 chimeric ion channel has lipid-dependent ligand-binding energetics. *J Biol Chem*. 289(14):9535-46
3. Arrigoni, C., Schroeder, I., Romani, G., Van Etten, J.L., Thiel, G., and Moroni, A (2013) The voltage-sensing domain of a phosphatase gates the pore of a potassium channel. *J. Gen. Physiol.*, 141, 389–395
4. Cosentino, C., Alberio, L., Gazzarrini, S., Aquila, M., Romano, E., Cermenati, S., Zuccolini, P. et al. (2015) Engineering of a light-gated potassium channel. *Science*, 348, 707-710.
5. Christie, J.M., Arvai, A.S., Baxtger, K.J., Heilmann, M., Pratt, A.J., O'Hara, A., Kelly, S.M. et al. (2012) Plant UVR8 photoreceptor senses UV-B by tryptophan-mediated disruption of cross-dimer salt bridges. *Science*, 335, 1492-1496
6. Minor, D.L., Masseling, S.J., Jan, Y.N., and Jan, L.Y. (1999) Transmembrane structure of an inwardly rectifying potassium channel. *Cell* 96, 879-891
7. Chatelain, F.C., Gazzarrini, S., Fujiwara, Y., Arrigoni, C., Domigan, C., Ferrara, G., Pantoja, C., Thiel, G., Moroni, A., Minor, D.L. Jr. (2009) Selection of inhibitor-resistant viral potassium channels identifies a selectivity filter site that affects barium and amantadine block. PLoS One 16;4(10):e7496.
8. Elgoyhen, A.B., Vetter, D., Katz, E., Rothlin, C., Heinemann, S., and Boulter J. (2001) alpha10: Aa determinant of nicotinic cholinergic receptor function in mammalian vestibular and cochlear mechanosensory hair cells. *Proc Natl Acad Sci USA* 98, 3501–3506.
9. Krieg, P.A., and Melton, D.A. (1984) Functional messenger RNAs are produced by SP6 in vitro transcription of cloned cDNAs. *Nucleic Acids Res.* 12, 7057–7070.

10. Tang, W., Ruknudin, A., Yang, W.P., Shaw, S.Y., Knickerbocker, A. and Kurtz, S. (1995) Functional expression of a vertebrate inwardly rectifying K^+ channel in yeast. *Mol. Biol. Cell*, 6, 1231-1240

Figure Captions

Fig. 1: Schematic representation of the engineering principles of the light-activated K^+ channel and of the yeast-based screening assay used to identify functional light-driven K+ channels. (A) The prototype light-gated K^+ channel (LK) was engineered by fusing the LOV2-Jα domain (L) to the viral K^+ channel Kcv (K). K and LK are inserted in the lipid membrane while L is cytosolic. N and C indicate the first and the last aminoacid of each construct. (B) Yeast complementation assay for the detection of functional light-regulated K^+ channels: the mutant strain SGY1528 does not grow in low external K^+ concentration (4 mM) when it is transformed with L, neither in the dark nor in light. Expression of the functional K^+ channel Kcv (K), restores yeast growth, independently of light and dark growth conditions. Expression of LK, promotes differential yeast growth in light and dark, indicating light regulation of channel gating.

Fig. 2: Growth chamber for yeast-based light/dark complementation assay: (A) side view of the incubation chamber; (B) top view of the workbench. Detailed scheme of LED assembly and LED components is shown at the right side of each panel.

Fig. 3: PCR based cloning methods: (A) terminal extension PCR (TE-PCR) workflow; (B) overlap extension PCR (OE-PCR) workflow; (C) site directed mutagenesis (SDM-PCR) workflow.

Fig. 4: Gap repair-based library preparation in yeast. RE stands for restriction site; P stands for EP-PCR primer

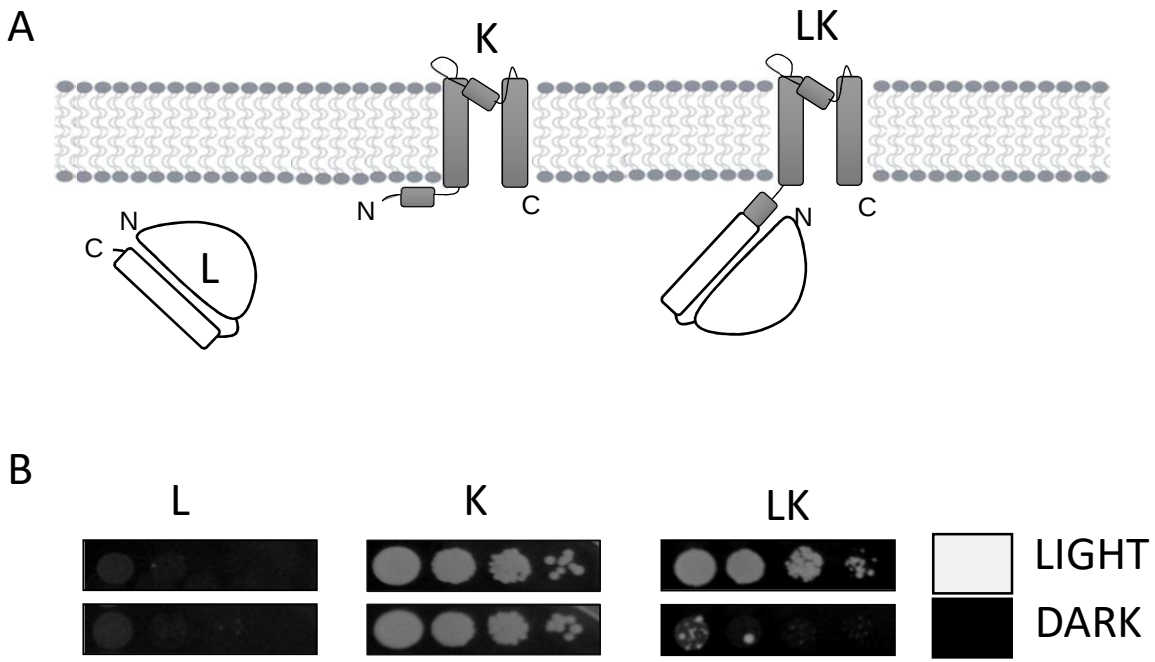

Figure 1

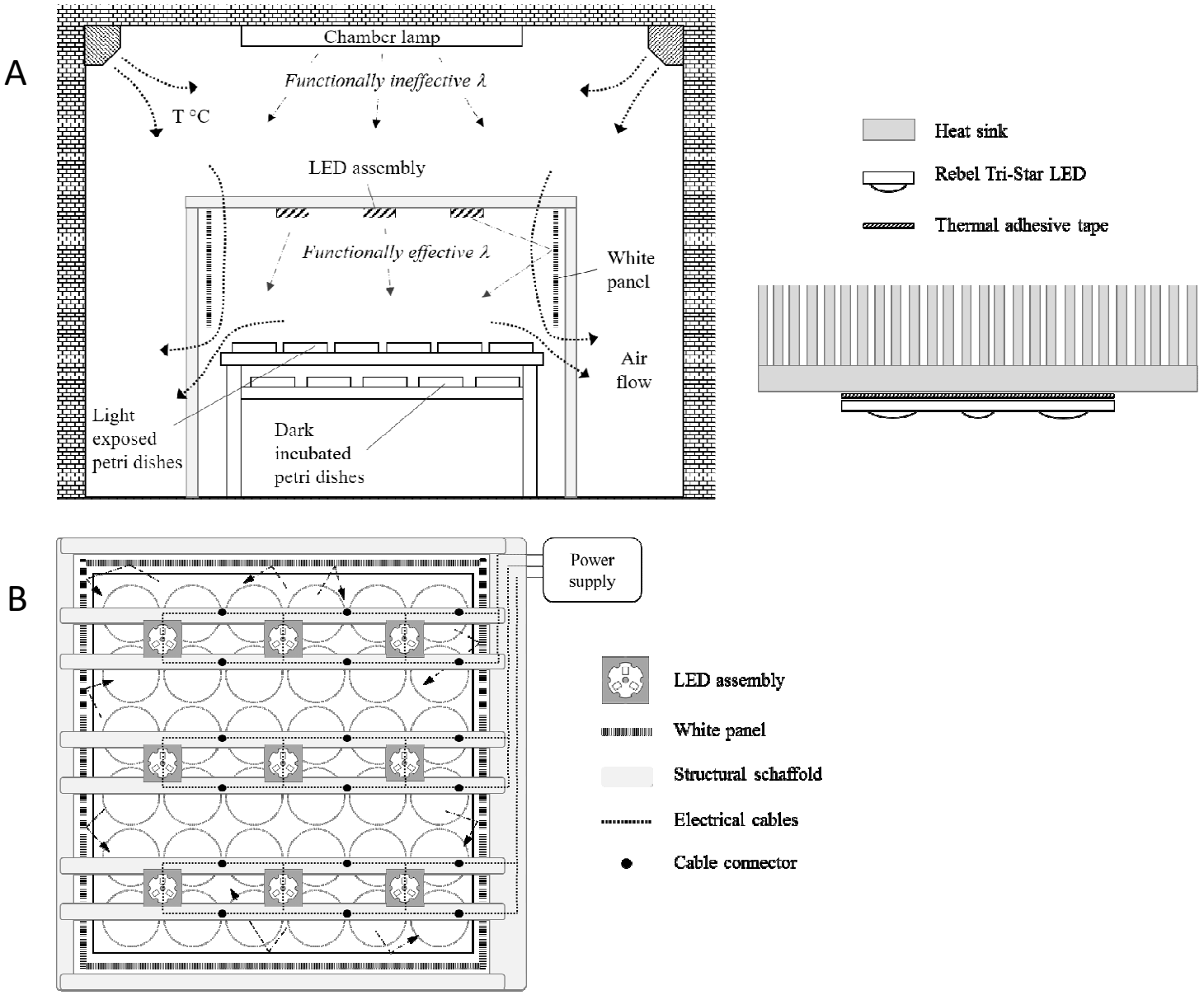
A
Chamber lamp
Functionally ineffective λ
T °C
LED assembly
Functionally effective λ
White pancl
Air flow
Light exposed petri dishes
Dark incubated petri dishes
Heat sink
Rebel Tri-Star LED
Thermal adhesive tape
B
Power supply
LED assembly
White panel
Structural schaffold
Electrical cables
Cable connector

Figure 2

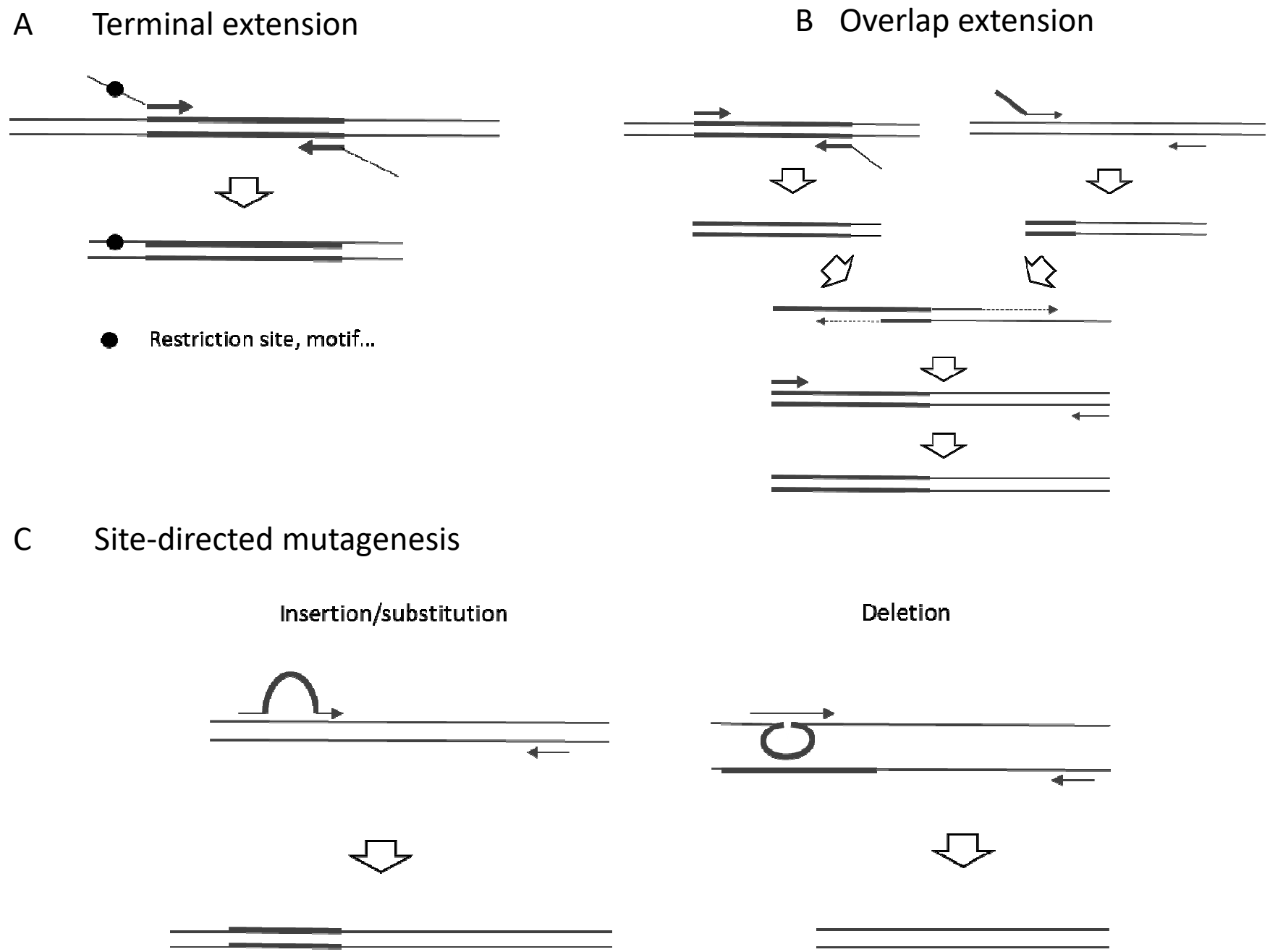
A Terminal extension
B Overlap extension
Restriction site, motif...
C Site-directed mutagenesis
Insertion/substitution
Deletion

Figure 3

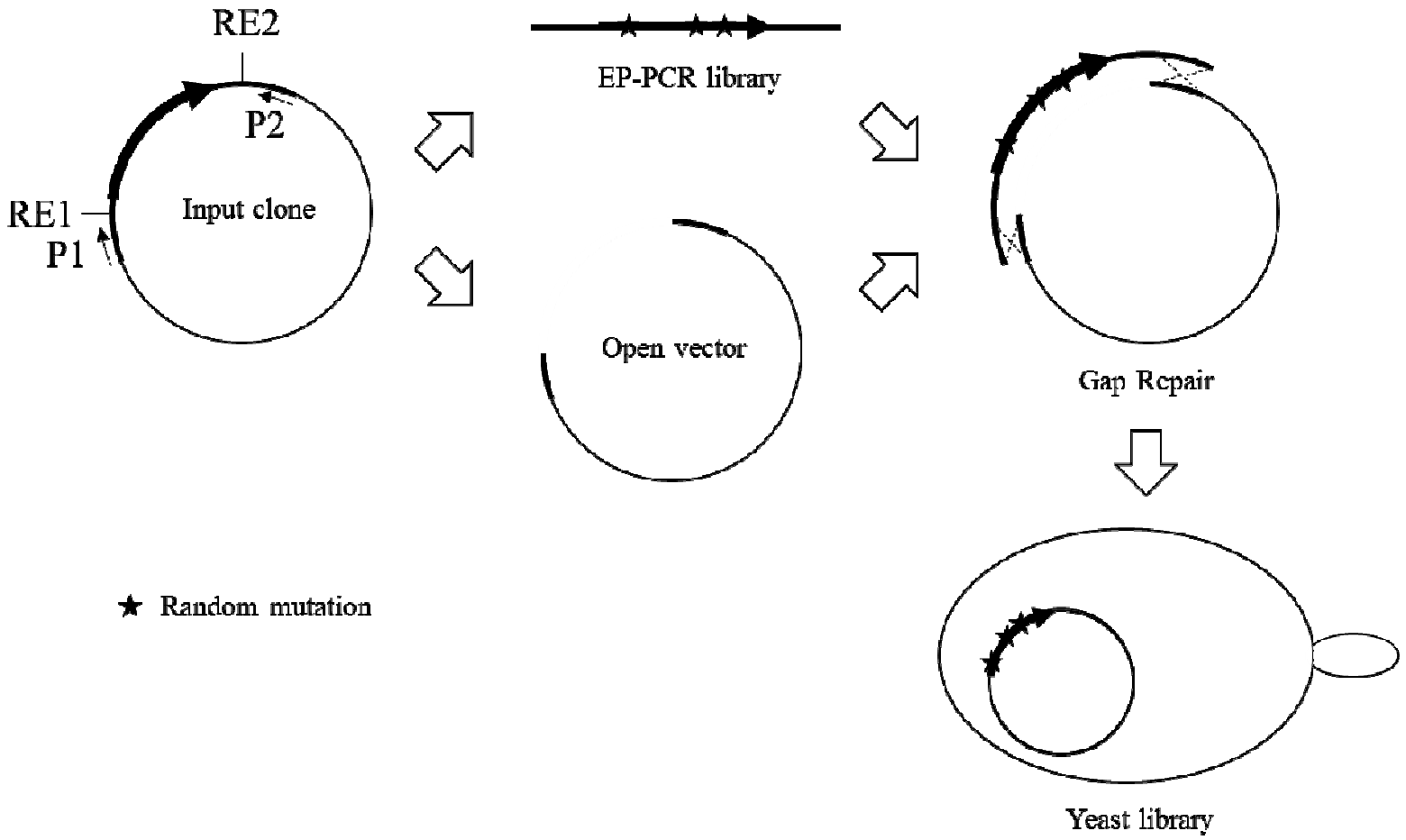
RE2
P2
RE1
P1
Input clone
EP-PCR library
Open vector
Gap Repair
Yeast library
★ Random mutation

Figure 4

PART III

MATERIALS AND METHODS

1 - Molecular biology

1.1 - Constructs Preparation

All constructs described in Part I were prepared by means of overlapping PCR [80].
A complete list of the ID codes of the sequences used to obtain each construct is provided in Supplementary Table 1, details regarding each construct sequences are indicated in Supplementary Table 2.

1.2 – Insertion of mutations

QuikChange Lightening ® (Agilent Technologies) was used to introduce point mutations described in Part I, paragraph 3.7; all the mutations introduced follow the residue numeration used for the original sequence of AsLOV2 domain.

1.3 – Expression vectors

Constructs were cloned in pYES2-Met25 vector [81] for expression in *S. cerevisiae*, in pcDNA3.1+ for expression in HEK293T and in pCS2+ for zebrafish.

Protein name	Organism source	Sequence
AsPhototropin1	*Avena sativa*	GeneBank: AAC05083.1
LAMP1	*Homo sapiens*	GeneBank: J03263.1
Gαo	*Homo sapiens*	CCDS: 10756.1
mKir2.1	*Mus musculus*	Gene ID: 16518
mTASK1	*Mus musculus*	NCBI gene: 16527
mTASK3	*Mus musculus*	NCBI gene: 223604
KAT1	*Arabidopsis thaliana*	Gene ID: 834666
PMA	*Zea maize*	Gene ID: 542048

Table 1

ID of all the gene sequences used in the present study

CONSTRUCT NUMBER	CONSTRUCT NAME	SEQUENCE DETAILS
1	Kcv	Kcv PBCV-1 (1-94)
2	L	AsPhotI (404-546) - LOV2-Ja
3	myL	my (1-8)::LOV2 (404-546)
4	myLK	my (1-8)::LOV2 (404-546) ::PBCV-1 (3-94)
5	myLK33	my (1-8) A7T::LOV2 (404-546) N538A ::PBCV-1 (3-94) P13L
6	BLINK1	my(1-8)::LOV2 (404-537) ::PBCV-1 (3-94)
7	Δ6	my (1-8)::LOV2 (404-540) ::PBCV-1 (3-94)
8	Δ3	my (1-8)::LOV2 (404-543) ::PBCV-1 (3-94)
9	AnBLINK1	my(1-8)::LOV2 (391-537) I532A ::PBCV-1 (3-94)
10	nBLINK1	my(1-8)::LOV2 (398-537) I532A ::PBCV-1 (3-94)
11	GID BLINK1	my(1-8)::LOV2 (401-537) I532A ::PBCV-1 (3-94)
12	TJSK+	RFP(1-234)::TM23 (380-405)::my(1-8)::LOV2 (404-537) ::PBCV-1 (3-94)
13	myG18 BLINK1	GNAO(1-18)::LOV2 (404-537) ::PBCV-1 (3-94)
14	myG26 BLINK1	GNAO(1-26)::LOV2 (404-537) ::PBCV-1 (3-94)
15	BLINK1-EYFP	my(1-8)::LOV2 (404-537) ::PBCV-1 (3-94):: eNpHR3.0 (291-559)
16	BLINK1-ER	my(1-8)::LOV2 (404-537) ::PBCV-1 (3-94):: mKir2.1 (374-380)
17	BLINK1-TS	my(1-8)::LOV2 (404-537) ::PBCV-1 (3-94):: mKir2.1 (233-252)
18	BKir	my(1-8)::LOV2 (404-537) ::PBCV-1 (3-94):: mKir2.1 (180-428)
19	BKir2	my(1-8)::LOV2 (404-537) ::PBCV-1 (3-94):: mKir2.1 (233-428)
20	BKir3	my(1-8)::LOV2 (404-537) ::PBCV-1 (3-94):: mKir2.1 (233-380)
21	BT1D	my(1-8)::LOV2 (404-537) ::PBCV-1 (3-94):: mTASK1 (245-394) S393D
22	BT3D	my(1-8)::LOV2 (404-537) ::PBCV-1 (3-94)::mTASK3 (245-402) S401D
23	BK6S	my(1-8)::LOV2 (404-537) ::PBCV-1 (3-94):: KAT1 (506-677)
24	BK6D/BLINK2	my(1-8)::LOV2 (404-537) ::PBCV-1 (3-94):: KAT1 (506-677) S676D
25	BLINK2.1	my(1-8)::LOV2 (404-537) ::PBCV-1 (3-94) :: KAT1 (506-677) S676D, EEWRD 524-528 DIDAE
26	BLINK2.2	my(1-8)::LOV2 (404-537) ::PBCV-1 (3-94):: KAT1 (506-677) S676D LMDAI 547-551 DIDAE
27	BLINK-KAT1	my(1-8)::LOV2 (404-537) ::PBCV-1 (3-94):: KAT1 (303-677) S676D
28	BLINK2.3	my(1-8)::LOV2 (404-537) ::PBCV-1 (3-94):: KAT1 (506-671)::PMHA (943-948) T947D
29	BLINK2 I427V	my(1-8)::LOV2 (404-537) I427V ::PBCV-1 (3-94):: KAT1 (506-677) S676D
30	BLINK2 V416T	my(1-8)::LOV2 (404-537) V416T ::PBCV-1 (3-94):: KAT1 (506-677) S676D
31	BLINK2 N414A	my(1-8)::LOV2 (404-537) N414A ::PBCV-1 (3-94):: KAT1 (506-677) S676D
32	BLINK2 Q513H	my(1-8)::LOV2 (404-537) Q513H ::PBCV-1 (3-94):: KAT1 (506-677) S676D
33	BLINK2 N414A+Q513H	my(1-8)::LOV2 (404-537) N414A Q513H::PBCV-1 (3-94):: KAT1 (506-677) S676D
34	BLINK2 Q513D	my(1-8)::LOV2 (404-537) Q513D ::PBCV-1 (3-94):: KAT1 (506-677) S676D

Table 2

List of all the constructs examined in the present work. Details about chimeras construction are indicated, residues are numbered according to the native protein sequence.

2 – Western blot analysis

Western blot analysis was performed on proteins produced and purified from *S. cerevisiae*.

2.1 - Yeast growing conditions

Yeast expression of BLINK1 and myLK33 was achieved by functional complementation in the *S. cerevisiae* strain SGY1528 (*MATa ade2–1 can1–100 his3–11,15 leu2–3,112 trp1–1 ura3–1 trk1::HIS3 trk2::TRP1* [81], lacking the endogenous K+ transporters. Therefore, this strain is not able to grow on media supplemented with K^+ lower than 100 mM.

Transformed yeast colonies were inoculated in non-selective medium (SD -Ura, 100 mM KCl) and grown overnight to stationary phase. Cultures were then diluted to OD600=0.8 and 7µl of 10-fold serial dilutions were spotted onto selective plates (SEL -Ura -Met with 0.5, 1, 4 mM KCl). Twin plates were prepared for each K^+ concentration and were either incubated 4 days at 30°C in presence of blue light or grown in the dark. Non-selective and selective media were prepared as previously described [81]**.** Solid media were obtained adding 15g/l agar with low potassium content (SIGMA #A7921).

2.2 - Western blot

Yeast cells grown on selective medium for 3 days at 30 °C were collected from plates, resuspended in water and pelleted (1,500 x *g*, 20 min). Pellet was resuspended in Breaking Buffer (50 mM NaH_2PO_4*H2O, 1 mM EDTA, 5 % (w/v) glycerol, 5µM Leupeptin, 1µM Pepstatin, 0.1mM PMSF, 5mM DTT) and lysis was performed by vortexing in the presence of glass beads (425-600 µm, Sigma-Aldrich). The lysate was centrifuged (4000 x *g*, 5 min) to remove cell debris. Then, the Eppendorf tube was centrifuged (15,000 x *g*, 1 hour) at 4°C and the supernatant was discarded. The obtained microsomes were resuspended in Breaking Buffer, quantified using Bradford reagent (Biorad) and stored at -80°C.

13µg/lane of total protein were separated in SDS-PAGE on 4-20% tris-glycine denaturating gel (Novex). Proteins were blotted on a PVDF membrane and blocked in 5% dry milk in TBST solution for 4 hours and then incubated with primary anti-Kcv 8D6 monoclonal antibody [72] at 4 °C overnight. Then the blots were rinsed in TBST for 3 X 10 min and incubated with alkaline phosphatase-conjugated secondary antibody for 1 hour. Antibody binding was detected using SIGMAFAST BCIP/NBT tablet (Sigma).

3 - Immunocytochemistry

HEK293T cells were transfected with TurboFect Transfection Reagent (Thermo Scientific) according the producer protocol (see Paragraph 4.1), and after one to two days were treated as follows.
Cells used for surface staining were incubated first with blocking solution containing 2% BSA in PBS and then 1 hour with anti-Kcv 8D6 monoclonal antibody [72], washed briefly with blocking solution and incubated 1 hour with Alexa Fluor® 594 AffiniPure secondary antibody and Hoechst dye.
Cells used for intracellular staining were fixed with 4%PFA in PBS, incubated with blocking solution containing 2% BSA and 0.2% Triton-X in PBS and then treated as described for non-permeabilized samples.
Confocal microscopy analyses were performed using Leica SP2 (http://www.leica-microsystems.com) laser scanning confocal imaging system. Images were acquired using a 63x oil lens, images manipulation was done using Fiji-ImageJ.

4 – Electrophysiology recordings in HEK 293T cells

4.1 - Cell culture and transfection protocol

HEK293T cells were cultured in Dulbecco's modified Eagle's medium (Euroclone) supplemented with 10% fetal bovine serum (Euroclone), 100 IU/mL of penicillin, 100 μg/ml of streptomycin, and stored in a 37 °C humidified incubator with 5% CO_2. Transfections were performed with TurboFect Transfection Reagent (Thermo Scientific) according the producer protocol: cDNAs inserted in pcDNA3.1+ were co-transfected in HEK293T with a plasmid containing green fluorescent protein (GFP) and incubated in dark.

4.2 - Patch clamp recordings

One to two days after transfection, HEK293T cells were dispersed by trypsin-EDTA treatment and seeded on 35-mm plastic petri dishes to allow single cell measurements. Cells showing GFP signal were selected for patch clamp measurements.
Membrane currents were recorded in whole cell configuration using a Dagan 3900A patch-clamp amplifier and digitized using a Digidata 1322A controlled by pCLAMP 9.2.
The pipette solution contained: 10 mM NaCl, 130 mM KCl, 2 mM ATP-Magnesium salt, 1mM EGTA and 5 mM HEPES–KOH buffer (pH 7.2).

The extracellular bath's solution contained: 100 mM KCl, 80 mM D-Mannitol, 1.8 mM $CaCl_2$, 1 mM $MgCl_2$ and 5 mM HEPES–KOH buffer (pH 7.4). When different KCl concentrations were used, the osmolarity was adjusted to 290 mOsm with D-mannitol. The channel blocker $BaCl_2$ was applied to the external solution at a concentration of 5 mM.
The voltage protocols applied consisted in a step protocol of 20 mV steps from + 60 to -140 mV, or in a gap free protocol clamping the cell membrane at E_K for 24 seconds and at -60 for 6 seconds to extend the duration of the recording. E_K was estimated using Nernst equation.

5 - Microinjections and touch response assays in zebrafish

Channels and GFP constructs inserted in pCS2+ were linearized with *Not*I and transcribed with Sp6 RNA polymerase, using the mMESSAGE mMACHINE® SP6 Transcription Kit (Ambion) and following manufacturer's instructions. 200pg/embryo of RNA in water (W3500, Sigma-Aldrich) was injected in embryos at the 1- to 2-cell stage. Injection mix was supplemented with rhodamine-dextran (D1817, Molecular Probes) as a tracer. Injected embryos were grown in E3 medium (5 mM NaCl, 0.17 mM KCl, 0.33mM MgSO4, 0.33 mM CaCl2) at 28.5 °C and manually dechorionated at 1 day post-fertilization (1dpf). The escape response was tested 2 days post-fertilization, according to the following procedure: using a microloader tip, a gentle stimulus was applied to the tail of the embryos and their reaction observed at 5X magnification under a stereo microscope as previously described for BLINK1 [31].

6 - Light conditions

Light irradiation of the different model systems used in this study was obtained as follows.
Yeast plates were grown either in dark or irradiated by a custom-made array of light emitting diodes (LEDs) (Royal-Blue LED, λ 447 ± 10 nm, LUXEON Rebel LED) allowing homogeneous illumination of the samples (2 ± 0.2 $\mu W/mm^2$) in a controlled temperature chamber. The same system was used for illumination of zebrafish embryos, but with a higher intensity, 80 $\mu W/mm^2$.
Transfected HEK293T cells were kept in the dark prior to the assays and all preliminary operations were performed under red light illumination (MRH2060-20T, LUXEON Rebel LEDs Red-Orange (617 nm)). Blue light illumination was obtained using a light-emitting diode (Royal Blue, 455 nm, High-Power LED; Thorlabs) at 80 $\mu W/mm^2$. Light power was measured using a light power meter (Thorlabs).